Toward A Generalized Signal Processing Framework for Inter-Subject Associative BCI

by

Simanto Saha

M.Phil. in Electrical and Electronic Engineering
The University of Adelaide, Australia, 2020

A thesis submitted to fulfil requirements for the degree of

Doctor of Philosophy

in

Faculty of Engineering
The University of Sydney, Australia

2025

THE UNIVERSITY OF
SYDNEY

Principal Supervisor:

Professor Alistair McEwan, School of Biomedical Engineering

Co-Supervisors:

Professor Omid Kavehei, School of Biomedical Engineering

Dr. Petra Karlsson, Sydney Medical School

Dr. Collin Anderson, School of Medical Sciences

“Om Satyam Shivam Sundaram"
Truth, Auspiciousness, and Beauty

Statement of Originality

I certify that this work contains no material which has been accepted for the award of any other degree or diploma in my name, in any university or other tertiary institution and, to the best of my knowledge and belief, contains no material previously published or written by another person, except where due reference has been made in the text. In addition, I certify that this work will only be used in a submission in my name for any other degree or diploma in any university or other tertiary institution with the prior approval of the University of Sydney or any partner institution responsible for the joint award of this degree.

The author acknowledges that the copyright of the published works contained within the thesis resides with those works' copyright holder(s).

I give permission for the digital version of my thesis to be made available on the web via the University's digital research repository, the Library Search, and web search engines unless the University has granted permission to restrict access for a period of time.

Signed

Date

Authorship Attribution Statement

This thesis contains materials that have been published or are in the process of publication in journals. I contributed significantly to each chapter of this thesis and appendices. I have been the corresponding author of the publication associated with this thesis; otherwise, permission has been obtained from the corresponding author. An author's contribution statement is presented at the beginning of each chapter.

Signed

Date

As the supervisor for the candidature upon which this thesis is based, I can confirm that the authorship attribution statements above are correct.

Signed

Date

Abstract

Neural decoding enables the translation of the brain's electrical and hemodynamic activities into clinical diagnosis and treatment or control signals to operate assistive and rehabilitative technologies (ARTs). Brain-computer interfaces (BCIs) utilize brain signals and enable healthy individuals and people with disabilities to interact with their surroundings by operating ARTs. The primary objective of this thesis is to evaluate BCIs as state-of-the-art ARTs for people with disabilities and to develop digital signal processing (DSP) algorithms for generalized BCIs that translate the brain's electrical or hemodynamic activities into active or passive tangible outputs.

Neuroimaging is a crucial element of BCI, and electroencephalography (EEG) is a non-invasive neuroimaging technique that captures the brain's electrical activities associated with users' thoughts, intentions, and cognitive states. Notwithstanding, due to covariate shifts, inherent inter-subject variabilities of EEG signals hinder the development of generalized DSP and pattern recognition algorithms for BCI. Covariate shifts describe the difference between training and testing feature spaces, demanding adjustment to the classifier boundaries for consistent outcomes. Some studies demonstrated data-driven covariate shift adaptation or transfer learning strategies to compensate for the inter-subject variabilities, while others proposed BCI performance predictors. Nevertheless, further investigations are essential for a fully zero-training BCI that does not require training samples from a new target user.

An inter-subject associative BCI refers to a fully zero-training neural decoding algorithm when a group of users shares similar EEG features so that the algorithm can perform well for a user when trained on other users' data from the same group. However, only a few studies attempted to quantify inter-subject associativity, *i.e.*, identifying task-related EEG features that exhibit unchanged feature domains across subjects, minimizing the chance of covariate shift occurrence. Quantifying inter-subject associativity complements data-driven transfer learning and delivers good BCI performance without any training data. Data-driven conventional techniques, including common spatial pattern (CSP), are prone to overfitting and often demonstrate inconsistent classification accuracies. However, recently introduced convolutional neural network (CNN)-based architectures are deep learning techniques that

inherently learn features from data with nonlinear activation functions while optimizing the models' predictive capabilities.

This thesis presents six chapters, including a review that evaluates the state-of-the-art BCI-based ARTs by integrating the International Classification of Functioning, Disability, and Health framework across the lifespan, highlighting the influence of brain changes during development and aging on the design and ethical use of BCI technologies. While user needs are central to adaptable design strategies for providing individualized BCI-based ARTs to people with disabilities, generalized DSP and pattern recognition algorithms offer scalability across users. Inter-subject associative BCIs are practical, given that reliable inter-subject BCI performance predictors exist. A novel Bhattacharya distance-based predictor was developed for a CSP-based BCI classification framework. The CSP-based methods were compared with novel BCI classification pipelines utilizing a $1-$dimensional convolutional neural network (1D-CNN) architecture, which can employ multi-dimensional sequences for feature learning. Various feature representation techniques, such as bandpass-filtered EEG signals, power spectral density (PSD) sequences, and bi-channel cross-power spectral density (CPSD) sequences, were used to train the proposed 1D-CNN architectures. The proposed methods were tested on motor imagery (MI) and speech classification tasks from EEG signals. Results implicated that 1D-CNN, utilizing time-domain EEG signals, produced better classification accuracies than frequency-embedded PSD or CPSD sequences and CSP-based methods for intra- and inter-subject MI classification. However, the proposed 1D-CNN with PSD sequences outperformed the results of time-domain EEG signals for intra-subject speech BCI.

Predicting inter-subject associativity can foster a fully zero-training BCI development for classifying MI and text classification tasks. The proposed CNN-based architecture is a novel option for classifying multi-channel time-domain EEG signals, likely highlighting generic feature learning for intra- and inter-subject BCI. Such nonlinear learning functions would promote generalized algorithms for BCIs, inherently compensating for inter-subject EEG variabilities. In addition to generic feature learning using the proposed 1D-CNN architecture, results suggest that spectral representations of EEG signals, *i.e.*, PSD, and CPSD sequences are potential alternative representations to temporal EEG signals. Thus, this thesis highlights the importance of EEG signal preprocessing and representation using DSP techniques, even when deep learning architectures such as 1D-CNN are designed to learn features from raw signals directly.

Acknowledgements

I would like to convey my deepest gratitude to my principal supervisor, Professor Alistair McEwan, for his generous support and guidance throughout my candidature. First, I am indebted to him for believing in my research aptitude, with an offer of a PhD position in his group. His continuous guidance helped me understand the state-of-the-art assistive and rehabilitative technologies and the underlying design philosophy for assisting people with disabilities. He provided me access to his strong collaboration networks across local and global research communities of neural rehabilitation technologies. Pursuing a PhD is challenging; he was always there to support me in overcoming difficult personal and student life situations and keeping me on track to a successful and timely thesis completion. He inspired me to do an internship during my PhD to gain valuable industry experience.

I am also very thankful to my co-supervisors, Professor Omid Kavehei, Dr. Petra Karlsson, and Dr. Collin Anderson, for their support throughout my candidature.

A special thank you goes to my MPhil supervisor, Associate Professor Mathias Baumert, for his continued support to my research career. I would also like to acknowledge the tremendous support from my industry mentor, Mr. James Wagner, and everyone in the Advanced Technology Group for all their help during my internship at Dolby Australia.

Finally, I would like to thank my family and friends for keeping me always psychologically up during the challenging time of pursuing a PhD. I am and will always be indebted to my mum and dad for their unconditional love and mental support while I continue my studies in Australia. Thanks to my darling wife, Dyuti, for being compassionate, even when I spent the weekends on my research activities.

I acknowledge the support of a Research Training Program Scholarship to conduct the research reported in this thesis during my PhD candidature.

Honors and Awards

Award

- **Dean's Commendation for Master by Research Thesis Excellence**
  by the University of Adelaide, 2020

Scholarships

- **APR Intern Program Scholarship** by The University of Sydney 2024
- **University of Sydney International Stipend Scholarship** 2021
- **University of Sydney Tuition Fee Scholarship** 2021
- **Leo J Mahar Scholarship** by the University of Adelaide 2018
- **Full Fee Scholarship** by the University of Adelaide 2018

Travel Grants

- **Research Travel Scholarship** by the University of Adelaide 2019
- **IEEE EMBS Student Travel Award** by IEEE 2019
- **Travel Allowance** by the School of EEE (the University of Adelaide) 2019

Conventions

This thesis is typeset using the MiKTeX software. TeXstudio was used as text editor interfaced to MiKTeX. MATLAB® and `BioRender.com` were used to produce schematic diagrams and other drawings. Harvard style is used for referencing and citation in this thesis. North American spelling is adopted througout the thesis (`www.Merriam-Webster.com`). For grammatical accuracy and writing assistance, `www.grammarly.com` was used. No other tools, including recent artificial intelligence-based language models, were used to prepare the materials for this thesis unless explicitly mentioned.

Publications

Journal Articles

- **Saha, S.**, Karlsson, P., Anderson, C., Kavehei, O. and McEwan, A., Individualized Brain-Computer Interface for People with Disabilities: A Review. – Under Review. [Chapter 2]
- **Saha, S.**, Baumert, M. and McEwan, A., Time-Domain Versus Frequency-Embedded EEG Sequences for Sensorimotor BCI Using 1D-CNN. – Under Review. [Chapter 4]
- **Saha, S.**, Wagner, J and McEwan, A., Frequency-Embedded Sequence Learning for Multi-Class EEG-to-Text Interface. – Under Review. [Chapter 5]
- **Saha, S.**, Linz, D., Saha, D., McEwan, A. and Baumert, M., 2024. Overcoming uncertainties in electrogram-based atrial fibrillation mapping: A review. *Cardiovascular Engineering and Technology*, 15(1), pp.52-64. [Appendix B]

Conference Papers

- **Saha, S.**, Baumert, M. and McEwan, A., 2023, July. Can Inter-Subject Associativity Predict Data-Driven BCI Performance?. In *2023 45th Annual International Conference of the IEEE Engineering in Medicine & Biology Society (EMBC)* (pp. 1-4). IEEE. [Chapter 3]
- **Saha, S.**, Alam, R.U., Samore, A., Goodwin, A., Wong, M.L.S., McEwan, A. and Anderson, C., 2023, October. Time-Embedded EEG Sequence Learning for Comatose Patients' Prognosis. In *2023 Computing in Cardiology (CinC)* (Vol. 50, pp. 1-4). IEEE. [Appendix A]

Contents

List of Figures

List of Tables

1 Introduction

NEURAL decoding enables the translation of the brain's electrical and hemodynamic activities into clinical diagnosis and prognosis or control signals to operate assistive and rehabilitative technologies (ARTs). The primary objective of this thesis is to develop generalized neural decoding frameworks featuring advanced digital signal processing and pattern recognition algorithms for electroencephalography (EEG)-based brain-computer interfaces (BCIs). EEG signals are highly variable over time and across users; thus, developing a generalized neural decoding algorithm is challenging. This thesis presents novel BCI performance predictors and generalizable neural decoding algorithms using time/frequency representations of EEG signals and $1-$dimensional convolutional neural network (1D-CNN) architectures for intra- and inter-subject BCIs. The proposed 1D-CNN methods demonstrate promising performance for BCI for decoding imagined movements and speech. This chapter provides an introduction to neural decoding and an overview of the contents and organization of this thesis.

1.1 Neural Decoding

Medical technologies are evolving in diverse application areas through significant advancements in neuroimaging modalities, digital signal processing (DSP), and pattern recognition algorithms. There are implantable and non-implantable signal acquisition modalities featuring advanced neural sensors to capture the brain's electrical and hemodynamic activities. The brain signals require various DSP techniques to eliminate noises or artifacts and enhance the signal-to-noise ratio, followed by handcrafted feature extraction for classification using machine learning techniques or feature learning by deep learning algorithms to classify an intended task (Craik *et al.*, 2019; Lotte *et al.*, 2018; Hosseini *et al.*, 2020; Motamedi-Fakhr *et al.*, 2014; Lotte *et al.*, 2007; Bashashati *et al.*, 2007). Figure 1.1 illustrates a simplified DSP block diagram for clinical diagnosis, prognosis, and brain-computer interface (BCI) applications. Clinical applications include the detection of epilepsy or sleep disturbances and predicting a patient's recovery in an intensive care unit (ICU) (Wang *et al.*, 2023b; Phan *et al.*, 2023; Saha *et al.*, 2023a).

1.1.1 Brain-Computer Interfaces

A BCI is a bidirectional communication link between the brain and a computer or other external devices, enabling the decoding and encoding neural information from and to the brain described in more detail in chapter 2. This thesis aims to develop novel DSP and pattern recognition algorithms for neural decoding of movement and speech using electroencephalography EEG signals, which could offer assistive and rehabilitative technologies (ARTs) to people with disabilities. Typically, a neural decoder or BCI translates brain signals into control signals to operate diverse ARTs, such as controlling a wheelchair or prosthetic arm (Naser and Bhattacharya, 2023; Flesher *et al.*, 2021).

EEG signals are highly nonlinear and nonstationary, hindering the reproducibility of a neural decoding algorithm across sessions and subjects (Saha and Baumert, 2020; Saha *et al.*, 2019b, 2017b,a). Inter-session and inter-subject variabilities are prominent in BCI. Thus, session- and subject-specific calibration is essential to operating a BCI with high accuracy. EEG signal variabilities cause covariate shifts, which occur when distributions between the training and testing feature spaces differ due to inter-session and inter-subject variabilities. Studies addressed this issue using covariate shift adaptation or transfer learning techniques (Wei and Ding, 2023; Chen *et al.*, 2022; Azab *et al.*, 2019; He and Wu, 2019; Azab *et al.*, 2018; Jayaram *et al.*, 2016). Other studies found neurophysiological markers

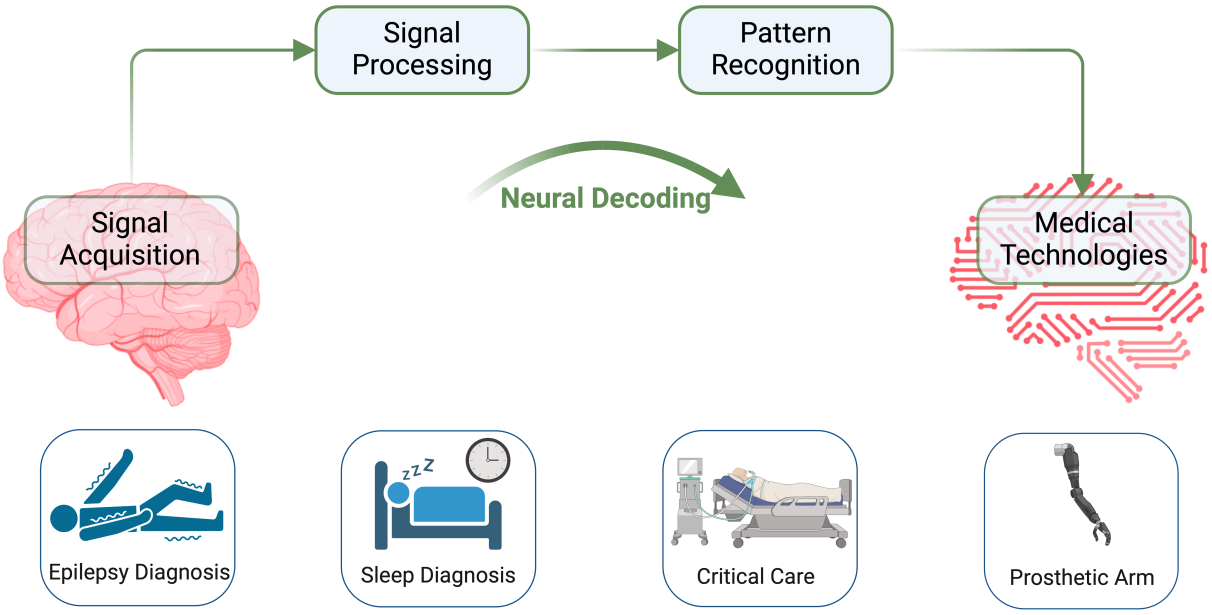

Figure 1.1. A simplified block diagram of neural signal processing pipeline for the diagnosis and prognosis of clinical conditions or controlling ARTs.

predicting BCI performance. Irrespective of the inter-subject variabilities, some studies also investigated inter-subject associative features for a fully zero-training BCI, which enables a new user to operate a BCI without any training session for calibration (Saha *et al.*, 2019b; Wronkiewicz *et al.*, 2015; Kang and Choi, 2014; Kang *et al.*, 2009).

This thesis presents a novel Bhattacharyya distance-based predictor for motor imagery (MI) classification in both intra- and inter-subject BCI settings. The predictor shows promising results correlating with BCI classification accuracies, suggesting inter-subject associative BCIs are feasible. This thesis also proposes DSP algorithms for fully zero-training inter-subject MI BCIs featuring 1-dimensional convolutional neural network (1D-CNN) architectures, replacing conventional handcrafted feature engineering for decoding imagined movement and speech from EEG signals. Typically, 1D-CNN architectures can use multi-channel sequence data, such as time-domain multi-channel EEG signals. This thesis investigates the spectral representation of multi-channel EEG signals featuring power spectral density (PSD) estimation for 1D-CNN. The underlying assumption is that frequency-embedded feature representation may perform better than time-domain signals. Comparative results exhibit time-domain EEG signals outperform frequency-embedded PSD sequences for MI classification. In contrast, the frequency-embedded PSD sequences beat time-domain EEG

signals for speech decoding. This thesis also presents a novel cross-power spectral density (CPSD)-based representation of EEG signals for training 1D-CNN.

1.2 Thesis Structure

This (Chapter 1) is an introduction followed by a state-of-the-art narrative review in chapter 2. Chapter 3 demonstrates a novel performance predictor for intra- and inter-subject BCIs. That reports MI classification results using a common spatial pattern (CSP)-based neural decoding algorithm and their correlation with the proposed Bhattacharyya distance-based performance predictor. Notably, CSP is a widely used technique for MI classification. Chapter 4 presents a novel 1D-CNN architecture-based DSP pipeline for decoding MI tasks, *i.e.*, right hand and right foot MI utilizing time-domain EEG signals, frequency-embedded PSD and CPSD sequences. The results benchmarked with that achieved using two CSP-based classification frameworks illustrate the significance of frequency-embedded feature representation for 1D-CNN. Chapter 5 also utilizes 1D-CNN architecture-based neural decoding framework for classifying multi-class imagined speech in the context of intra- and inter-subject BCIs. This study compares the results of time-domain EEG signals and frequency-embedded PSD sequences, respectively. Then, chapter 6 discusses the significant contributions, study limitations, and future outlook of the proposed DSP algorithms for inter-subject BCI, followed by a conclusion. As supplementary materials, appendix A explains a DSP algorithm for predicting patients' recovery post-stroke coma in ICUs. Finally, appendix B presents a contemporary (narrative) review of critical elements of atrial fibrillation mapping and their engineering perspectives.

Chapter Context:

This chapter briefly introduced neural decoding in the context of clinical diagnosis, prognosis, and BCI and describes the structure and organization of this thesis. The next chapter follows a thorough literature review on BCI-based ARTs for people with disabilities and highlights the key translational elements of state-of-the-art BCIs.

Individualized Brain-Computer Interface for People with Disabilities

2

BRAIN-computer interfaces (BCIs) facilitate functional interaction between the brain and external devices, enabling users to bypass their typical peripheral motor actions to control assistive and rehabilitative technologies (ARTs). This chapter critically evaluates the state-of-the-art BCI-based ARTs by integrating the International Classification of Functioning, Disability, and Health (ICF) framework across the lifespan, highlighting the influence of brain changes during development and aging on the design and ethical use of BCI technologies. As direct human-computer interfaces, BCI-based ARTs offer extended degrees of freedom via augmented mobility, cognition and communication, especially to people with disabilities. However, the innovation in BCI-based ARTs is guided by the complexity of disability types and levels of function across users that define individual needs. Therefore, an adaptable design is essential for tailoring a BCI-based ART that can fulfill user-specific requirements, which may hinder the scalability of BCIs for their widespread adoption across users with disabilities. The tradeoffs between implantable and non-implantable BCIs are explored along with complex decisions around informed consent for people with communication or cognitive disabilities and pediatric settings. Non-implantable BCIs offer broader accessibility and transferability across users due to reproducible signal acquisition and decoding algorithms, making them suited for a more comprehensive user group. This chapter contributes to the field by providing a lifespan- and ICF-informed discussion of BCI-based ARTs, emphasizing the need for adaptable designs that align the evolving functional and developmental needs of users with disabilities.

The contents of this chapter have been submitted for publication as:

Saha, S., Karlsson, P., Anderson, C., Kavehei, O. and McEwan, A., Individualized Brain-Computer Interface for People with Disabilities: A Review. – Under Review.

Author Contributions: SS conceived this review's idea, developed the initial proposal, prepared graphical illustrations, wrote the original draft, and edited and finalized the manuscript. PK, CA, OK, and AM reviewed the original draft and provided feedback. All authors read and approved the final manuscript for publication.

2.1 Introduction

Neurological disorders such as stroke, spinal cord injury, amyotrophic lateral sclerosis, and cerebral palsy cause functional disabilities and often have associated impairments that impact communication, cognition and mobility, thus, quality of life (Metzger *et al.*, 2023; Bekteshi *et al.*, 2023; Hallett *et al.*, 2022; Monforte *et al.*, 2021; Makris *et al.*, 2021; Micera *et al.*, 2020; Goulet *et al.*, 2019; Milekovic *et al.*, 2018; Goldstein and Abrahams, 2013). Multiple factors, from personal and environmental contexts to social and welfare elements, impact people with disabilities and their ability to participate in everyday life. In 2002, the World Health Organization (WHO) proposed a psychosocial model of disability, the International Classification of Functioning, Disability and Health (ICF) (Organization *et al.*, 2002; Andresen *et al.*, 2016; Hill *et al.*, 2015). The ICF framework helps to explain the often-complex neurological disorders' interplay with contextual factors (*i.e.*, personal and social circumstances). It also assists in identifying individualized user needs to improve the operational abilities of people with disabilities. Individualized requirements include assistive and rehabilitative technologies (ARTs), which support users in regaining healthy functional abilities or performing daily life tasks (Mohammadi *et al.*, 2023; Zhu *et al.*, 2022; Edughele *et al.*, 2022; Andresen *et al.*, 2016; Stamford *et al.*, 2015; Hill *et al.*, 2015). Figure 2.1 illustrates the complex interplay between the diverse psychosocial and health-related factors for assessing the needs of people with functional disabilities due to neurological incidents.

A brain-computer interface (BCI) facilitates functional interaction between the brain and a computer, enabling the decoding and encoding of neural information from and into the brain (Card *et al.*, 2024; Willett *et al.*, 2023; Huggins *et al.*, 2022; Karlsson *et al.*, 2022; Orlandi *et al.*, 2021; Mrachacz-Kersting *et al.*, 2021; Willett *et al.*, 2021; Saha *et al.*, 2021; Moses *et al.*, 2021; Flesher *et al.*, 2021; Mrachacz-Kersting *et al.*, 2016; Rao *et al.*, 2014; Moghimi *et al.*, 2013). It provides novel ways of communication for end-users intending to interact with their surroundings through ARTs. Figure 2.2 illustrates a simplified block diagram of a bidirectional BCI and its application in diverse ARTs for people with disabilities. Neural decoding utilizes implantable or non-implantable neuroimaging modalities to record electrical and hemodynamic responses of the brain corresponding to a user's intentions or cognitive states (Patrick-Krueger *et al.*, 2024; Edelman *et al.*, 2024; Karikari and Koshechkin, 2023; Saha *et al.*, 2021; Martini *et al.*, 2020; Moghimi *et al.*, 2013; Min *et al.*, 2010). The captured brain signals are classified through digital signal processing (DSP) and pattern recognition algorithms (Lotte *et al.*, 2018; Krusienski *et al.*, 2011; Bashashati *et al.*, 2007; Lotte *et al.*, 2007) to use them to operate different types of ARTs, for example, wheelchairs,

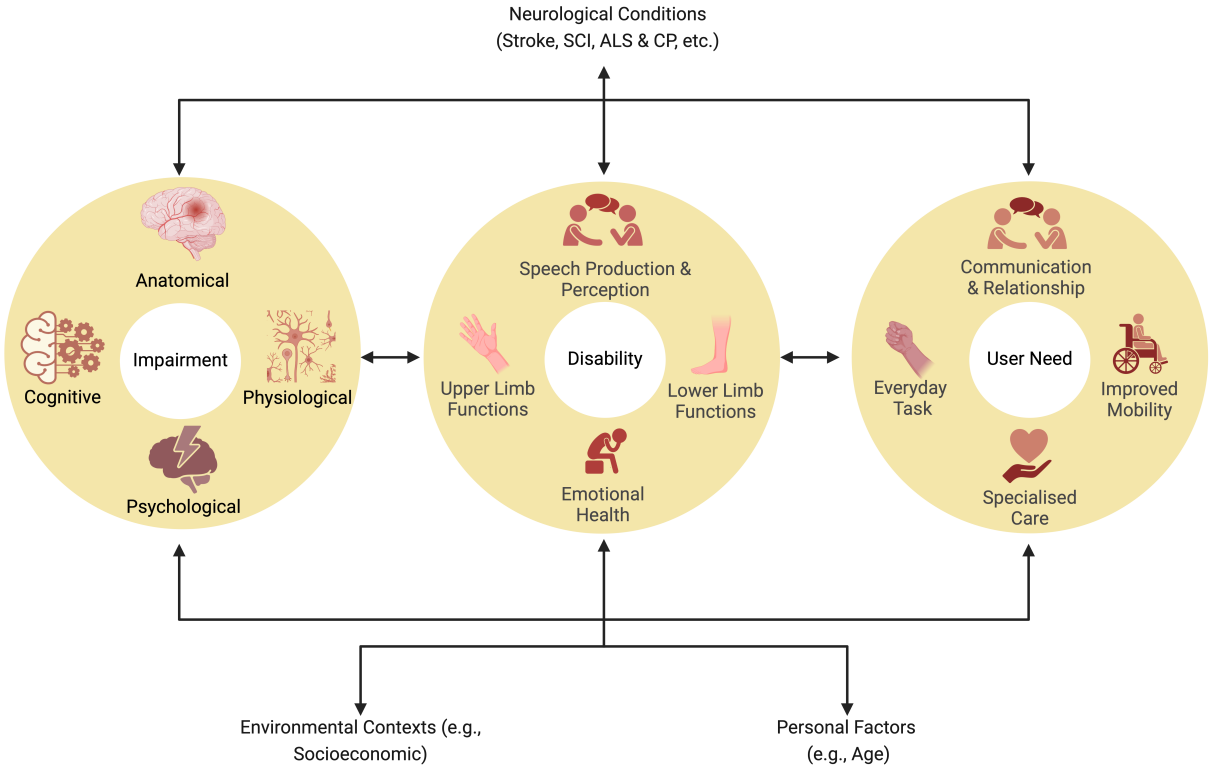

Figure 2.1. The complex interplays between psychosocial and health-related factors defining the user needs of people with disabilities. [SCI: spinal cord injury, ALS: amyotrophic lateral sclerosis, CP: cerebral palsy. Figure inspired from the WHO ICF framework]

prosthetic arms, virtual reality, and stimulation modalities (Flesher *et al.*, 2021; Saha *et al.*, 2021; Mrachacz-Kersting *et al.*, 2021, 2016; Cao *et al.*, 2014). The stimulation modalities are core components of neural encoding and, thus, for rehabilitative BCI.

Some of the most successful applications of BCI-based ARTs have benefitted people with movement and speech disabilities (Card *et al.*, 2024; Willett *et al.*, 2023, 2021; Moses *et al.*, 2021; Flesher *et al.*, 2021; Huggins *et al.*, 2022; Karlsson *et al.*, 2022; Orlandi *et al.*, 2021; Moghimi *et al.*, 2013). Studies showed that people with severe disabilities to generate pronounced speech could use their thoughts, *i.e.*, brain signals, to produce texts on a computer screen to communicate with their surroundings (Willett *et al.*, 2023, 2021; Moses *et al.*, 2021). At the same time, a BCI can rehabilitate impaired functional abilities by integrating neuroprosthetic and neurostimulation modalities (Mrachacz-Kersting *et al.*, 2021, 2016). Diversity in disability types and levels of impairment across users demand individualized design of BCI-based ARTs for fulfilling user needs. Weighing the value of BCI-based ARTs over conventional technologies is critical for their mass adoption by people with disabilities, while the ARTs assist them in participating in mainstream socioeconomic life.

This chapter evaluates the current state of BCI-based ARTs, their critical elements and manifold translational aspects. While the personalization of BCI applications is essential for fulfilling individualized user needs, generalizing neural decoding algorithms to provide calibration-free requirements promotes scalability and mass dissemination of BCI across diverse user cohorts. However, developing a generalized BCI algorithm is challenging, especially when using EEG signals, due to the inherent signal variation over time and across subjects. This thesis illustrates in Chapter 3 a novel Bhattacharyya distance-based BCI performance predictor to evaluate the impact of EEG signal variability on BCI performance. Then, novel neural decoding algorithms for classifying imagined movements and speech using time/frequency feature representation techniques and 1D-CNN architectures in Chapters 4 and 5, respectively. Replacing conventional handcrafted feature engineering with the proposed 1D-CNN promotes generic feature learning from EEG signals for inter-subject associative generalized BCIs.

2.2 Assistive and Rehabilitative Technologies

The principles of BCI-based assistive or communication technologies rely on how brain signals are translated into machine commands, for example, using two distinct brain activity patterns to control a switch (on/off) (Cao *et al.*, 2014). These can take active, reactive and passive forms of translation through a BCI. Decoding users' intentions or thoughts directly is an active BCI, such as detecting imagined movements and speech (Willett *et al.*, 2023; Moses *et al.*, 2021; Saha *et al.*, 2021; Willett *et al.*, 2021; Acı *et al.*, 2019; Aricò *et al.*, 2018; Zander *et al.*, 2009). Typically, the decoded movement or speech classes are represented on an electronic device or used for controlling ARTs. However, the success of these applications relies on how accurately the DSP and pattern recognition algorithms can classify brain activities (Lotte *et al.*, 2018; Krusienski *et al.*, 2011; Bashashati *et al.*, 2007; Lotte *et al.*, 2007). Visual and auditory evoked potentials are signals due to external stimulation and define reactive BCI applications. Reactive BCIs are suitable for people who have severe disabilities, for example, individuals in completely locked-in states. Depending on the disability type and severity, the specific signal type is selected to meet individualized user needs. For example, a visually impaired cannot use a visually evoked potential-based BCI but may exploit an auditory cue-based stimulation when their auditory senses are intact. Likewise, visual stimulation is appropriate for users with intact vision. While reactive BCIs are time-synchronized, active ones offer intuitive use for functional autonomy. Finally, a passive BCI is applicable when monitoring users' affective states, such as detecting

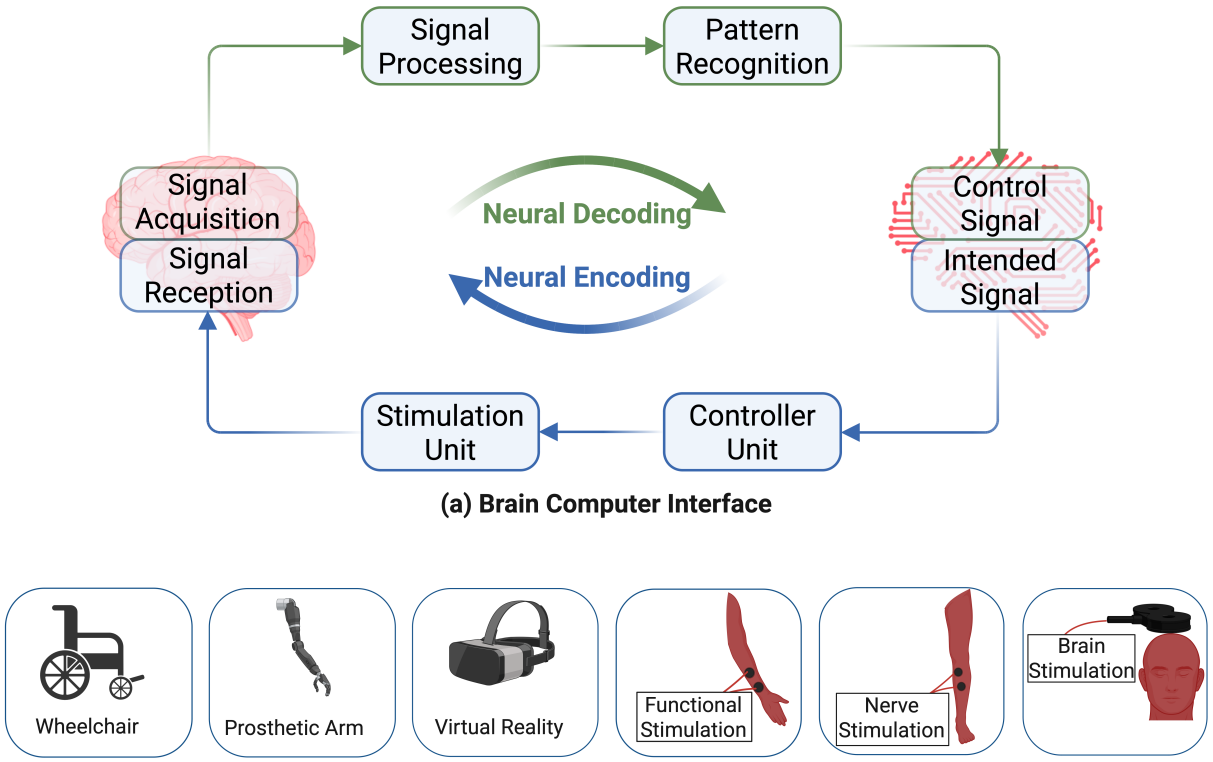

Figure 2.2. The block diagram of a bidirectional brain-computer interface with peripheral assistive and rehabilitative technologies.

drowsiness. There is no one-size-fits-all; nonetheless, BCI-based ARTs require preliminary assessments of users' perspectives of gaining functional autonomy while fulfilling individualized needs (French *et al.*, 2024; Huggins *et al.*, 2015; Nijboer *et al.*, 2014; Huggins *et al.*, 2011).

The principles of rehabilitative BCIs rely on promoting neuroplasticity, which refers to the adaptive behavior of central and peripheral neural networks. Neuroplasticity is a critical ingredient of the motor learning process and is at the center of BCI-driven rehabilitation (Gao *et al.*, 2022; Flesher *et al.*, 2021; Saha and Baumert, 2020; Dobkin, 2007). For upper/lower limb rehabilitation, a BCI can induce neuroplasticity by attaching external rehabilitation devices such as robotic exoskeletons or by encoding neural information via functional/nerve stimulation modalities (Flesher *et al.*, 2021; Mrachacz-Kersting *et al.*, 2021; Soekadar *et al.*, 2016; Mrachacz-Kersting *et al.*, 2016; Orsborn *et al.*, 2014; Dobkin, 2007). Functional electrical stimulation is a stimulation modality that reorganizes the paretic neural networks of an upper or lower limb. A BCI-driven exoskeleton can also assist users in

regaining motor control and functional abilities (Flesher *et al.*, 2021). Studies showed motor imagery-based BCI-driven transcranial magnetic stimulation or transcranial direct current stimulation could restimulate affected brain areas to regain impaired motor control or learn new skills to perform essential daily life tasks post-rehabilitation (Flesher *et al.*, 2021; Yang *et al.*, 2021b; Mrachacz-Kersting *et al.*, 2016; Rao *et al.*, 2014).

2.3 Advances in BCI Technologies

2.3.1 Neuroimaging and neurostimulation modalities

The practical usability of a BCI depends on various factors, primarily the user-centric design of ARTs to fulfil user needs (French *et al.*, 2024; Saha *et al.*, 2021; Martini *et al.*, 2020; Min *et al.*, 2010). Neuroimaging is a critical element of BCIs, which defines their appropriateness across diverse user groups with different types of disabilities (Patrick-Krueger *et al.*, 2024; Edelman *et al.*, 2024; Karikari and Koshechkin, 2023; Moghimi *et al.*, 2013). Typically, no single modality offers the spatial, spectral and temporal resolution for mapping all required complex brain functions, resulting in limited BCI control signals (Saha *et al.*, 2021; Martini *et al.*, 2020; Min *et al.*, 2010). However, recently developed implantable speech BCIs have demonstrated up to 50-word decoding by integrating language models (Willett *et al.*, 2023, 2021; Moses *et al.*, 2021). Electroencephalography (EEG), magnetoencephalography (MEG), electrocorticography (ECoG) and microelectrode array (MEA) capture fine temporal features (*i.e.*, electrical activities). However, the sensors are either sparsely distributed (spatially) or localized within an area of interest only. Functional magnetic resonance imaging (fMRI) records high-resolution spatial features of the brain, but the unmanageable size and slow hemodynamic signals are unsuitable for many real-time applications (Sitaram *et al.*, 2007). As an alternative, functional near-infrared spectroscopy (fNIRS) has lower spatial resolution but is more practical, mainly due to its portability and ease of use (Naseer and Hong, 2015). On the other hand, electric and magnetic field-based neuroimaging techniques, *i.e.*, EEG and MEG, offer better speed and bandwidth. MEG lacks portability and is barely usable outside a specialized setting (Bu *et al.*, 2023).

From a translational perspective, EEG is still one of the most viable neuroimaging modalities due to its portability, easy maintenance and low cost. It does not involve any surgical procedure, like craniotomy for implantable ECoG and MEA. Moreover, it could promote

wearable BCIs using tiny recording setups like ear EEG (Kaongoen *et al.*, 2023). However, EEG signals are highly nonstationary and nonlinear due to time-variant and subject-specific anatomical, psychological, physiological and environmental factors (Saha *et al.*, 2023b, 2021; Saha and Baumert, 2020; Saha *et al.*, 2019b, 2017b,a). Furthermore, EEG signals do not offer the required spatial resolution for mapping localized brain functions because the signals attenuate through the outer brain layers, skull, scalp, skin and hairs (Miinalainen *et al.*, 2019; Cohen, 2017). This issue is somewhat alleviated with implantable ECoG and MEA, which record functionally relevant localized signals (Vansteensel *et al.*, 2016). However, the invasiveness associated with craniotomy diminishes the utility of these neuroimaging modalities, specifically in cases where the long-term trajectory of user benefits and risk factors is unconvinced to the stakeholders. There are less invasive alternatives, such as Stentrode, a new type of neuroimaging introduced by Synchron^{TM} (Oxley *et al.*, 2016). This system does not require craniotomy. Instead, it is computer-guided, with a minimally invasive procedure to place the Stentrode into a blood vessel. Studies have found that the signals are comparable to their more invasive counterparts, such as ECoG and MEA. A limitation of Stentrode is that it records brain signals from only the major blood vessels; thus, a question remains if this technology is scalable to any brain area. Sub-scalp EEG has recently become another viable option for recording finer resolution signals than EEG and requires less maintenance than ECoG and MEA (Duun-Henriksen *et al.*, 2020). Generally, signal quality tends to improve with increasing invasiveness in current neuroimaging modalities of BCI (Figure 2.3).

Neurostimulation modalities externally modulate neural activities in a target brain area to repair paretic functional abilities by rendering neuroplasticity (Flesher *et al.*, 2021; Mrachacz-Kersting *et al.*, 2016). They are critical elements of rehabilitative BCIs, mostly restimulating impacted neural networks in the brain and central and peripheral nervous systems. Studies proposed BCI-based rehabilitation strategies featuring transcranial magnetic stimulation and direct/alternating current stimulation for repairing stroke lesions in the brain (Keser *et al.*, 2022; Van der Groen *et al.*, 2022; Yang *et al.*, 2021b; Antal and Herrmann, 2016). Transcranial random noise stimulation is an alternating current stimulation that generates electrical noise with varying amplitude and frequency. The implantable options include deep brain stimulation and intracortical microstimulation via MEA and Stentrode (Allert *et al.*, 2018; Willett *et al.*, 2023, 2021; Oxley *et al.*, 2016). While the primary applications of neurostimulation techniques are in neurorehabilitation, they can also be used to improve signal quality and users' ability to operate a BCI. Lorach *et al.* developed a rehabilitative BCI featuring epidural nerve stimulation for rectifying spinal cord injury (Lorach *et al.*,

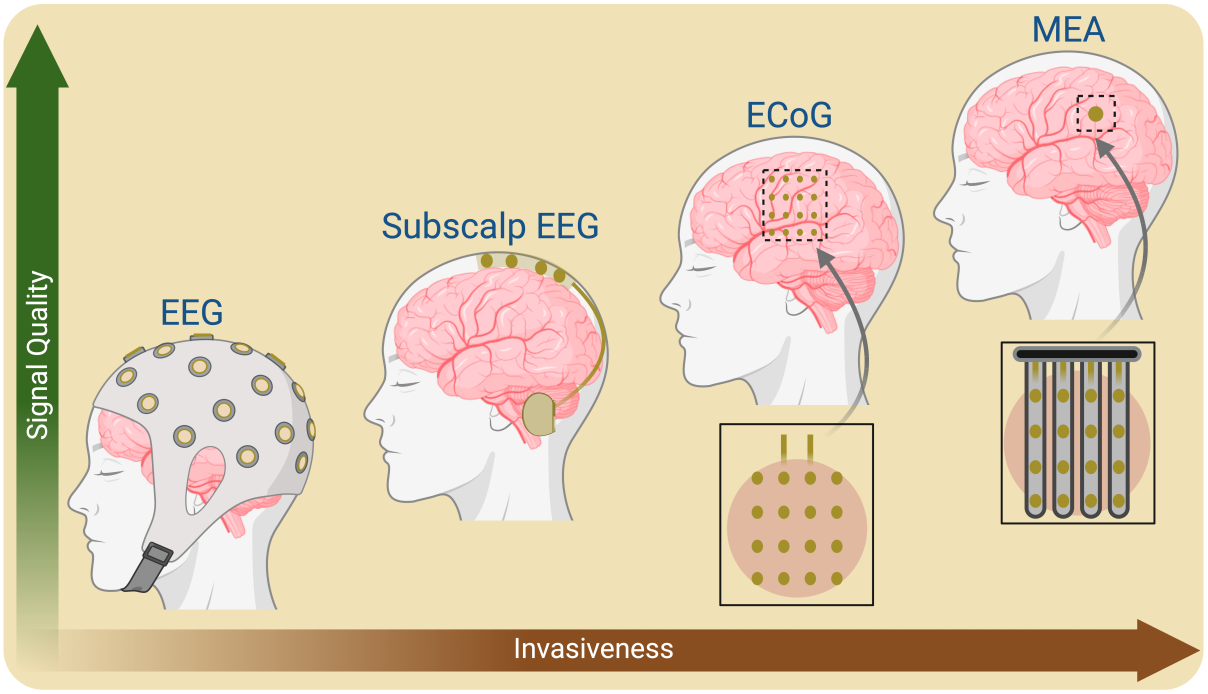

Figure 2.3. A schematic illustration of signal quality and invasiveness of neuroimaging modalities to record brain's electrical activities.

2023). Other studies presented BCI-driven functional electrical stimulation for rehabilitating impaired upper or lower limb functions (Brunner *et al.*, 2024; Jovanovic *et al.*, 2021; Mrachacz-Kersting *et al.*, 2021, 2016).

2.3.2 Neural Signal Processing and Pattern Recognition

The most advanced BCIs utilize the brain's electrical activities recorded through neuroimaging techniques such as EEG, ECoG and MEA (Edelman *et al.*, 2024; Willett *et al.*, 2023, 2021; Moses *et al.*, 2021; Sponheim *et al.*, 2021; Saha *et al.*, 2021; Edelman *et al.*, 2019; Oxley *et al.*, 2016; Rao *et al.*, 2014; LaFleur *et al.*, 2013). Other state-of-the-art modalities include MEG to measure magnetic fields produced by the brain's electrical currents and fNIRS to record the brain's hemodynamic activities (Bu *et al.*, 2023; Naseer and Hong, 2015). These methods output time-domain signals corresponding to the user's intentions or cognitive states. Traditionally, various DSP techniques filter out undesired noises or artefacts from raw neural signals to enhance the detectability of user's intentions or cognitive states (Lotte *et al.*, 2018; Krusienski *et al.*, 2011; Bashashati *et al.*, 2007; Lotte *et al.*,

2.3.2 Neural Signal Processing and Pattern Recognition

2007). Then, handcrafted feature extraction follows a classifier to evaluate the decoding accuracy of a BCI. However, with the recent developments in artificial intelligence-based algorithms, nonlinear activation functions replace handcrafted feature engineering for attributing more generic features associated with users' intentions or cognitive states (Barmpas *et al.*, 2023; Roy *et al.*, 2020; Fahimi *et al.*, 2019). Convolutional neural network (CNN)-based architectures are popular among the state-of-the-art artificial intelligence techniques. The raw neural signals may require preprocessing to enhance signal quality and transformation to represent the signals as compatible with CNN or other architectures (Kamble *et al.*, 2023a,b; García-Salinas *et al.*, 2023). For example, raw neural signals are directly compatible as input to a 1-dimensional CNN or long short-term memory network architecture; however, the time-domain signals are incompatible as input to 2-dimensional CNN architectures. In this case, converting time-domain neural signals into 2-dimensional images through time-frequency analyses such as short-time Fourier transform and wavelet transform is essential.

The time-domain neural signals fluctuate over time and across users due to diversity in anatomical, physiological, psychological and cognitive characteristics (Saha and Baumert, 2020). These inter-session and inter-subject variabilities cause differences in training and testing feature distributions, leading to covariate shifts. For covariate shift adaptation, a BCI typically requires tedious calibration using data from a new target subject or the same subject on a new session. This issue is predominantly more challenging for people with disabilities than healthy users who have limited residual functional communication abilities. Studies proposed various transfer learning strategies in BCI decoding algorithms for covariate shift adaptation (Azab *et al.*, 2019, 2018; Jayaram *et al.*, 2016). Inter-session and inter-subject domain adaptation is an example of transfer learning in BCI. However, most methods still require fewer training samples for calibration when a fully zero-training BCI promotes wide dissemination of this technology across diverse user groups. Inter-subject associative BCI is feasible when subjects share similar brain dynamics (Saha *et al.*, 2023b, 2019b, 2017b,a). Quantifying inter-subject associativity predicts the performance of fully zero-training BCI. From a translational perspective, generalized decoding algorithms can disseminate BCI-based ARTs to a large cohort by minimizing the calibration requirements (Roy *et al.*, 2020; Saha *et al.*, 2017b). Even so, a large cohort of people $(15-30\%)$ encounter BCI deficiency, which refers to BCI system's inability to interpret users' brain signals (Park and Jun, 2024; Bamdadian *et al.*, 2015; Vidaurre and Blankertz, 2010).

2.4 Socioeconomic Outlook of BCI Technologies

2.4.1 Personalized and user-centric design

The clinical distinction of neurological incidents defines disability types and promotes individualization of BCI-based ARTs. While a group of users encounters developmental disabilities like people with cerebral palsy, others experience acquired disabilities due to neurological incidents such as stroke, amyotrophic lateral sclerosis, and spinal cord injury (Metzger *et al.*, 2023; Bekteshi *et al.*, 2023; Hallett *et al.*, 2022; Monforte *et al.*, 2021; Makris *et al.*, 2021; Micera *et al.*, 2020; Goulet *et al.*, 2019; Milekovic *et al.*, 2018; Goldstein and Abrahams, 2013). Due to the diverse types and severities of impairments that reflect individualized user needs (Seghier and Price, 2018; Park *et al.*, 2016), the user-centric and personalized design of BCI-based ARTs can fulfil the requirements of people with disabilities (French *et al.*, 2024; Branco *et al.*, 2023; Saha *et al.*, 2021; Martin *et al.*, 2018). A BCI-controlled stimulation modality can strengthen corticomuscular coherence to induce plasticity in impacted upper/lower limb neural or impaired spinal cord networks (Brunner *et al.*, 2024; Lorach *et al.*, 2023; Jovanovic *et al.*, 2021; Mrachacz-Kersting *et al.*, 2021, 2016). Brain stimulation modalities in conjunction with BCI can augment residual brain functions of users post-neurological incidents (Willett *et al.*, 2023; Keser *et al.*, 2022; Van der Groen *et al.*, 2022; Willett *et al.*, 2021; Yang *et al.*, 2021b; Allert *et al.*, 2018; Antal and Herrmann, 2016; Oxley *et al.*, 2016). A BCI-driven neurofeedback regulates the cortical-subcortical networks and also assists in modulating brain signals for cognitive or functional recovery (Silversmith *et al.*, 2021; Sitaram *et al.*, 2017; Orsborn *et al.*, 2014). Notably, both neurofeedback and stimulation may involve decoding users' intentions from brain activities to operate ARTs.

Other assistive technologies, such as eye-tracking and voice-controlled devices (Sunny *et al.*, 2021; Tran *et al.*, 2020), may offer better assistance for users than BCI-based ARTs. However, there are obvious circumstances when BCI outperforms other existing ARTs. A BCI typically exploits residual brain functions explicitly without any peripheral muscular input, and this is critical for people with severe disabilities post-neurological incidents (Willett *et al.*, 2023; Moses *et al.*, 2021). Users with limited or no functional abilities may not operate an eye-tracking or voice-controlled device. By utilizing residual brain functions, BCI-based ARTs can provide effective rehabilitation interventions or alternative communication links for users to interact with their surroundings. Thus, the appropriateness of BCI-based ARTs highly depends on individual circumstances. Nonetheless, the rapid evolution of BCI

technologies in recent years makes them suitable for manifold applications for diverse user cohorts (Edelman *et al.*, 2024; Karikari and Koshechkin, 2023; Lopez-Bernal *et al.*, 2022; Karlsson *et al.*, 2022; Saha *et al.*, 2021).

2.4.2 Implantation lifespan and brain development

The appropriateness of a neuroimaging modality requires careful consideration, weighing up risks and benefits (Rubin *et al.*, 2023; Leuthardt *et al.*, 2021; Sierra-Mercado *et al.*, 2019), especially in cases of implantable BCI-based ARTs for people of different ages with diverse disabilities. Current implantable electrodes are increasingly biocompatible, provide good-quality signals for up to several years, and hold a promise to operate a BCI successfully. However, findings show that the neural signal quality deteriorates over time (Ferguson *et al.*, 2019), and reimplanting sensors is a complex task due to surgical risk factors (Sponheim *et al.*, 2021; Viana *et al.*, 2021; Woeppel *et al.*, 2021; Sierra-Mercado *et al.*, 2019). The necessity of reimplantation and post-operative maintenance are critical aspects of an implantable BCIs over the lifespan of a user. An implantable BCI is often permanent, and the device is kept inside the brain due to anatomical changes in complex brain structure and risk factors associated with surgical extraction before potential reimplantation (Fry *et al.*, 2023). A question remains whether the current implantable BCI can offer long-term use while minimizing the chances of reimplantation.

In pediatric BCI, where the benefits of early implantation might take advantage of neurodevelopment and plasticity, the changing environment around implanted sensors over the lifespan is another essential aspect. Around $90-95\%$ of human brain growth occurs by the age of $5-7$ years, although cognitive experiences evolve over the lifetime (Zhou *et al.*, 2024; Bethlehem *et al.*, 2022; Hedman *et al.*, 2012; Brown and Jernigan, 2012; Peters, 2006) (Figure 2.4). Non-implantable neuroimaging, specifically EEG, offers BCI-based ARTs for pediatric users living with movement and speech disabilities (Kelly *et al.*, 2023; Jadavji *et al.*, 2022). However, there is a lack of studies to substantiate the potential use of implantable BCI for pediatric users. The human brain undergoes anatomical transformations during its lifespan; for example, it expands and shrinks in the early and late ages (Bethlehem *et al.*, 2022). Moreover, electrode displacements post-implantation may contribute to increased chances of reimplantation (Göransson *et al.*, 2021; Morishita *et al.*, 2017; Lumsden *et al.*, 2015). As neural technologies advance and growing evidences are accessible for researchers and clinicians, the BCI-based ARTs may soon evolve in children

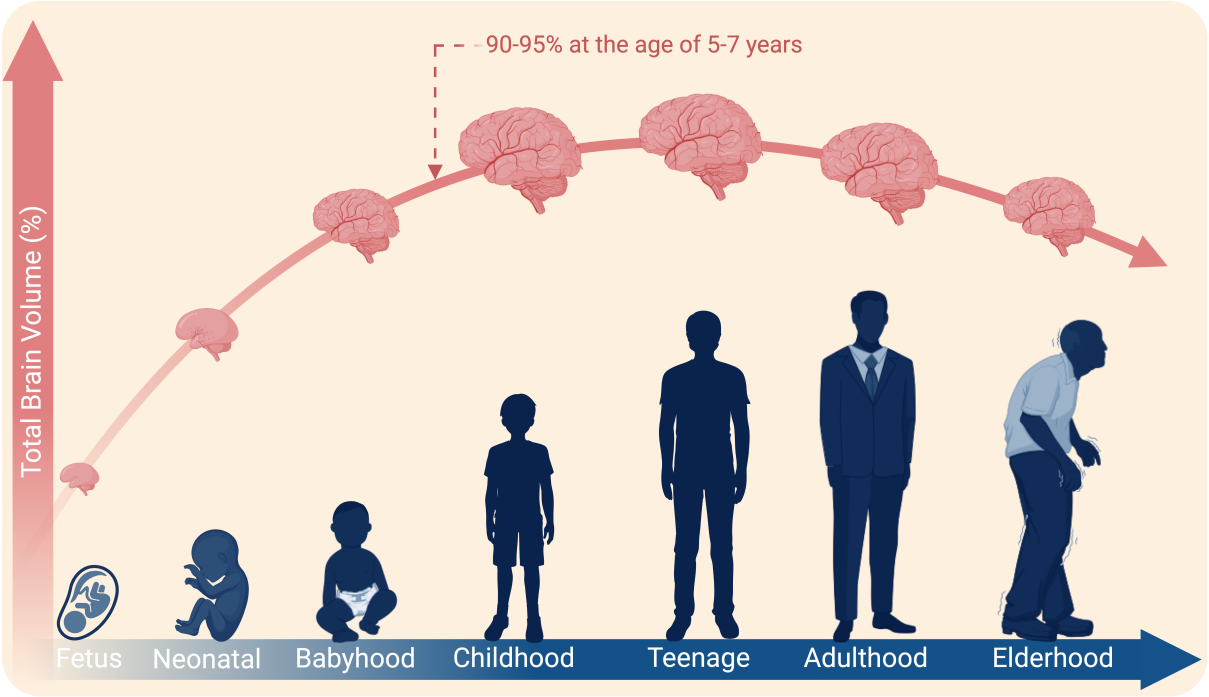

Figure 2.4. A schematic timeline illustrating changes in total brain volume: $90 - 95\%$ growth occurs within the age of $5 - 7$ years.

with severe disabilities after careful technical and ethical considerations (Bergeron *et al.*, 2023).

2.4.3 User perspectives and socioeconomic challenges

BCI-based ARTs can assist people with disabilities in accessing mainstream socioeconomic life, where they can contribute to the ethical and economic dynamics of society. Regardless of scientific breakthroughs, users' perspectives on using BCI-based ARTs and their safety are critical (Patrick-Krueger *et al.*, 2024; Soldado-Magraner *et al.*, 2024; Bergeron *et al.*, 2023; Saha *et al.*, 2021; Naufel and Klein, 2020; Sample *et al.*, 2019; Klein and Ojemann, 2016; Nijboer *et al.*, 2013). All stakeholders must ensure the ethical use of BCI. Informed consent from the users or their caregivers is the precursor to using a BCI. However, there is still scope for discussion to acquire consent after adequately making the user aware of the risk factors and the expected benefits. Some users with disabilities may experience cognitive or communication difficulties; thus, ensuring they are fully informed about risks and benefits may be challenging (Willett *et al.*, 2023, 2021; Moses *et al.*, 2021; Vansteensel *et al.*, 2016). Consent is tricky in children (Bergeron *et al.*, 2023); for example, their perspective of using a BCI may change by the time they reach adulthood. They may question their parent's

or guardian's decision on whether or not to implant a BCI in their early years. Studies underlined the importance of engaging BCI stakeholders considering ethics policies to ensure transparent communication with users before obtaining consent (Patrick-Krueger *et al.*, 2024; Soldado-Magraner *et al.*, 2024; Bergeron *et al.*, 2023; Saha *et al.*, 2021; Naufel and Klein, 2020; Sample *et al.*, 2019).

Standardizing BCI-based ARTs and their lawful utilization are crucial for positive societal change (Patrick-Krueger *et al.*, 2024; Soldado-Magraner *et al.*, 2024; Bergeron *et al.*, 2023; Chandler *et al.*, 2022). BCI is an emerging field, and authorities should act promptly to set up regulations that include all stakeholders' opinions due to the fast evolution of BCI-based ARTs in diverse areas. The Brain/Neural Computer Interaction Horizon 2020 project defined six primary objectives of BCI: (1) restore (*e.g.*, unlocking the residual ability of completely locked-in), (2) replace (*e.g.*, BCI-based ARTs), (3) enhance (*e.g.*, improved user experience in video games), (4) supplement (*e.g.*, interactive virtual/augmented/mixed reality glasses), (5) improve (*e.g.*, upper/lower limb rehabilitation post stroke), and (6) research tools (*e.g.*, decoding brain activity with real-time neurofeedback) (Brunner *et al.*, 2015). The development of regulatory guidelines may address the socioeconomic concerns and reflect the defined objectives of BCIs in these application areas. Patrick-Krueger *et al.* discussed the clinical perspectives of implantable BCIs and the importance of regulatory approvals after clinical trials of the state-of-the-art technologies (Patrick-Krueger *et al.*, 2024). A question remains whether introducing BCI guidelines could limit their use after carefully evaluating the risks versus benefits and socioeconomic impact trajectories (Patrick-Krueger *et al.*, 2024; Soldado-Magraner *et al.*, 2024; Coin and Dubljević, 2023; Sample *et al.*, 2019).

Emerging cybersecurity measures are also essential translational elements of BCI-based ARTs. Confidentiality, integrity and availability are critical cybersecurity components to ensure ethical BCI use (Liv and Greenbaum, 2023; Bernal *et al.*, 2023). Confidentiality prevents unauthorized access to sensitive neural data, integrity ensures data precision, and availability maintains the infrastructure to provide secured data access to authorized stakeholders (Goodman and Rowland, 2021). Illicit access to signature neural activities mapped to passwords or visual and auditory stimulus and their manipulation can damage an individual's social presence (Armengol-Urpi *et al.*, 2023; Ienca and Haselager, 2016). Wireless BCI systems may be hackable, so adequate cybersecurity measures are essential (Bernal *et al.*, 2023; Ajrawi *et al.*, 2021; Ienca and Haselager, 2016). It is particularly hazardous when a BCI can potentially alter functional neural circuitry in the short and long term, inducing threats to users' fundamental characteristics such as personalities, memories and

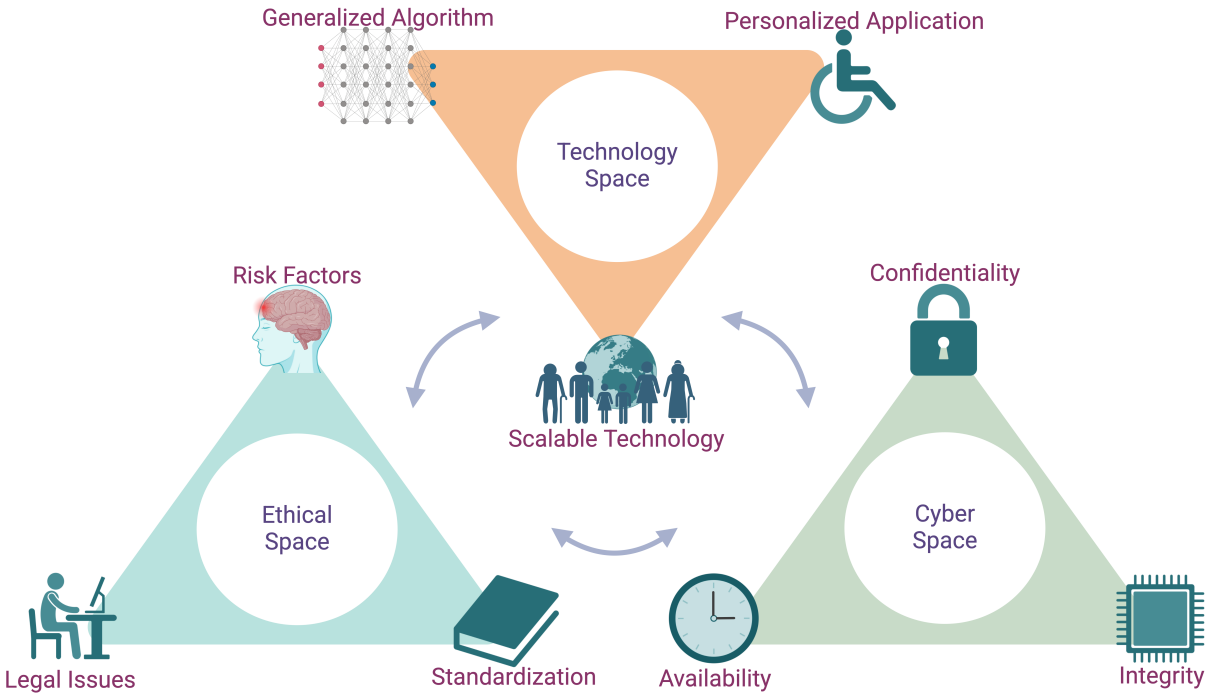

Figure 2.5. The translational outlook of a BCI and their key components.

emotions (Steinert and Friedrich, 2020; Ienca and Haselager, 2016). Altering human cognitive capacity is challenging because it is unclear whether mental changes are reversible (Dunlap *et al.*, 2020; Schmitz-Luhn *et al.*, 2012). Generally, exploiting neural data can modify the expected BCI outcome for unethical or unsafe control of ARTs. Integrated cryptographic encryption and access control into BCI may offer a more secure option, fulfilling BCI cybersecurity requirements. Figure 2.5 illustrates the translational components of BCIs, from technology standardization to ethics policies, algorithm development and essential cybersecurity measures that promote BCIs as promising ARTs for people with disabilities, contributing to their widespread dissemination.

2.5 Conclusion

Advancements in state-of-the-art neuroimaging and artificial intelligence technologies are expanding BCI-based ARTs for people with disabilities. BCI can offer unconventional communication links between the brain and ARTs, even when their conventional alternatives are impractical. A generalizable DSP and pattern recognition algorithm is a precursor to widening accessibility to this technology for mass. Meanwhile, personalizing BCI applications based on user needs is inevitable. Due to the sensitivity of neural data and the inherent

personal information they potentially preserve, a set of guidelines for the lawful utilization of BCI technology is critical while taking all stakeholders into the decision-making process.

Chapter Context:

This chapter presented a contemporary literature review on BCI-based ARTs for people with disabilities, highlighting the key translational elements of state-of-the-art BCIs. While personalization of BCI applications fulfills individualized user needs, generalized DSP and pattern recognition algorithms offer scalability for widespread dissemination across diverse and large user groups. As the aim of this thesis, the following three chapters present novel DSP and pattern recognition algorithms for neural decoding of movement and speech and how they contribute to the generalization of BCIs.

The next chapter demonstrates a novel performance predictor for intra- and inter-subject BCIs, classifying two MI tasks using a neural decoding framework featuring CSP, PCA and LDA. Inter-subject BCI performance predictor promotes the concept of inter-subject associative BCI, a step toward generalized neural decoding algorithms.

Can Inter-Subject Associativity Predict Data-Driven BCI Performance?

3

INTRA- and inter-subject variabilities cause covariate shifts in training and testing feature spaces, resulting in low sensorimotor (SMR) brain-computer interface (BCI) performance for practical implementation. Studies involving data-driven transfer learning strategies demonstrated improving BCI performance by covariate shift adaptation. The aim of this study is to illustrate if inter-subject associativity (*e.g.*, subjects having similar SMR brain dynamics) can predict inter-subject classification performance. A BCI classification pipeline with a common spatial pattern (CSP), principal component analysis (PCA) and linear discriminant analysis (LDA) was implemented for performance evaluation. Both intra- and inter-subject BCI were evaluated in $5-$fold cross-validation settings. Furthermore, a Bhattacharyya distance-based covariate shift score (CSS) was proposed for assessing the difference between training and testing feature distributions. Pearson correlation analysis was performed to draw the relationship between BCI performance and CSS. Intra-subject classification accuracies were significantly and negatively correlated with CSS ($r = -0.94$, $p < 0.05$). For the inter-subject experiment, BCI classification accuracies were also highly and negatively associated with CSS ($r = -0.61$, $p < 0.05$). However, this data-driven BCI evaluation framework does not necessarily manifest inter-subject associativity in BCI performance, requiring further investigations for a conclusion. If it predicts BCI performance successfully, inter-subject associativity could reduce time-consuming and annoying subject-specific calibration for the users.

The contents of this chapter was published in 2023 45th Annual International Conference of the IEEE Engineering in Medicine & Biology Society (EMBC) as:

Saha, S., Baumert, M. and McEwan, A., 2023, July. Can Inter-Subject Associativity Predict Data-Driven BCI Performance?. In *2023 45th Annual International Conference of the IEEE Engineering in Medicine & Biology Society (EMBC)* (pp. 1-4). IEEE.

Author Contributions: SS conceptualized the Bhattacharyya distance-based performance predictor for intra- and inter-subject BCIs and experimental settings, implemented MATLAB codes, generated results, produced figures, wrote the original manuscript, and edited the final version. SS, MB, and AM participated in interpreting the results. MB and AM reviewed the original draft and provided feedback. All authors read and approved the final version.

3.1 Introduction

A brain computer interface (BCI) is a direct interface between the brain and a computer or other peripheral devices (Saha *et al.*, 2021). It provides assistive and rehabilitative technologies (ARTs), benefitting people with functional disabilities. Motor imagery (MI)-based BCI can intuitively control ARTs (Saha *et al.*, 2021). Nevertheless, MI-based BCI performance varies over time and across subjects (Saha and Baumert, 2020; Sannelli *et al.*, 2019; Saha *et al.*, 2017b, 2019b, 2017a; Wei and Ding, 2023). Intrinsic intra- and inter-subject variabilities in EEG dynamics promote covariate shift, resulting in poor reproducibility of BCI performance on different sessions and individuals.

Studies addressed the covariate shift primarily by data-driven transfer learning strategies (Chen *et al.*, 2022; Jayaram *et al.*, 2016; Azab *et al.*, 2019; He and Wu, 2019; Wei and Ding, 2023). Other studies proposed BCI performance predictors for potentially generalizing the EEG signal processing pipeline (Benaroch *et al.*, 2022; Kwon *et al.*, 2020; Rimbert *et al.*, 2019; Vidaurre *et al.*, 2020; Lee *et al.*, 2020; Darvishi *et al.*, 2018). Saha *et al.* proposed *inter-subject associativity* as a subject-independent BCI performance predictor (Saha and Baumert, 2020; Saha *et al.*, 2017b, 2019b, 2017a). Data-driven covariate shift adaptation strategies include widely used domain adaptation techniques (Chen *et al.*, 2022; Jayaram *et al.*, 2016; Azab *et al.*, 2019; He and Wu, 2019; Wei and Ding, 2023). However, previous studies proposed that (*inter-subject associative*) subjects having similar brain dynamics could complement inter-subject information transfer, resulting in good inter-subject BCI performance (Saha and Baumert, 2020; Sannelli *et al.*, 2019; Saha *et al.*, 2019b, 2017a,b; Wronkiewicz *et al.*, 2015; Kang and Choi, 2014; Kang *et al.*, 2009).

This study aims to quantify covariate shift for intra- and inter-subject BCI and to investigate if our proposed Bhattacharrya distance-based BCI performance predictor manifests inter-subject associativity from the brain dynamics perspective. Inter-subject associativity refers to task-related neural substrates contributing to EEG features, which are inter-subject generalizable for a BCI with no or minimum calibration requirement (Wei and Ding, 2023; Kwak *et al.*, 2023; Saha *et al.*, 2023b; Benaroch *et al.*, 2022; Wang *et al.*, 2021; Kwon *et al.*, 2020; Rimbert *et al.*, 2019; Saha *et al.*, 2017b; Wronkiewicz *et al.*, 2015; Kang and Choi, 2014; Kang *et al.*, 2009). The proposed predictor quantifies the distance between training and testing (inter-subject) feature spaces, thus evaluating intra- and inter-subject variabilities of EEG signals. A fully zero-training BCI is challenging due to intra- and inter-subject EEG signal variabilities; however, identifying inter-subject associative subjects complements transfer learning strategies in BCI.

3.2 Materials and Methods

3.2.1 About the dataset

The dataset IVa from *BCI Competition III*[1] was used to evaluate intra- and inter-subject classification pipeline. The EEG signals were recorded from five healthy individuals in single-trial MI-based BCI paradigm. Subjects were instructed to perform any of two MI tasks (*i.e.*, right hand (RH) and right foot (RF)) while sitting comfortably in an armchair. One hundred eighteen electrodes (Extended $10/20$ System) were used to record raw EEG signals. The sampling rate was 1 KHz but later downsampled to 100 Hz. The dataset consists of 280 trials for each subject, and the ratio between the RH and RF is $1:1$. Each trial has a duration of 3.5 s, but we selected 2.5 s of EEG signals, 0.5 s after the visual cue.

3.2.2 Intra- and Inter-Subject BCI

Figure 3.1 illustrates the block diagram of the proposed BCI classification pipeline. A total of 280 trials were used for both intra- and inter-subject experiments. EEG signals were bandpass-filtered using a 4^{th} order Butterworth filter with corner frequencies of 4 Hz and 32 Hz, followed by the common spatial pattern (CSP) technique. The CSP algorithm is described in the following section. The algorithm projects EEG channels such that the first channel attributes the most separable feature for a class, and the last channel provides the most separable feature for another class. Class-specific importance of the channels decreases as we move to the central channel, contributing insignificance to the classification performance. Thus, the first three channels for RH and the last three channels for RF were selected for feature extraction. Then, the variances from the selected six channels were calculated as features following the principal component analysis (PCA) to reduce the $6-$dimensional feature space to a $2-$dimensional feature space. Then, the $2-$dimensional feature spaces were investigated for intra- and inter-subject covariate shifts. These $2-$dimensional PCA-extracted features were also used to evaluate the proposed BCI performance and calculate the covariate shift score (CSS).

The experiment was conducted in a $5-$fold cross-validation format, where 280 trials were divided into five equal subsets in the order they appear in the dataset. For intra-subject BCI, each of the five subsets was used as testing data, and the remaining four subsets were used as training data for the CSP-based algorithm. The subsets were shuffled until each of the

[1] http://www.bbci.de/competition/iii/desc_IVa.html

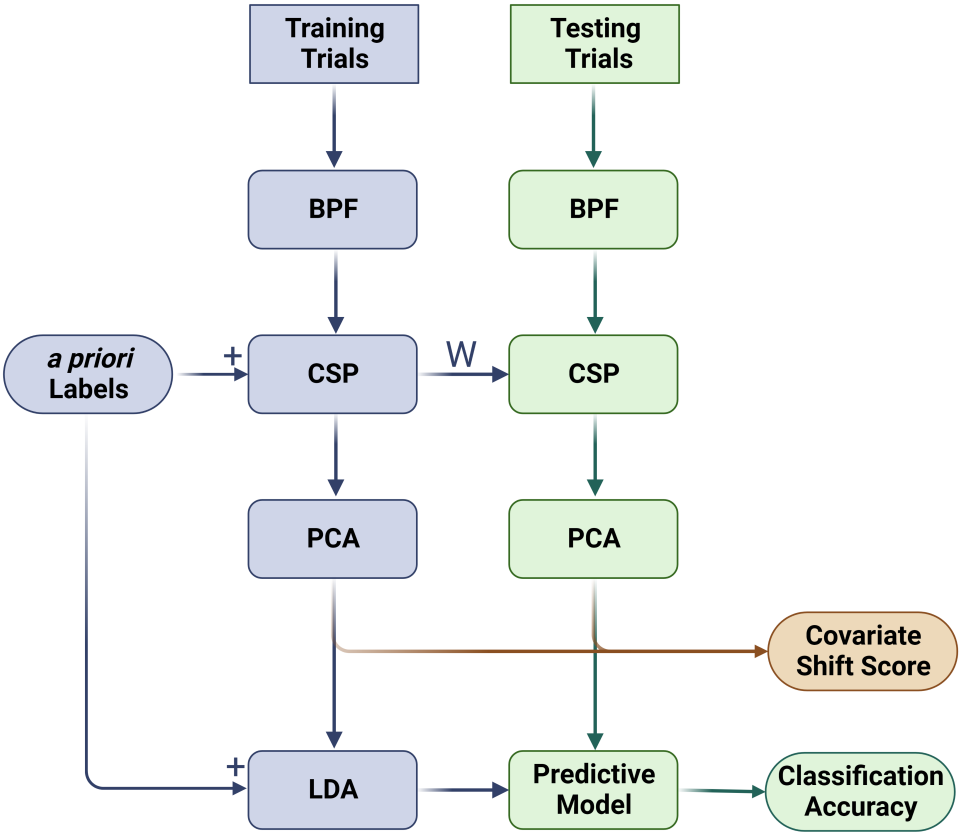

Figure 3.1. The block diagram of the proposed BCI signal processing pipeline.

five subsets was used as the testing data. All 280 trials were taken from a single subject for the intra-subject experiment. Mean$\pm$SD (Standard Deviation) was calculated over five runs. For the inter-subject experiment, two subjects were chosen for training and testing, respectively, but the available 280 trials of each subject were divided into five subsets. Any four subsets from the first subject were used to train, and any one subset from the other subject was used to test the BCI, keeping it analogous to the intra-subject experimentation. Thus, a total of 25 BCI runs result from inter-subject BCI. Mean$\pm$SD was approximated over 25 runs.

A linear discriminant analysis (LDA) classifier was used to evaluate intra- and inter-subject BCI classification accuracy. Then, the proposed CSS was approximated as the distance between $2-$dimensional training and testing feature spaces using Bhattacharyya distance as described in 3.2.4. The Pearson correlation analysis was performed to determine the BCI performance (Mean values) association with CSS for intra- and inter-subject BCI, respectively.

3.2.3 Common Spatial Pattern CSP

CSP approximates a transformation of multi-channel EEG signals for maximizing the difference between two classes. The transformed EEG signals are estimated by calculating sample-based covariance matrices on the training trials. Assume that an EEG trial is represented by E and of size $N \times P$, where N is the number of channels and P is the number of data samples per trial. In the CSP algorithm, the sample-based covariance matrix of a trial E is approximated after normalizing it with the total variance as follows

$$S_i = \frac{E_i E_i^{'}}{trace(E_i E_i^{'})}, \qquad S_j = \frac{E_j E_j^{'}}{trace(E_j E_j^{'})}. \tag{3.1}$$

Where $^{'}$ denotes the transpose of a matrix and i and j represent two classes, respectively. The composite spatial covariance matrix can be factorized using singular value decomposition as,

$$S = \overline{S_i} + \overline{S_j} = U_0 \Lambda U_0^{'}, \tag{3.2}$$

where $\overline{S_i}$ and $\overline{S_j}$ indicate the average of covariance matrices approximated from the training trials for class i and class j, respectively. U_0 and Λ symbolize the matrix of eigenvectors and the diagonal matrix of eigenvalues, respectively. Then, the whitening transformation matrix is,

$$Q = \sqrt{\Lambda^{-1}} U_0^{'}, \tag{3.3}$$

which transforms the average covariance matrices as follows:

$$R_i = Q S_i Q^{'}, \qquad R_j = Q S_j Q^{'}. \tag{3.4}$$

Notably, R_i and R_j share common eigenvectors, *i.e.*, if $R_i = U \Lambda_i U^{'}$, then $R_j = U \Lambda_j U^{'}$ and $\Lambda_i + \Lambda_j = I$. I is the identity matrix. Finally, the projection matrix is depicted as,

$$W = U^{'} Q. \tag{3.5}$$

Then, the projected EEG signals can be determined as

$$Z = W E. \tag{3.6}$$

The columns of W^{-1} are common spatial patterns. More details of CSP algorithm can be found in (Lu *et al.*, 2010; Ramoser *et al.*, 2000).

3.2.4 Covariate Shift Score Calculation

In this study, only six CSP channels were selected to calculate the variance from each channel, followed by applying PCA to reduce the feature dimension to $2-$dimensional. The Bhattacharyya distance was used to calculate class-specific distances between the training and testing feature distributions. Let's assume P_{tr} and P_{te} are two probability distributions for the $2-$dimensional training and testing features extracted from PCA. Then, the Bhattacharyya distance is defined as follows:

$$D_B = -\ln(BC(P_{tr}, P_{te})), \tag{3.7}$$

where, BC refers to the Bhattacharyya coefficient and can be calculated as

$$BC(P_{tr}, P_{te}) = \sum_{x \in X} \sqrt{P_{tr}(x) P_{te}(x)}. \tag{3.8}$$

Here, X is the domain of P_{tr} and P_{te}.

Class-specific distance between $2-$dimensional training and testing features, *i.e.*, P_{tr} and P_{te}, was calculated across classes and averaged over the 5 and 25 runs for cross-validation settings, respectively, and to get intra- and inter-subject CSS. Thus, CSS was estimated as a single value for each subject (intra-subject) or each subject pair (inter-subject).

3.3 Results And Discussion

The highest classification accuracy $(\%)$ achieved for subject *al* was 91.79 ± 5.59, and the lowest classification accuracy achieved for subject *av* was 58.93 ± 8.38 for intra-subject BCI. The CSS for the subjects *al* and *av* were 0.84 and 1.39, respectively. Increasing CSS is inversely associated with classification accuracy, as shown in Figure 3.2. Pearson correlation analysis revealed a strong correlation between CSS and classification accuracy ($r = -0.94$, $p < 0.05$). Previous studies also reported the poorest BCI performance using CSP for subject *av* (Saha *et al.*, 2016; Lu *et al.*, 2010).

Figure 3.3 illustrates the inter-subject BCI classification accuracies and CSS values. Interestingly, the inter-subject classification accuracies were mostly asymmetric, *i.e.*, altering training and testing subjects within a subject pair dramatically caused poorer performance (Saha *et al.*, 2017a, 2019b). For example, the classification accuracy for the subject pair *aa - al* was 84.79 ± 17.00; however, altering the training and testing subjects demonstrated

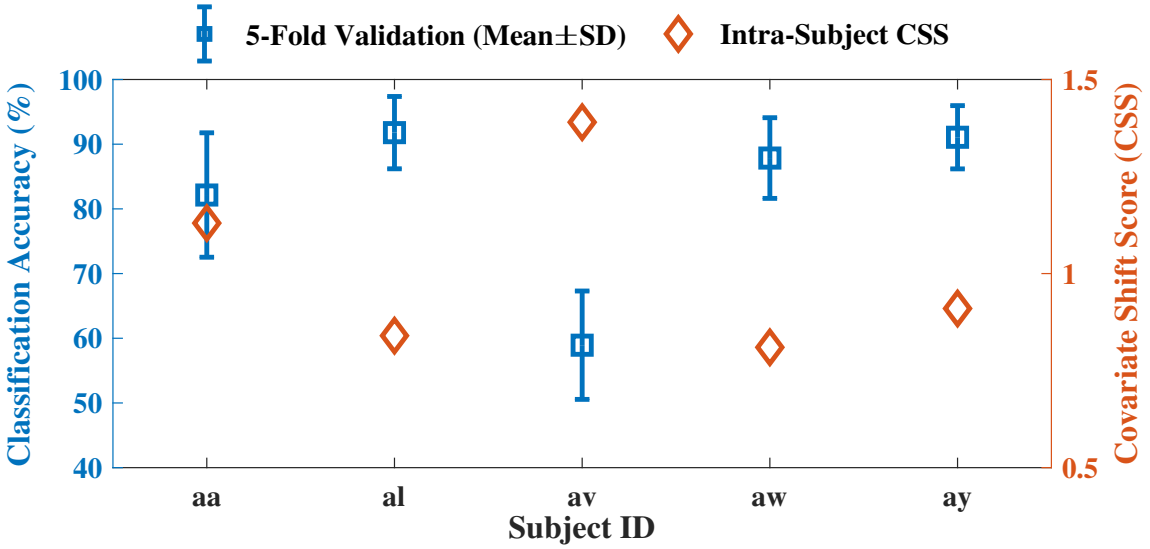

Figure 3.2. Illustration of intra-subject BCI performance metrics.

relatively lower classification accuracy (59.93 ± 10.64). On the contrary, the classification accuracies were 86.71 ± 9.45 and 85.57 ± 15.57 for the subject pairs *al* - *ay* and *ay* - *al*, respectively. Previous studies supported the asymmetric nature of the proposed inter-subject BCI performance (Saha *et al.*, 2019b, 2017b,a). Figure 3.4 illustrates training and testing feature spaces remaining closer and classifier boundary for the subject pair *aa* - *ay* when the classification reaches one of the maxima at 98.21 out of 25 runs.

For the inter-subject BCI, the highest classification accuracy for subject pair *al* - *ay* was 86.71 ± 9.45, and a total of six subject pairs showed good classification accuracies (Mean $> 80\%$). As comparable to the intra-subject BCI, inter-subject CSS values were also negatively correlated with the classification accuracies. Pearson correlation analysis suggested a significant correlation between the BCI performance metrics ($r = -0.61$, $p < 0.05$). Figure 3.5 shows the correlation scatter plot for the inter-subject classification accuracy and CSS.

Studies investigated potential sources of EEG signal variation over time and across subjects (Cueva *et al.*, 2025; Saha *et al.*, 2023b; Saha and Baumert, 2020; Saha *et al.*, 2019b, 2017b; Wronkiewicz *et al.*, 2015; Kasahara *et al.*, 2015; Kang and Choi, 2014; Hammer *et al.*, 2012; Kang *et al.*, 2009). They identified a long list of time-variant and subject-specific neurological, neuroanatomical and physiological characteristics contributing to nonstationary EEG signals, causing covariate shifts in training and testing feature distributions and, thus, impacting BCI performance. The Bhattacharyya distance-based predictor quantifies the intra- and inter-subject variabilities correlating MI classification performance. The aim is

to eliminate the requirement of any testing trials for a fully-zero training BCI. However, the Bhattacharyya distance-based predictor requires training and testing samples for calculation. It is an impractical solution as testing trials are unseen data and are expected only to be used to evaluate the BCI without any prior calculations.

The proposed CSS is a Bhattacharrya distance-based and simple BCI performance predictor. Although a strong correlation has been found between CSS and classification accuracies, interpreting the intra- and inter-subject CSS may require further investigations. The proposed BCI is based on data-driven CSP and PCA methods, and data-driven strategies are prone to overfitting leading to covariate shift between the training and testing feature spaces (Saha and Baumert, 2020; Jayaram *et al.*, 2016; Sannelli *et al.*, 2016). Specifically, the asymmetric nature of inter-subject BCI performance implicates CSS as a data-driven BCI performance predictor. A question remains: does CSS measure *inter-subject associativity*? Results indicate CSS is just a data-driven measure, not demonstrating *inter-subject*

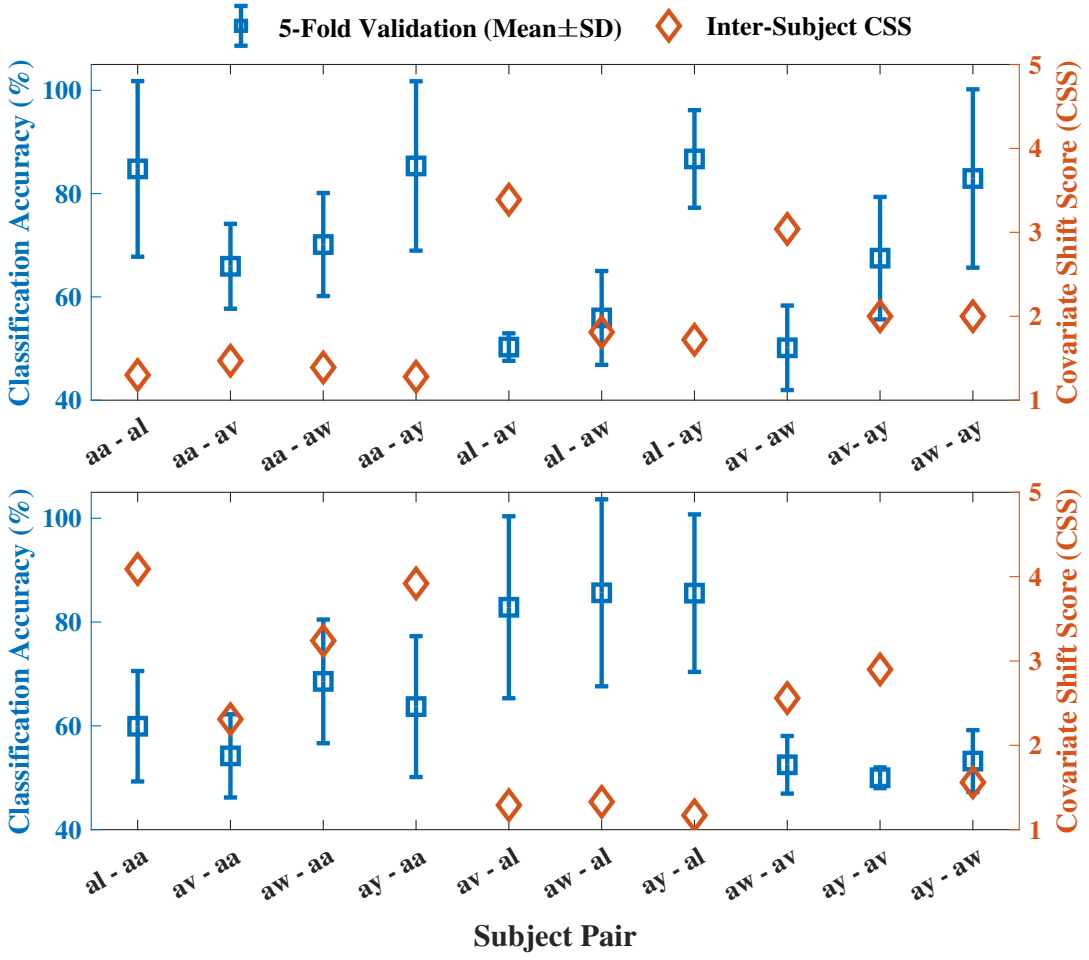

Figure 3.3. Illustration of inter-subject BCI performance metrics.

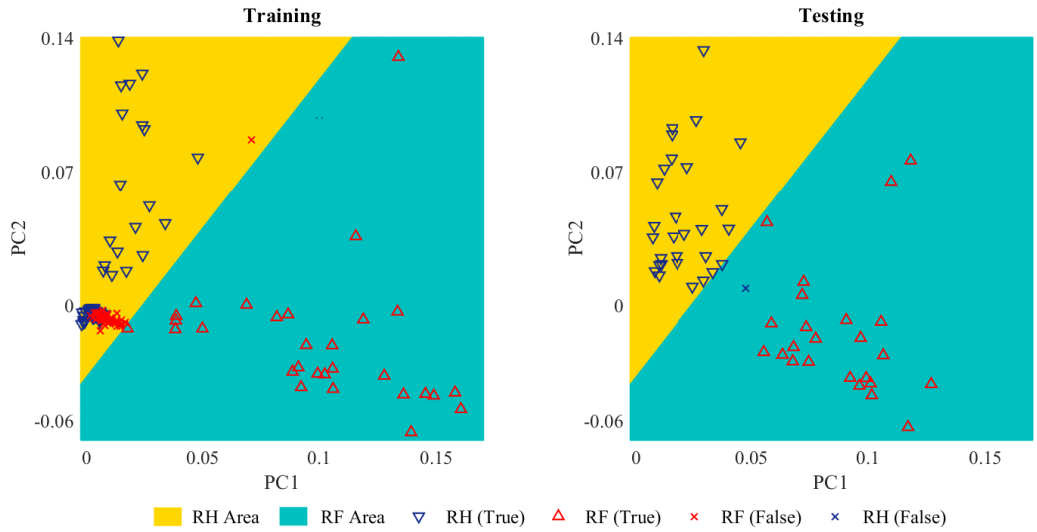

Figure 3.4. Visualizing training and testing feature spaces and classifier boundary for subject pair *aa* - *ay*, when the classification accuracy was 98.21% [PC: principal component; RH: right hand; RF: right foot].

associativity in the true sense. It could be anticipated that *inter-subject associativity* to be the manifestation of EEG dynamics (*i.e.*, the reflection of SMR brain dynamics). It would offer a more generalized predictor for BCI performance irrespective of changing the training and testing subjects (Saha and Baumert, 2020; Benaroch *et al.*, 2022; Lee *et al.*, 2020; Sannelli *et al.*, 2019; Vidaurre *et al.*, 2020).

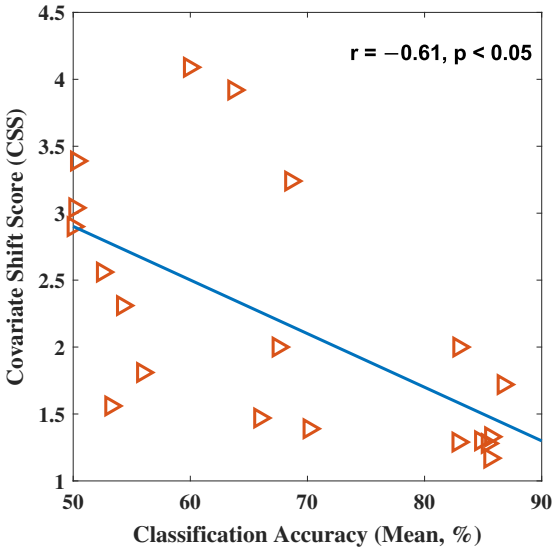

Figure 3.5. Correlation scatter plot of the inter-subject BCI performance metrics.

3.4 Conclusion

If it predicts BCI performance successfully, inter-subject associativity could reduce time-consuming and annoying subject-specific calibration for the users. The proposed inter-subject BCI should be extended to a larger dataset to investigate *inter-subject associativity* further that predicts BCI performance independent of data-driven techniques, notwithstanding the order of training and testing subjects. In addition, more extensive experiments may quantify *inter-subject associativity* in a pooled-subject context featuring more than two subjects having associative brain dynamics; however, this study was restricted to pairwise quantification.

Chapter Context:

This chapter presented a novel performance predictor for intra- and inter-subject BCI performance, classifying two MI tasks using a neural decoding framework featuring CSP, PCA and LDA. Inter-subject BCI performance predictor promotes the concept of inter-subject associative BCI by utilizing *a priori* information on across-subject differences in EEG features in transfer learning strategies, a step toward generalized neural decoding algorithms. Although impractical because all training and testing trials were used to calculate the CSS, the proposed predictor quantifies intra- and inter-subject variabilities, demonstrating their impact on BCI performance.

Training and testing feature spaces characterized by conventional handcrafted feature engineering, often revealing inter-subject differences, causing covariate shifts and hindering the development of generalized DSP and pattern recognition algorithms for BCIs. The next chapter proposes an AI-based feature learning for classifying MI tasks, replacing handcrafted feature extraction. The classification pipeline demonstrates raw EEG signals converted into time-domain EEG signals, frequency-embedded PSD and CPSD sequences for training 1D-CNN. The proposed method was benchmarked with the CSP-based classifiers with and without PCA presented in Chapter 3 and demonstrated the capabilities of 1D-CNN to learn features by nonlinear activation functions while optimizing BCI performance.

Time/Frequency EEG Sequence Learning for Sensorimotor BCI

4

THIS chapter proposed a motor imagery (MI) classification pipeline featuring a $1-$dimensional convolutional neural network (1D-CNN) with different time/frequency feature representation techniques. The objective was to classify right hand (RH) versus right foot (RF) MI tasks in both intra- and inter-subject (pairwise and pooled) BCI settings using a 1D-CNN architecture trained on time-domain bandpass-filtered electroencephalography (EEG) signals, frequency-embedded power spectral density (PSD) and cross-power spectral density (CPSD) sequences. The EEG signals were bandpass-filtered with 4 Hz and 32 Hz cut-off frequencies, and PSD/CPSD sequences were estimated in the same frequency range. Thus, the number of input channels for 1D-CNN was N, N or $N \times N$ for EEG signals, PSD or CPSD sequences. We used dataset IVa from BCI Competition III in $5-$fold cross-validation settings to evaluate intra-subject, inter-subject (pairwise) and inter-subject (pooled) BCI classification accuracies. We compared the performance of the proposed methods with classification algorithms featuring common spatial patterns (CSP) for benchmarking. The best overall classification accuracies ($\%$) for intra-subject, inter-subject (pairwise) and inter-subject (pooled) BCIs were 86.57 ± 11.69, 70.80 ± 9.21 and 76.61 ± 12.37 using 1D-CNN with time-domain EEG signals. The average classification accuracies using 1D-CNN with frequency-embedded PSD sequences were 82.57 ± 10.20, 69.32 ± 7.46 and 71.32 ± 7.96 for intra-subject, inter-subject (pairwise) and inter-subject (pooled) BCIs. The proposed time/frequency feature representation techniques with 1D-CNN outperformed CSP-based algorithms (p-value < 0.05).

The contents of this chapter have been submitted for publication as:

Saha, S., Baumert, M. and McEwan, A., Time-Domain Versus Frequency-Embedded EEG Sequences for Sensorimotor BCI Using 1D-CNN. – Under Review.

Author Contributions: SS conceptualized the CPSD and 1D-CNN-based neural decoding framework for intra- and inter-subject MI-BCI experiments, implemented MATLAB codes, generated results, produced figures, wrote the original draft and edited the final version. SS, MB, and AM participated in interpreting the results. MB and AM reviewed the original draft and provided feedback. All authors read and approved the final version.

4.1 Introduction

A brain-computer interface (BCI) translates the brain's electrical or hemodynamic activities into active or passive tangible outputs (Saha *et al.*, 2021). It is an alternative link for human-computer interaction featuring diverse assisitive and rehabilitative technologies (ARTs) for healthy individuals and people with disabilities. Sensorimotor BCI, specifically motor imagery (MI) is a widely explored signal type for operating ARTs. MI refers to kinaesthetic imagination of a motor task that reflects similar brain dynamics corresponding to the actual motor action (Roberts *et al.*, 2020; Zich *et al.*, 2015; Jeannerod and Decety, 1995). Thus, a MI-BCI is used to rehabilitate people with upper/lower limb disabilities as well as providing assistive technologies for healthy individuals (Saha *et al.*, 2021).

Electroencephalography (EEG) is the most widely used and a non-invasive neuroimaging technique that captures the electrical activities of the brain for decoding user intentions or cognitive states through a BCI. However, EEG signals are highly nonlinear and nonstationary mainifested in inter-session and inter-subject variabilities (Saha *et al.*, 2023b; Saha and Baumert, 2020; Saha *et al.*, 2017b,a, 2019b). The intrinsic fluctuations in the brain dynamics demand session and subject-specific calibration for an EEG signal processing algorithm. That often requires subjects to spend significant time and efforts to learn modulating their brain signals and calibrate a BCI. This hinders generalizability and reproducibility of BCI model parameters across sessions and subjects (Saha *et al.*, 2023b, 2021; Saha and Baumert, 2020; Saha *et al.*, 2019b, 2017b,a; Jayaram *et al.*, 2016).

Inherent variabilities of EEG signals cause covariate shift when feature spaces for training and testing data splits does not share a common distribution (Saha and Baumert, 2020). Previous studies demonstrated performance variation for inter-session and inter-subject BCI when using supervised data transformation techniques (Wei and Ding, 2023; Saha *et al.*, 2019b, 2017b,a). Common spatial pattern (CSP) is the most popular method to transform multi-channel EEG signals for classifying MI tasks (Lu *et al.*, 2010). Recently, deep learning-based techniques including $1-$dimensional or $2-$dimensional convolutional neural network (CNN) architectures have been used in BCI (Wang *et al.*, 2023a; Kiranyaz *et al.*, 2021; Pérez-Zapata *et al.*, 2018; Kiranyaz *et al.*, 2015b). EEG signals may require some preprocessing and feature representation depending on the type of architecture. For example, EEG signals are converted into $2-$dimensional images via wavelet or short-time Fourier transforms for a 2D-CNN (Wang *et al.*, 2023a). For a 1D-CNN, the raw EEG signals may be used as input (Kiranyaz *et al.*, 2021, 2015b). Other studies demonstrated state-of-the-art artificial intelligence techniques such as long short-term memory

and attention-based architectures for MI classification (Wang *et al.*, 2023a; Ahn *et al.*, 2022).

This study proposes an MI classification pipeline featuring 1D-CNN with three different input feature representation techniques. A 1D-CNN can inherently utilize multi-channel $1-$dimensional sequential data for feature learning. We compare three input feature representation techniques, *i.e.*, time-domain EEG signals, frequency-embedded power spectral density (PSD) and bi-channel cross-power spectral density (CPSD) sequences. A comparative study among the proposed input feature representation techniques and CSP-based algorithms in intra- and inter-subject BCI settings demonstrates the potential of 1D-CNN for MI classification.

4.2 Materials and Methods

Figure 4.1 illustrates the proposed framework for classifying MI tasks in both intra- and inter-subject experimental settings. The proposed 1D-CNN was trained using one of the time-domain EEG signals, frequency-embedded PSD and CPSD sequences. To benchmark the proposed method featuring different input feature representation techniques, two CSP-based classification pipelines were implemented and evaluated in the same experimental settings. For single-trial MI classification, the CSP is one of the most widely used filtering techniques (Ramoser *et al.*, 2000; Lu *et al.*, 2010). Saha *et al.* proposed an MI-BCI classification algorithm comprising a bandpass filter, CSP, principal component analysis (PCA) and linear discriminant analysis (LDA) (Saha *et al.*, 2023b). After CSP, we selected six channels, the first and last three channels, to calculate the variance from each channel. We compared the classification accuracies achieved without and with PCA, respectively, to examine the impact of PCA on BCI performance. Notably, PCA is an unsupervised technique that may reduce the separation between two classes and, thus, the BCI performance. For details of CSP algorithm, please refer to (Ramoser *et al.*, 2000; Lu *et al.*, 2010; Saha *et al.*, 2023b).

4.2.1 Motor Imagery Dataset

The proposed MI classification framework was validated on the dataset IVa from BCI Competition III[2]. The dataset comprised single-trial EEG signals for $2-$class MI tasks,

[2]https://www.bbci.de/competition/iii/desc_IVa.html

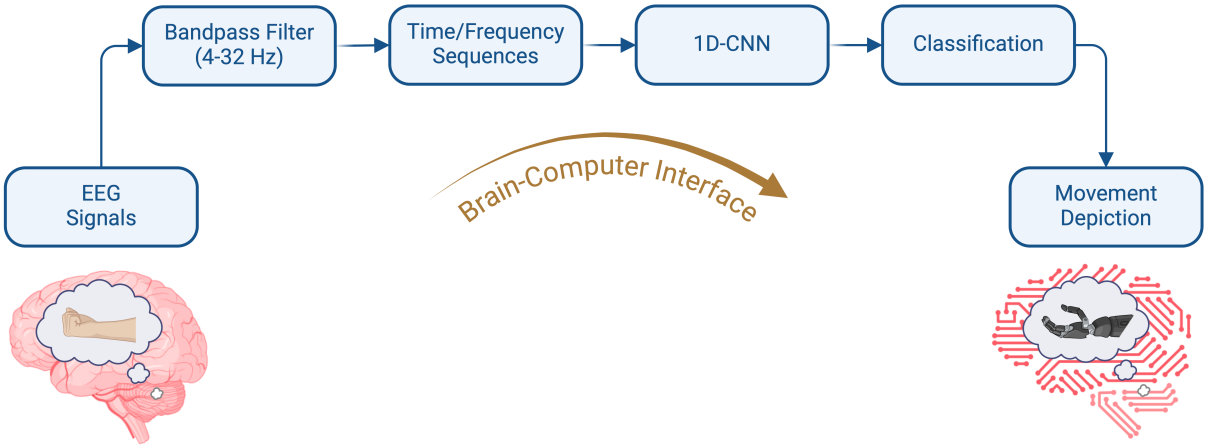

Figure 4.1. A simplified block diagram of the proposed signal processing pipeline for intra- and inter-subject motor imagery classification using a 1D-CNN architecture. [EEG = electroencephalography; 1D-CNN = 1−dimensional convolutional neural network]

i.e., right hand (RH) and right foot (RF), collected from five healthy individuals. Data were recorded using an extended $10/20$ EEG system when each subject was sitting in a comfortable armchair. The sampling rate is $Fs = 100$ Hz. Each subject had 280 trials, and the split between RH and RF is 50%. The trial duration is 3.5 s, but only 2.5 s of EEG signals after 0.25 s of the visual cue were selected. The PSD and CPSD sequences were calculated from each trial in a frequency range of $4 - 32$ Hz. Figure 4.2 shows class-specifc bandpass-filtered EEG signals from two channels, *i.e.*, $C3$ and $F3$ and their corresponding PSD and CPSD sequences for RH and RF tasks, respectively.

4.2.2 Time/Frequency Input Sequences

We trained the proposed BCI algorithm, *i.e.*, 1D-CNN architecture using bandpass-filtered time-domain EEG signals, frequency-embedded PSD or CPSD sequences. First, we applied a 4^{th} order Butterworth bandpass filter with cut-off frequencies of 4 Hz and 32 Hz for extracting MI-related temporal EEG signals as input to 1D-CNN. Then, we calculated PSD and CPSD sequences using the modified Welch periodogram method (Welch, 1967).

The PSD approximates the per unit frequency-embedded power distribution of a time-domain EEG signal, and is defined as follows:

$$P_x(\omega) = \sum_{m=-\infty}^{\infty} x(m)e^{-j\omega m}. \tag{4.1}$$

Here, $x(m)$ is a time series. For N EEG channels, there were N frequency-embedded PSD sequences as input to the 1D-CNN.

Similarly, the CPSD approximates the per unit frequency-embedded bi-channel power distribution and defined as follows:

$$P_{xy}(\omega) = \sum_{m=-\infty}^{\infty} R_{xy}(m) e^{-j\omega m}. \tag{4.2}$$

Here, $R_{xy}(m)$ is the cross-correlation sequence and formulated as

$$R_{xy}(m) = E\{x_{n+m} y_n^*\} = E\{x_n y_{n+m}^*\}. \tag{4.3}$$

Here, x_n and y_n are jointly stationary random signals, $-\infty < n < \infty$, $-\infty < m < \infty$, $\omega = 2\pi f$, and $E\{.\}$ refers to the expected value operator. In this study, an underlying assumption is that any two EEG signals are jointly stationary. For N channels, there are N auto-correlation sequences as CPSD was estimated from the same signal, and the remaining are cross-channel sequences.

We used the modified Welch periodogram method with a $256-$point discrete Fourier transform, precisely the computationally efficient fast Fourier transform (FFT) algorithm. The sampling rate of the EEG signals was $Fs = 100$, and the signal length of a single trial was 2.5 s, resulting in 250 samples/trial. For the $256-$point FFT, the signals were extended by zero padding to match the FFT length, and the PSD/CPSD approximation is a special case because the FFT length is greater than the signal length. There was no averaging for a single FFT spectrum. However, the Welch method was more likely to produce a smoother spectrum than a simple FFT approximation.

The length of each time-domain EEG signal was 250. For both PSD and CPSD sequences, only the spectrum from 4 to 32 Hz. The sampling rate is $Fs = 100$ and length of FFT is $NFFT = 256$. Thus, the frequency resolution is $\Delta f = \frac{Fs}{NFFT} = \frac{100}{256} = 0.306$ and length of a PSD/CPSD sequence is $L_{PSD/CPSD} = \frac{NFFT}{2} + 1 = 129$. But a frequency range (4 Hz to 32 Hz) for MI was selected for classification, resulting the length of PSD/CPSD sequences being 71 (approximated).

4.2.3 Convolutional Neural Network

A 1D-CNN can be used to learn local features from sequential data such as time-domain EEG signals and frequency-embedded PSD or CPSD sequences in this study (Kiranyaz *et al.*,

2021, 2015b). A sequence is passed through one or more convolution layers, each comprising a set of $1-$dimensional filters/kernels. The kernels are slid across the input sequence while calculating the dot product at each point defined by the stride (number of steps for moving kernels). The following equation refers to the convolution operation:

$$y_k = b_k + \sum_{n=0}^{M-1} s_n h_{k-n}. \tag{4.4}$$

Here, s is a $1-$dimensional sequence, h is the kernel, b is a bias term, M is the number of elements in s, y is the output vector, and k defines the stride. The input sequences are passed through the 1D-CNN layers while predicting the output. Then, both bias and kernel weights are learnable parameters tuned through backpropagation that allows updating the bias and weights while minimizing the loss, *i.e.*, cross-entropy loss.

Convolution is a linear operation, and adding a nonlinear activation function introduces nonlinear feature learning from time-domain EEG signals, frequency-embedded PSD or CPSD sequences. A rectified linear unit (ReLU) was used in this study and defined for an input s as follows (Krizhevsky *et al.*, 2012):

$$f(s) = \begin{cases} s, & \text{if } s > 1 \\ 0, & \text{otherwise.} \end{cases} \tag{4.5}$$

For more details on 1D-CNN, please refer to (Kiranyaz *et al.*, 2021, 2015a,b).

For N EEG channels, the number of input channels is N for both EEG and PSD input sequences and $N \times N$ for CPSD sequences. Table 4.1 describes the details of the proposed 1D-CNN architecture. The dataset comprised $N = 118$ EEG channels resulting in 118 EEG, 118 PSD or $118 \times 118 = 13924$ CPSD sequences. Thus, the number of channels in the input layer is $C = 118$, $C = 118$ or $C = 13924$, respectively, for EEG, PSD and CPSD sequences. The architecture comprised of three 1D-CNN layers with varying kernel sizes and numbers. A dropout layer with a probability of 0.2 was included after each layer to lessen the chance of overfitting. An $L2$ regularization (0.1) was included as another measurement to prevent overfitting. A $1-$dimensional average pooling layer was added after the first two 1D-CNN layers to reduce the feature space dimensions. After the third layer, a global average pooling layer was included followed by a fully connected layer. A softmax layer was then used to map class-specific probability distributions for classification of MI tasks.

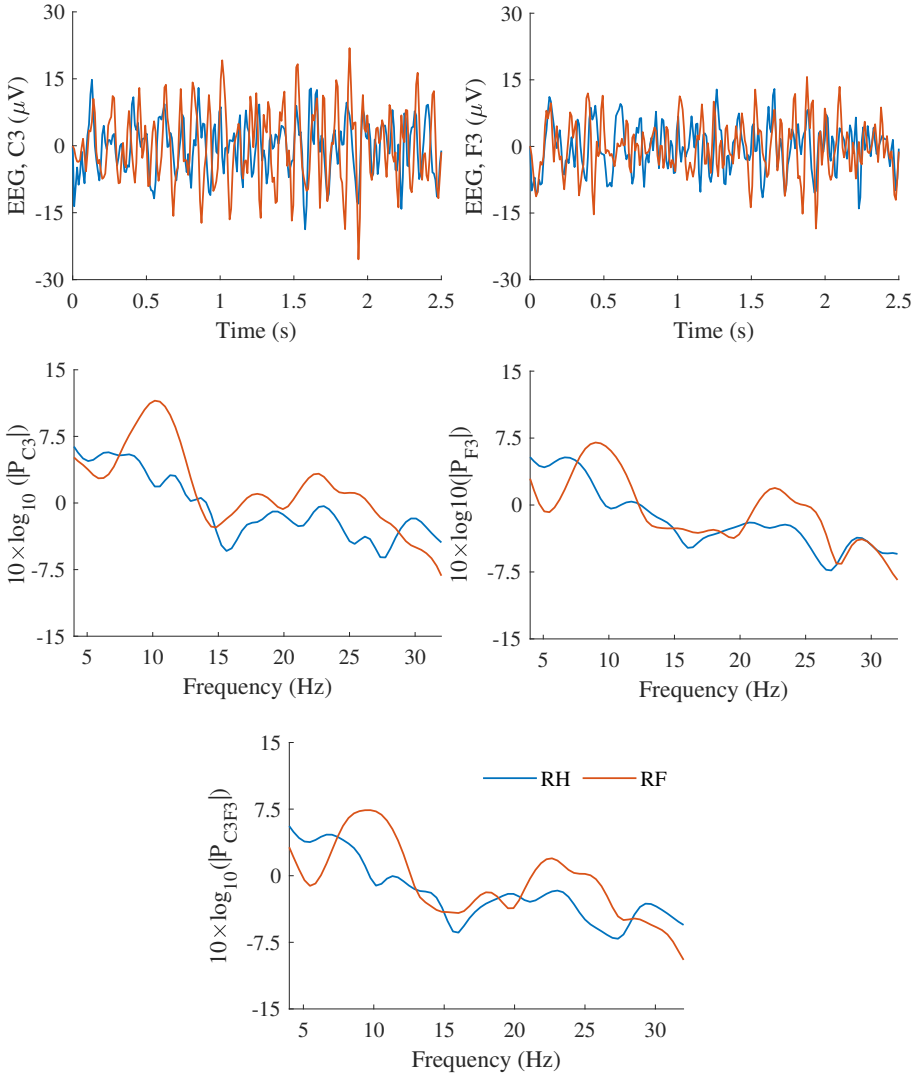

Figure 4.2. Examples of class-specific time-domain EEG signals, frequency-embedded PSD and CPSD sequences. [EEG: electroencephalography, PSD: power spectral density and CPSD: cross-power spectral density.]

4.2.4 Performance Evaluation of Intra- and Inter-Subject BCI

Table 4.2 shows the data distributions for training (70%), validation (10%) and testing sets (20%). The data were used in a $5-$fold cross-validation format to evaluate intra- and inter-subject BCI classification accuracies. For intra-subject BCI, data from each subject were divided into 5 subsets keeping 1 subset for evaluation. Each of the 5 subsets were shuffled and used as testing set interchangeably. The last one eighth of the training trials were used as valdation set to monitor the training of 1D-CNN models. The model with the best validation loss was selected for evaluting the testing accuray. Notably, the cross-validation setting was similar to Chapter 3, except the validation data were selected as the latest trials from each training set.

Layer #	Type	Kernel	Stride	Padding	Activations	Learnable Properties
1	Input = $\begin{cases} EEG, \\ PSD \text{ or} \\ CPSD \end{cases}$	–	–	–	$\begin{cases} 118 \times 1 \times 250, \\ 118 \times 1 \times 71 \text{ or} \\ 13924 \times 1 \times 71 \end{cases}$	–
2	1D-CNN	64 @ 7×1	1	'same'	$64 \times 1 \times 71$	Weights $\begin{cases} 7 \times 118 \times 64, \\ 7 \times 118 \times 64 \text{ or} \\ 7 \times 13924 \times 64 \end{cases}$ Bias 1×64
3	Dropout (20%)	–	–	–	$64 \times 1 \times 71$	–
4	ReLU	–	–	–	$64 \times 1 \times 71$	–
5	1–dimensional Average Pooling	64 @ 7×1	3	'same'	$64 \times 1 \times 24$	–
6	1D-CNN	32 @ 5×1	1	'same'	$32 \times 1 \times 24$	Weights $5 \times 64 \times 32$ Bias 1×32
7	Dropout (20%)	–	–	–	$32 \times 1 \times 24$	–
8	ReLU	–	–	–	$32 \times 1 \times 24$	–
9	1–dimensional Average Pooling	32 @ 5×1	2	'same'	$32 \times 1 \times 12$	–
10	1D-CNN	16 @ 3×1	1	'same'	$16 \times 1 \times 12$	Weights $3 \times 32 \times 16$ Bias 1×16
11	Dropout (20%)	–	–	–	$16 \times 1 \times 12$	–
12	ReLU	–	–	–	$16 \times 1 \times 12$	–
13	1–dimensional Global Average Pooling	–	–	–	16×1	–
14	Fully Connected	–			2×1	Weights 2×16 Bias 2×1
15	Softmax	–	–	–	2×1	–
16	Classification Output	–	–	–	2×1	–

Table 4.1. Detailed structure of the proposed 1D-CNN architecture. [1–dimensional: 1-dimensional, CNN: convolutional neural network, C: channel, B: batch and T: sequence length.]

	Training		Validation		Testing		Details
	#	Subject(s)	#	Subject(s)	#	Subject(s)	
Intra-Subject	196	$0.7 \times S_a$	28	$0.1 \times S_a$	56	$0.2 \times S_a$	$a/b/c/d/e = [1, 2, 3, 4, 5]$ $a \neq b \neq c \neq d \neq e$
Pairwise	196	$0.7 \times S_a$	28	$0.1 \times S_a$	56	$0.2 \times S_b$	
Pooled	980	$1.0 \times S_a + 1.0 \times S_b + 1.0 \times S_c + 0.5 \times S_d$	140	$0.5 \times S_d$	280	$1.0 \times S_e$	

Table 4.2. Distributions of data (# of trials) across training, validation and testing sets for intra-subject and inter-subject (pairwise and pooled) experiments. [Total number of trials/subject: $S_1/S_2/S_3/S_4/S_5$]

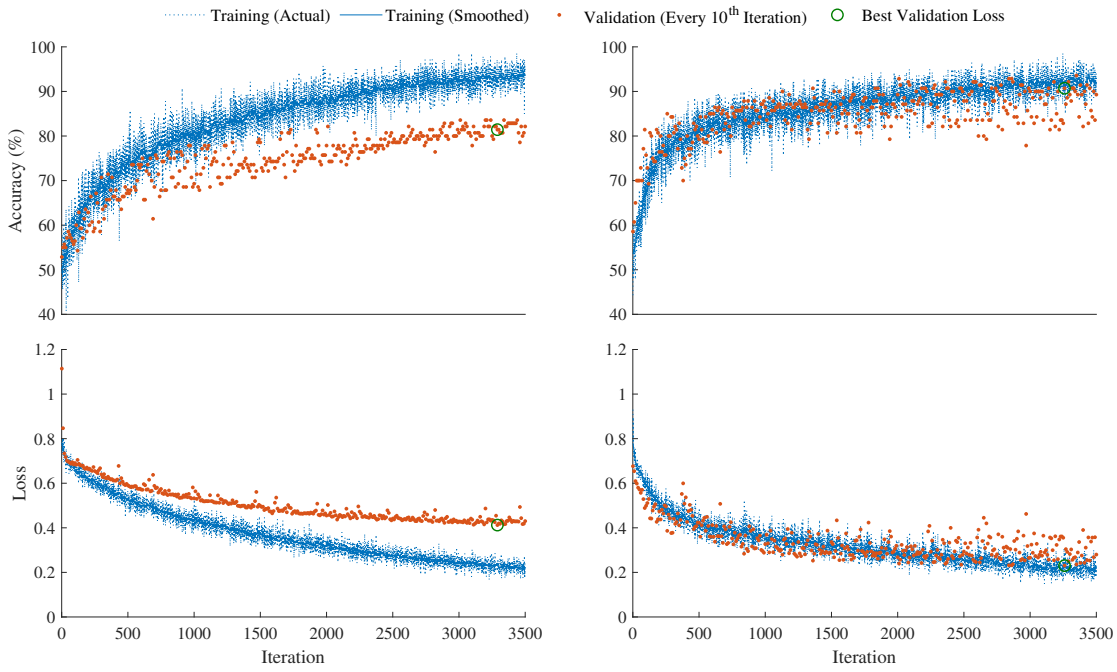

Figure 4.3. Illustration of accuracy and loss curves for the validation and testing subject pairs $aw - ay$ and $al - av$ (lef-right) in pooled BCI experiment. The lowest validation loss model was selected for evaluation.

Two experimental settings were used for evaluating inter-subject BCI. First, the data distributions similar to their intra-subject counterparts were used for pairwise inter-subject MI classification. When the training and validation trials from one subject were used to train the 1D-CNN models, the testing trials were from another subject. A total of 25 classification accuracies were calculated using different combinations of training, validation and testing sets. For both intra-subject and inter-subject (pairwise) BCI, the batch sizes during training 1D-CNN models were $[7, 14, 28, 56]$.

Finally, the inter-subject (pooled) BCI was implemented considering a leave-one-subject-out cross-validation. In this case, trials from four subjects were used to train and select best validation model. The selected model was applied on another subject to determine the accuracy. The batch sizes during the training were $[35, 70, 140, 280]$. The followings are the learning rates that were used in all experiments: $[1e^{-5}, 3e^{-5}, 5e^{-5}, 7e^{-5}, 9e^{-5}, 11e^{-5}, 13e^{-5}]$. The combinations of batch sizes and learning rates attribute 28 training sessions. Each session was run twice, totalling 56 1D-CNN models. Notably, the validation loss was evaluated in every 10^{th} epoch and the model with the best validation loss was selected for each session. The best accuracy on unseen testing set was reported in this chapter. Figure 4.3 shows training and validation metrics, *i.e.*, accuracy and loss curves for the validation and testing subject pairs $aw - ay$ and $al - av$ (lef-right) in pooled BCI experiment.

Subject	CSP		1D-CNN		
	without PCA	with PCA	EEG	PSD	CPSD
	Mean±SD	Mean±SD	Mean±SD	Mean±SD	Mean±SD
aa	81.07 ± 11.82	80.36 ± 13.06	76.78 ± 10.71	76.79 ± 6.31	80.72 ± 4.45
al	92.50 ± 4.45	91.43 ± 5.56	96.07 ± 1.95	95.71 ± 2.03	91.79 ± 2.71
av	58.57 ± 11.25	57.86 ± 8.04	72.50 ± 7.64	72.50 ± 6.75	68.22 ± 4.79
aw	86.78 ± 4.48	84.28 ± 6.96	92.14 ± 4.66	78.57 ± 6.05	80.36 ± 8.75
ay	92.50 ± 4.62	90.36 ± 6.39	95.36 ± 2.39	89.29 ± 6.05	88.21 ± 2.04
Overall	82.28 ± 14.82	80.86 ± 14.63	86.57 ± 11.69	82.57 ± 10.20	81.86 ± 9.50

Table 4.3. Intra-subject BCI classification accuracies ($\%$) for a $5-$fold validation setup. [CSP = common spatial pattern, 1D-CNN = $1-$dimensional convolutional neural network, SD = standard deviation; Mean±SD calculated on 5 runs for each subject.]

4.2.5 Computing Resources

The proposed algorithm was implemented in MATLAB $2023b$. The software was installed on a desktop computer with the following specifications: Windows 11 Pro, 12^{th} Gen Intel® Core^{TM} $i9-12900K$, RAM 32.0 GB. The computer comprises a NVIDIA GeForce RTX 3080, which was used to train the proposed 1D-CNN models.

4.3 Results

4.3.1 Intra-Subject BCI

Table 4.3 lists the classification accuracies ($\%$) for intra-subject BCI. The overall classification accuracies (Mean±SD) are 82.28 ± 14.82, 80.86 ± 14.63, 86.57 ± 11.69, 82.57 ± 10.20 and 81.86 ± 9.50 using CSP without and with PCA, and 1D-CNN with EEG, PSD and CPSD sequences, respectively, the best being 1D-CNN with EEG signals. Interestingly, the performance of CSP without PCA is slightly higher than that achieved using PCA. For subject av, the accuracies using 1D-CNN and EEG signals and PSD sequences are 72.50 ± 7.64 and 72.50 ± 6.75, respectively, noticeably beating the performances of CSP-based methods.

4.3.2 Inter-Subject (Pairwise) BCI

Table 4.4 shows inter-subject (pairwise) MI classification accuracies. The all-around inter-subject BCI classification results (mean±SD) are 67.06 ± 16.78, 65.89 ± 17.38, 70.80 ± 9.21, 69.32 ± 7.46 and 70.20 ± 6.04, respectively, using CSP without and with PCA, and 1D-CNN

Subject Pair	CSP		1D-CNN		
	without PCA	with PCA	EEG	PSD	CPSD
	Mean±SD	Mean±SD	Mean±SD	Mean±SD	Mean±SD
aa - al	84.28 ± 13.26	81.50 ± 16.51	76.64 ± 7.76	67.71 ± 6.50	72.78 ± 4.59
al - aa	56.64 ± 7.32	55.28 ± 7.42	73.36 ± 6.64	65.21 ± 4.19	68.14 ± 4.96
aa - av	60.21 ± 10.38	64.93 ± 8.55	65.43 ± 4.31	69.00 ± 3.57	73.21 ± 4.83
av - aa	54.14 ± 13.30	53.21 ± 9.74	66.43 ± 6.19	70.00 ± 4.12	69.86 ± 5.93
aa - aw	69.86 ± 11.94	68.07 ± 11.03	67.93 ± 4.17	65.79 ± 6.63	69.43 ± 5.63
aw - aa	67.93 ± 8.12	62.07 ± 11.25	67.28 ± 5.02	67.93 ± 6.92	72.57 ± 4.72
aa - ay	78.64 ± 12.80	80.71 ± 16.12	81.36 ± 9.11	77.43 ± 4.15	72.00 ± 3.67
ay - aa	56.50 ± 10.03	64.36 ± 13.89	70.14 ± 7.76	71.78 ± 5.48	75.07 ± 2.89
al - av	52.64 ± 4.53	50.21 ± 2.26	64.28 ± 7.01	61.64 ± 5.58	65.36 ± 5.00
av - al	83.50 ± 13.15	78.28 ± 16.49	71.28 ± 5.23	75.79 ± 3.34	70.43 ± 3.42
al - aw	65.50 ± 12.23	58.36 ± 12.38	66.14 ± 4.76	63.29 ± 7.29	68.07 ± 5.70
aw - al	84.64 ± 17.02	85.28 ± 17.95	72.50 ± 6.18	70.50 ± 4.41	75.78 ± 3.58
al - ay	74.86 ± 14.78	81.21 ± 8.53	85.36 ± 5.18	74.07 ± 5.51	70.79 ± 4.97
ay - al	84.86 ± 18.31	85.00 ± 17.77	85.28 ± 6.21	76.93 ± 9.99	79.78 ± 6.03
av - aw	55.78 ± 7.79	50.86 ± 5.83	61.50 ± 4.41	63.78 ± 5.87	62.86 ± 2.68
aw - av	54.28 ± 10.80	50.28 ± 2.34	66.86 ± 3.75	63.50 ± 3.75	66.07 ± 4.81
av - ay	60.78 ± 15.40	65.07 ± 11.32	73.50 ± 6.02	77.93 ± 5.13	67.71 ± 3.45
ay - av	51.28 ± 2.45	50.00 ± 2.00	61.71 ± 5.65	71.71 ± 6.55	71.43 ± 4.61
aw - ay	81.21 ± 15.20	80.14 ± 16.93	76.79 ± 5.94	66.14 ± 5.19	68.71 ± 3.57
ay - aw	63.64 ± 9.00	53.00 ± 7.57	62.21 ± 4.77	66.28 ± 5.56	63.93 ± 4.64
Overall	67.06 ± 16.78	65.89 ± 17.38	70.80 ± 9.21	69.32 ± 7.46	70.20 ± 6.04

Table 4.4. Inter-subject (Pairwise) BCI classification accuracies (%) for a $5-$fold validation setup. [CSP = common spatial pattern, 1D-CNN = $1-$dimensional convolutional neural network, SD = standard deviation; Mean±SD calculated on 25 runs for each subject pair.]

with EEG, PSD and CPSD sequences. In some cases, CSP outperforms 1D-CNN, for example, for subject pair $aa-al$, $av-al$, $aw-al$ and $aw-ay$. Unlike intra-subject BCIs, there are cases when CSP with PCA outperforms without PCA, *i.e.*, for subject pairs $aa-ay$ and $aw-al$.

Interestingly, the inter-subject classification accuracies are mostly asymmetric, *i.e.*, altering training and testing subjects within a subject pair showed poorer performance. This is sometimes more prominent for CSP than 1D-CNN. For example, the classification accuracies for subject pairs $aa-al$ and $al-aa$ are 84.28 ± 13.26 and 56.64 ± 7.32 using CSP without PCA demonstrates more asymmetric performance than the accuracies achieved using 1D-CNN and EEG signals, *i.e.*, 76.64 ± 7.76 and 73.36 ± 6.64. Similarly, for subject pairs $aa-ay$ and $ay-aa$ the classification accuracies using CSP with PCA are 80.71 ± 16.12 and 64.36 ± 13.89, respectively, while the classification accuracies using 1D-CNN and CPSD

Validation-Testing Subject Pair	CSP		1D-CNN		
	without PCA	with PCA	EEG	PSD	CPSD
al-aa	50.00	50.00	63.93	64.64	65.00
av-aa	50.00	50.00	77.14	65.00	70.36
aw-aa	50.00	50.00	80.36	67.86	68.57
ay-aa	52.14	50.00	73.93	64.29	64.64
aa-al	80.36	80.00	90.71	85.71	80.00
av-al	81.43	74.28	92.50	84.29	77.14
aw-al	73.57	64.28	91.43	78.21	73.21
ay-al	68.93	59.28	90.71	80.36	78.21
aa-av	52.50	50.00	58.21	67.50	65.36
al-av	49.64	49.64	62.86	68.57	67.50
aw-av	53.93	52.50	60.00	69.29	62.14
ay-av	51.07	49.64	55.00	66.43	65.71
aa-aw	54.64	48.57	69.64	65.71	62.86
al-aw	59.28	63.93	68.21	57.14	61.79
av-aw	51.07	46.78	75.00	65.36	63.21
ay-aw	57.86	45.71	74.29	64.29	61.07
aa-ay	57.14	54.28	86.79	75.36	77.50
al-ay	53.21	51.07	83.21	77.50	73.93
av-ay	50.00	53.93	89.29	79.29	73.57
aw-ay	50.00	54.64	88.93	79.64	76.07
$Mean \pm SD$	57.34 ± 10.27	54.93 ± 9.12	76.61 ± 12.37	71.32 ± 7.96	69.39 ± 6.28

Table 4.5. Inter-subject (Pooled) BCI classification accuracies (%) for a $5-$fold validation setup. [CSP = common spatial pattern, 1D-CNN = $1-$dimensional convolutional neural network, SD = standard deviation; Mean±SD calculated on 20 runs for each subject.]

sequences are 72.00 ± 3.67 and 75.07 ± 2.89, respectively. Although the results might implicate 1D-CNN featuring more consistent BCI performance, CSP outperforms in many cases including subject pairs $aa-al$, $av-al$, $aw-al$ and $aw-ay$.

4.3.3 Inter-Subject (Pooled) BCI

Table 4.5 tabulates the inter-subject (pooled) BCI accuracies. The overall classification accuracies (%, Mean $\pm$ SD) are 57.34 ± 10.27, 54.93 ± 9.12, 76.61 ± 12.37, 71.32 ± 7.96 and 69.39 ± 6.28 using CSP without and with PCA, and 1D-CNN with EEG, PSD and CPSD sequences, respectively. In any of 4 cases, the classification accuracy for (*testing*) subject aa is surprisingly constant at 50.00% using CSP with PCA. However, the highest accuracy for testing subject aa using 1D-CNN with EEG signals is 80.36%. The best performance for

Wilcoxon signed rank test	Intra-Subject	Inter-Subject (Pairwise)	Inter-Subject (Pooled)
without PCA vs. with PCA	Yes	Yes	Yes
without PCA vs. EEG	Yes	Yes	Yes
without PCA vs. PSD	No	Yes	Yes
without PCA vs. CPSD	Yes	Yes	Yes
with PCA vs. EEG	Yes	Yes	Yes
with PCA vs. PSD	No	Yes	Yes
with PCA vs. CPSD	No	Yes	Yes
EEG vs. PSD	Yes	Yes	Yes
EEG vs. CPSD	Yes	Yes	Yes
PSD vs. CPSD	Yes	Yes	Yes
$p-$value (Friedman's Test)	0.0092	1.4328^{-15}	6.0669^{-13}

Table 4.6. Statistical comparison of intra-subject and inter-subject motor imagery classification accuracies achieved using the proposed algorithms.

testing subject al is 92.50% using with EEG signals. The classification accuracies using 1D-CNN with EEG signals for testing subject ay significantly outperforms CSP-based methods, the best performance being 89.29%.

4.3.4 Statistical Analysis

For comparisons, the performance metrics achieved using CSP without and with PCA, 1D-CNN with EEG, PSD and CPSD sequences were examined through statistical methods such as Friedman's test for the overall evaluation of all five algorithms followed by Wilcoxon signed rank test for pairwise comparison of the algorithms. Bonferroni Correction was applied to adjust the $p-$value calculated from the Wilcoxon signed rank test for performing multiple pairwise comparisons. For five algorithms in this study, there were 10 pairs of algorithms. Thus, the original $p-$values were multiplied by 10 to approximate the corresponding adjusted $p-$values. Table 4.6 shows that the classification accuracies achieved using the proposed algorithms differ significantly for intra-subject, inter-subject (pairwise) and inter-subject (pooled) BCIs, demonstrating $p-$value < 0.05 for overall statistical evaluation using Friedman's test with the number of replicates 5, 25 and 4, respectively, for intra-subject, inter-subject (pairwise) and inter-subject (pooled) BCIs.

For intra-subject BCI, all pairs of algorithms showed significant differences except CSP without PCA versus 1D-CNN with PSD, CSP with PCA versus 1D-CNN with PSD and CSP with PCA versus 1D-CNN with CPSD. All pairs in inter-subject (pairwise and pooled) BCIs illustrated significantly different ($p-$value < 0.05) classification accuracies. Figure 4.4 illustrates

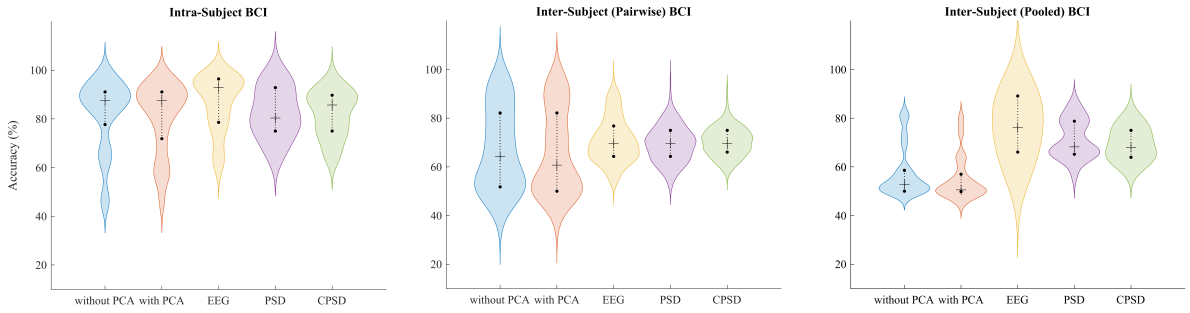

Figure 4.4. Comparison of classification accuracies illustrated by violin plots and median with interquartile range achieved using CSP without PCA and with PCA, 1D-CNN with EEG, PSD, and CPSD sequences for intra-subject, inter-subject (pairwise) and inter-subject (pooled) BCIs.

the distributions of classification accuracies using violin plots and median with interquartile range. Because the algorithms were evaluated on data from the same subjects, the classification accuracies (data) were paired, implicating repeated measurements from the same subjects using the intra-subject and inter-subject cross-validation settings.

4.4 Discussion

4.4.1 Study Significance in Current Literature

This study features a lightweight and straightforward 1D-CNN with different input feature representation techniques such as time-domain bandpass-filtered EEG signals, frequency-embedded PSD and CPSD sequences for intra-subject, inter-subject (pairwise) and inter-subject (pooled) MI classification. A comparative analysis of the proposed methods with conventional CSP-based algorithms complements the results. A 1D-CNN is intrinsically compatible with time-domain EEG input sequences and computationally less complex than its $2-$dimensional counterparts. The underlying rationale for using frequency-embedded PSD and CPSD sequences derives from contemporary studies implicating task-related cortical modulations as frequency-specific (Sasai *et al.*, 2021; Klimesch, 2018). Moreover, CPSD potentially attributes brain connectivity analysis-based features for MI classification (Leeuwis *et al.*, 2021; Gu *et al.*, 2020; Li *et al.*, 2019; Deco *et al.*, 2011). A previous investigation demonstrated different spectral estimation techniques, such as Yule-Walker and Welch methods, and used classifiers like LDA and support vector machines for sensorimotor BCI (Herman *et al.*, 2008). García-Salinas *et al.* transformed EEG signals into PSD

sequences for training a 2D-CNN model for classifying speech (García-Salinas *et al.*, 2023). Other studies utilized frequency-embedded PSD sequences in detecting neurological conditions such as epilepsy and Parkinson's disease (Liu *et al.*, 2023a; Göker, 2023). Wang *et al.* proposed PSD and CPSD estimation for identifying brain activities associated with Alzheimer's disease (Wang *et al.*, 2015). PSD and CPSD are popular signal processing methods to investigate spectral contents of time-domain signals. Nevertheless, this paper demonstrates using PSD or CPSD sequences to train a 1D-CNN for MI classification and shows promising results, even for fully zero-training inter-subject (pairwise and pooled) BCIs. Transforming EEG signals into PSD and CPSD sequences for training 1D-CNN is a computationally more efficient option than their $2-$dimensional representations, such as using Wavelet or short-time Fourier transform for training higher dimensional CNN architectures. Notably, the number of learnable parameters for the proposed 1D-CNN architecture is 64786, 64786 and 6249874 when using time-domain EEG, frequency-embedded PSD and CPSD sequences, respectively. CPSD is computationally expensive ($> 96\times$learnable parameters for EEG/PSD), although the classification accuracies implicate CPSD never outperformed computationally more efficient EEG.

The best overall intra-subject classification accuracy ($\%$) achieved using 1D-CNN with time-domain EEG sequences was 86.57 ± 11.69, which outperformed CSP without PCA, 82.28 ± 14.82. The performance of 1D-CNN with PSD and CPSD sequences also beat the performance of CSP-based methods. Typically, CSP is highly prone to overfitting and does not necessarily produce the best accuracy. While this study utilized a rudimentary version of the CSP algorithm-based MI classification pipeline for benchmarking, there are improved CSP algorithms for BCI (Saha *et al.*, 2023b; Ramoser *et al.*, 2000). Faezmehr *et al.* integrated Kullback-Leibler Divergence into CSP for improved covariance estimation and achieved an overall accuracy of 89.8 ± 9.9 (Faezmehr *et al.*, 2024). Another study evaluated a filter-bank CSP-based algorithm on the same dataset as this study and achieved a classification accuracy of 88.62 ± 9.22 (Park and Chung, 2020). Future studies may include other state-of-the-art techniques, including modified CSP algorithms, to compare BCI performances.

The proposed 1D-CNN with time-domain EEG signals outperformed in inter-subject (pairwise and pooled) experiments compared to the CSP-based classification pipeline without PCA, *i.e.*, 70.80 ± 9.21 versus 67.06 ± 16.78 and 76.61 ± 12.37 versus 57.34 ± 10.27, respectively. Liu *et al.* proposed a spatiotemporal CNN for inter-subject MI classification using a leave-one-subject-out cross-validation (Liu *et al.*, 2022). Although that study achieved an

overall classification accuracy of 81.71 ± 9.27, the algorithm used 80% data from the target subject for training. In contrast, this study demonstrated fully zero-training inter-subject BCIs where no training samples are essential for algorithm training. Wimpff *et al.* also proposed a CNN and attention mechanism-based intra- and inter-subject BCIs that achieved classification accuracies of 78.35 ± 1.23 and 66.81 ± 2.51, respectively (Wimpff *et al.*, 2024). That study utilized a previously proposed method called EEG Conformer (Song *et al.*, 2022), showing BCI classification accuracies of 81.71 ± 0.54 and 73.37 ± 0.58, respectively, for intra- and inter-subject MI classifications.

The proposed PSD and CPSD are novel input feature representation techniques for MI classification using 1D-CNN. Comparative results suggest 1D-CNN with time-domain EEG signals outperformed frequency-embedded CPSD sequences in intra-subject and inter-subject (pairwise and pooled) BCIs. Furthermore, 1D-CNN with PSD sequences produced better overall classification accuracies than 1D-CNN with CPSD for intra-subject and inter-subject (pooled) BCIs; however, the classification accuracies were comparable. For inter-subject (pairwise) BCI, the average classification accuracy of 1D-CNN with CPSD sequences narrowly exceeded that achieved using PSD sequences. Thus, augmenting N input channels to $N \times N$ did not improve the performance significantly as with increased computational burden. However, this study demonstrated the performance of 1D-CNN using time/frequency multi-channel sequential input in intra-subject and inter-subject settings, suggesting the potential utility of these feature representations for EEG-based BCI applications.

4.4.2 Toward a fully zero-training BCI

Calibration requirements of BCIs hinder the generalizability of neural decoding algorithms due to the influence of time-variant and subject-specific factors on EEG signals (Saha and Baumert, 2020). EEG signals are highly nonlinear and nonstationary, and signal variation originates from the diversity of users' neuroanatomical, psychological, physiological, and cognitive traits, which causes covariate shifts. Covariate shifts occur when training and testing feature distributions differ, resulting in a trained classifier not performing well on unseen testing data when they come from the same training subject at a different time or from a new user. To compensate for inter-session and inter-subject variabilities, there are different covariate shift adaptation or transfer learning techniques, such as the domain adaption technique, that integrate prior knowledge of distributions of training (source) and testing (target) subjects in the classifier (Kumar *et al.*, 2024; Jayaram *et al.*, 2016; Li *et al.*, 2010). Kwak *et al.* proposed a resting EEG-based inter-subject baseline correction method

for reducing the calibration time to a minimum, just using $1-$minute baseline EEG from the target subject (Kwak *et al.*, 2023). Other studies propose different predictors of BCI performance; for example, psychological factors such as attention and motivation are neural correlates of MI-based BCI (Kleih-Dahms *et al.*, 2021; Hammer *et al.*, 2012). Kasahara *et al.* showed gray matter volume as a neurological predictor for sensorimotor BCI (Kasahara *et al.*, 2015). Other studies implicated the MI-related sources are different (spatially) across subjects, leading to poor inter-subject BCI performance; however, including knowledge of inter-subject associative sources in the classifier may deliver good inter-subject BCI performance (Saha *et al.*, 2019b; Wronkiewicz *et al.*, 2015). Although this study does not quantify inter-subject variability, the proposed input feature representation techniques for 1D-CNN demonstrate promising fully-zero training inter-subject BCI.

The impact of inter-subject variability is more prominent for people with disabilities who encounter neurological incidents than healthy individuals. The clinical characteristics of the disability type and severity define subject-specific EEG characteristics; for example, post-stroke brain lesion depicts the damaged neural circuits and residual functional abilities as evident by altered EEG patterns (Park *et al.*, 2016). Thus, the generalizability of a BCI classifier is challenging. Generalized, fully zero-training BCIs for healthy individuals may become precursors to BCIs for people with disabilities that require no or minimum calibration (Kwak *et al.*, 2023; Saha *et al.*, 2019b, 2017b). BCI calibration is a tedious process, often frustrating for users, especially those with disabilities. A zero or minimum calibration BCI can promote BCI-based assistive and rehabilitative technologies for mass dissemination across diverse communities (Saha *et al.*, 2021; Kübler *et al.*, 2014).

Inter-subject associative BCI refers to a generalized BCI that can accommodate a new target user with no or minimum calibration efforts, assuming the target subject shares the same task-related neural substrates as training subjects (Wei and Ding, 2023; Saha *et al.*, 2023b; Wang *et al.*, 2021; Saha *et al.*, 2017b). Irrespective of the intrinsic EEG variabilities, multiple subjects may share similar MI-related dynamics that aid the generalization of classification framework. Quantifying inter-subject associativity is a precursor to developing generalized BCI algorithms when subjects with associative task-related EEG characteristics can be preselected. Previous studies proposed inter-subject associative BCI for MI classification (Saha *et al.*, 2019b, 2017b,a; Wronkiewicz *et al.*, 2015). They were limited to a cross-subject paradigm. The proposed methods in this study demonstrate both cross-subject and pooled-subject BCI experiments.

The selection of validation subjects impacts the choice of optimal 1D-CNN models and, thus, the inter-subject (pooled) classification accuracies (Table 4.5). This study lacks quantification of inter-subject associativity or variability, which was essential to select the best validation subject to maximize the BCI performance on the testing subjects. Future studies may quantify inter-subject associativity or variability within the dataset, which could lead us to the optimal selection of a validation-testing pair of subjects. Prior inter-subject associativity measurement complements the performance of a fully zero-training BCI. Previous studies developed inter-subject associativity quantification strategies requiring training and testing data (Saha *et al.*, 2023b). Kwak *et al.* have recently proposed a $1-$minute resting EEG-based predictor for an inter-subject associative BCI, which is a practical solution (Kwak *et al.*, 2023). Brain resting state networks are functionally relevant and contribute to MI classification (Kwak *et al.*, 2023; Leeuwis *et al.*, 2021; Gu *et al.*, 2020; Li *et al.*, 2019; Deco *et al.*, 2011). Thus, if a resting EEG-based predictor is established, a new perspective toward identifying inter-subject associative users for a generalized BCI is realistic.

4.4.3 Motor Imagery for Rehabilitation

Motor imagery tasks share similar neural substrates to actual motor actions (Pérez-Velasco *et al.*, 2025; Roberts *et al.*, 2020; Zich *et al.*, 2015). Pérez-Velasco *et al.* demonstrated that a BCI classifier trained on motor execution data successfully applied to MI data featuring inter-task transfer learning (Pérez-Velasco *et al.*, 2025). Previous studies demonstrated MI-based BCI for assisting people with disabilities who may suffer from neurological conditions such as stroke, spinal cord injury, amyotrophic lateral sclerosis and cerebral palsy (Saha *et al.*, 2021). Depending on the disability type and severity, diverse personalized BCI applications exist. The underlying principle lies in restimulating impaired neural networks by inducing plasticity that refers to the inherent changeable characteristics of the neural circuits across the central and peripheral nervous systems (Brown and Milner, 2003).

Studies showed MI, in combination with functional electrical stimulation, assisted users in regaining the functionality of paretic upper limbs by inducing plasticity (Brunner *et al.*, 2024; Bhattacharyya *et al.*, 2019). Other studies showed MI training with transcranial magnetic or direct current stimulation may be used to repair affected brain areas post neurological incidents (Ortiz *et al.*, 2020; Foysal and Baker, 2020; Grami *et al.*, 2022; Blanco Mora *et al.*, 2024). BCI-driven neurofeedback and exoskeleton induce plasticity to rehabilitate impaired movements (Stefano Filho *et al.*, 2024; Ferrero *et al.*, 2023). Irrespective of the BCI design diversity, the goal is to maximize the MI classification accuracies for operating rehabilitative

technologies. However, session- and subject-specific training demands time and effort, which may diminish the utility of BCI for both healthy individuals and people with disabilities.

4.4.4 Limitation and Future Outlook

The proposed 1D-CNN with time/frequency input sequences demonstrated promising results, especially for inter-subject (pairwise and pooled) experiments, promoting a fully zero-training BCI. However, the dataset used in this study comprises EEG signals for two MI tasks from only five subjects, which limits the generalizability of the models in inter-subject settings. Future studies should include a large dataset with many subjects; for example, Dreyer *et al.* published a MI dataset of 87 subjects (Dreyer *et al.*, 2023). Such a dataset could strengthen the quantification of inter-subject variability and the performance of calibration-free BCI. The pairwise experiment in this study is tedious when using an extensive dataset, while the pooled experiment is a more feasible option. Quantifying inter-subject EEG signal variability or feature space is challenging, and this study does not include any BCI performance predictor. Studies have proposed inter-subject BCI performance predictors, although they require training and testing trials to quantify the inter-subject distance (Saha *et al.*, 2023b, 2019b; Wronkiewicz *et al.*, 2015). Kwak et al. proposed a 1−minute resting EEG-based inter-subject baseline correction, which can become a practical alternative when the requirement of calibration data is minimal (Kwak *et al.*, 2023). Thus, future studies may apply innovative methods to develop resting EEG-based predictors for an inter-subject associative BCI (Kwak *et al.*, 2023; Leeuwis *et al.*, 2021; Gu *et al.*, 2020; Li *et al.*, 2019; Deco *et al.*, 2011).

The design choices of the proposed 1D-CNN have been made heuristically based on previous experience with deep learning hyperparameters and trial and error. Considering a small dataset for intra-subject BCI, we selected three layers of 1D-CNN filters with varying sizes. The selection was finalized after a few iterations of experiments using varying filter sizes. The choice of ReLU activation and other hyperparameters, such as batch sizes and learning rates, were also based on experience. It is inconclusive from this study about the optimal parameter selection. Future studies may include hyperparameter optimization techniques such as grid search and Bayesian optimization (Wojciuk *et al.*, 2024). Thus, the results presented in this study may not be the optimal BCI classification accuracies. Due to the many experiments required for intra-subject, inter-subject (pairwise), and inter-subject (pooled) BCIs, we used a limited number of hyperparameter tuning for the proposed 1D-CNN. Further studies on systemically optimizing the hyperparameters, as well as CNN

architectures, may offer enhanced performance. Adding batch normalization would alleviate internal covariate shifts by better generalizing the 1D-CNN model during the training (Ioffe and Szegedy, 2015).

4.5 Conclusion

This study proposes a novel time/frequency EEG sequence learning technique for intra- and inter-subject MI-based BCIs. The proposed 1D-CNN classification framework outperforms the conventional CSP-based methods as implicated in the results from intra- and inter-subject studies. Further investigations should include larger datasets with more subjects and multi-class data for more comprehensive comparisons with other state-of-the-art machine learning and deep-learning methods for MI classification.

Chapter Context:

This chapter proposed an AI-based feature learning for classifying MI tasks, replacing handcrafted feature extraction. The classification pipeline demonstrates raw EEG signals converted into frequency-embedded PSD and CPSD sequences for training 1D-CNN. The proposed methods were benchmarked with the CSP-based classifiers, demonstrating the capabilities of 1D-CNN to learn features by nonlinear activation functions while optimizing BCI performance. The CPSD sequences may offer brain connectivity network-based features and become a novel feature representation for training 1D-CNN architecture for classifying MI tasks.

The next chapter demonstrates a modified version of the 1D-CNN architecture for classifying multi-class text classification tasks for intra- and inter-subject BCIs. Bandpass-filtered time-domain EEG signals and frequency-embedded PSD sequences were used as input for training the 1D-CNN model. The proposed BCI outperforms the state-of-the-art speech BCIs using non-invasive EEG signals.

Frequency-Embedded Sequence Learning for Multi-Class EEG-to-Text Interface

BRAIN-computer interface (BCI) is a state-of-the-art technology that decodes users' thoughts or intentions, for example, decoding speech from electroencephalography (EEG) signals. In this study, a multi-class (*i.e.*, 5 words or phrases) EEG-to-Text classification pipeline featuring a $1-$dimensional convolutional neural network (1D-CNN) architecture was proposed. The 1D-CNN was trained using both time-domain EEG signals and frequency embedded sequences. As preprocessing, a bandpass filter with cut-off frequencies of 4 Hz and 120 Hz followed by a notch filter at 60 Hz was applied. Then, the modified Welch periodogram method was used to transform EEG signals into frequency-embedded power spectral density (PSD) sequences. Then, the 1D-CNN models were trained for evaluating intra-subject, inter-subject (pairwise) and inter-subject (pooled) BCI performance. For intra-subject settings, the overall classification accuracies ($\%$, Mean $\pm$ Standard Deviation) 46.1 ± 5.1 and 64.4 ± 8.3 were achieved across 15 subjects using time-domain EEG signals and frequency-embedded PSD sequences, respectively. The maximum intra-subject accuracies were 54 and 82 using EEG signals and PSD sequences, respectively. For inter-subject (pairwise) BCI, the best accuracy of 42 was achieved using both EEG signals and PSD sequences. The classification accuracies for inter-subject (pooled) experiments were 23.3 ± 1.0 and 24.5 ± 0.4, respectively, when using EEG signals and PSD sequences.

The contents of this chapter have been submitted for publication as:

Saha, S., Wagner, J and McEwan, A., Frequency-Embedded Sequence Learning for Multi-Class EEG-to-Text Interface. – Under Review.

Author Contributions: SS conceptualized the PSD and 1D-CNN-based neural decoding framework for intra- and inter-subject speech BCI experiments, implemented Python and PyTorch codes, generated results, produced figures, wrote the original draft and edited the final version. JW helped SS with software-related and GPU server-related issues. SS, JW, and AM participated in interpreting the results. JW and AM reviewed the original draft and provided feedback. All authors read and approved the final version.

5.1 Introduction

A brain-computer interface (BCI) is an alternative and augmentative communication channel that users can use to interact with their surroundings (Saha *et al.*, 2021). It is particularly beneficial for people with disabilities who encounter neurological incidents such as stroke (Mrachacz-Kersting *et al.*, 2016), spinal cord injury (Lorach *et al.*, 2023), amyotrophic lateral sclerosis (Li and Nam, 2016) and cerebral palsy (Kelly *et al.*, 2023). Disabilities span across diverse types, including paretic upper/lower limb movements, affected vision, and speech production and perception. People in completely locked-in states barely have any residual movement and communication abilities to interact with the outer world (Card *et al.*, 2024; Willett *et al.*, 2023; Metzger *et al.*, 2023; Moses *et al.*, 2021). BCIs can act as rehabilitative and assistive technologies ARTs to help users regain functional independence, thus enhancing the quality of life.

A BCI can decode speech from brain activities recorded via different invasive or non-invasive neuroimaging modalities (Saha *et al.*, 2021). The state-of-the-art neural speech decoders exploited invasive recordings of the brains' electrical activities recorded through implanted electrocorticography and demonstrated excellent performance for decoding continuous speech (Card *et al.*, 2024; Willett *et al.*, 2023; Metzger *et al.*, 2023; Moses *et al.*, 2021). They demonstrated exceptionally high-performance speech BCI and decoded up to **50** words and formed thousands of sentences by integrating BCIs with language models. Neural decoding of speech can assist people with speech production difficulties due to impairments prompted by neurological conditions. However, invasive neuroimaging requires careful assessment of whether the potential benefits of a speech BCI outweigh the risk factors associated with surgical procedures. Due to the complex nature of invasive recordings, these studies were subject-specific, lacking generalizability (Card *et al.*, 2024; Willett *et al.*, 2023; Metzger *et al.*, 2023; Moses *et al.*, 2021).

On the other hand, non-invasive BCIs offer more generalizable options for better scalability for the widespread adoption of BCI-based ARTs across broad user groups (Edelman *et al.*, 2024; Saha *et al.*, 2021). However, there is a trade-off between the degrees of freedom versus invasiveness. For people in completely locked-in states, having only a limited number of communication abilities may be adequate to promote a BCI as a state-of-the-art communication technology (Vansteensel *et al.*, 2024). Thus, non-invasive speech BCI is appropriate in that context. Electroencephalography (EEG) is the most widely used

non-invasive neuroimaging modality to capture the brain's electrical activities. An EEG-to-Text interface decodes words or phrases when users pronounce or imagine them (Lopez-Bernal *et al.*, 2024; García-Salinas *et al.*, 2023; Pawar and Dhage, 2023; Kamble *et al.*, 2023b; Cooney *et al.*, 2022; Einizade *et al.*, 2022; Lee *et al.*, 2021; Li *et al.*, 2021a; Saha and Fels, 2019; Nguyen *et al.*, 2017).

Due to diversity in subject-specific and time-variant neuroanatomical, physiological and psychological factors, EEG signals are highly variable over time and across subjects (Saha and Baumert, 2020). Thus, developing a generalized digital signal processing and pattern recognition algorithm for an EEG-to-Text interface is challenging. From a pattern recognition perspective, the inherent variability of EEG signals causes covariate shift, which is a manifestation of unlike distributions in training and testing feature spaces (Saha and Baumert, 2020; Jayaram *et al.*, 2016). Many studies applied transfer learning strategies for covariate shift adaptation that require prior domain-specific knowledge of the training and testing data (Fahimi *et al.*, 2019; Azab *et al.*, 2019; He and Wu, 2019; Zanini *et al.*, 2017). Studies proposed generative adversarial network-based domain adaptation techniques for inter-subject motor imagery classification by minimizing the covariate shifts by aligning feature distributions from the training and target subjects (Yin *et al.*, 2024; Fahimi *et al.*, 2019; Jayaram *et al.*, 2016). Saha *et al.* proposed inter-session and inter-subject associative BCI that requires no training samples from a target subject (Saha *et al.*, 2023b, 2019b, 2017b,a). In this study, we evaluate the proposed classification pipeline for assessing both intra- and inter-subject performance.

Recent advances in deep learning algorithms replace the requirement of conventional handcrafted feature engineering with nonlinear activation functions for learning patterns from data inherently (Zhang *et al.*, 2021; Bashashati *et al.*, 2007). The motivation is to learn generic features by optimizing the learnable parameters. Most common deep learning techniques include $1-$dimensional or $2-$dimensional convolutional neural networks (1D-CNN or 2D-CNN), long short-term memory, self-attention and generative adversarial network architectures (Bhatt and Sharma, 2024; Yin *et al.*, 2024; Kamble *et al.*, 2023a; Liu *et al.*, 2023b; Li *et al.*, 2022; Lee *et al.*, 2021; Cooney *et al.*, 2021; Fahimi *et al.*, 2019; Jayaram *et al.*, 2016). Although raw data are often compatible as input to deep learning architectures, such as time-domain EEG signals for training 1D-CNN, some preprocessing and feature representation or augmentation may improve the performance. This study proposes a lightweight 1D-CNN architecture for EEG-to-Text decoding using time-domain EEG signals or frequency-embedded power spectral density (PSD) sequences for classifying multi-class

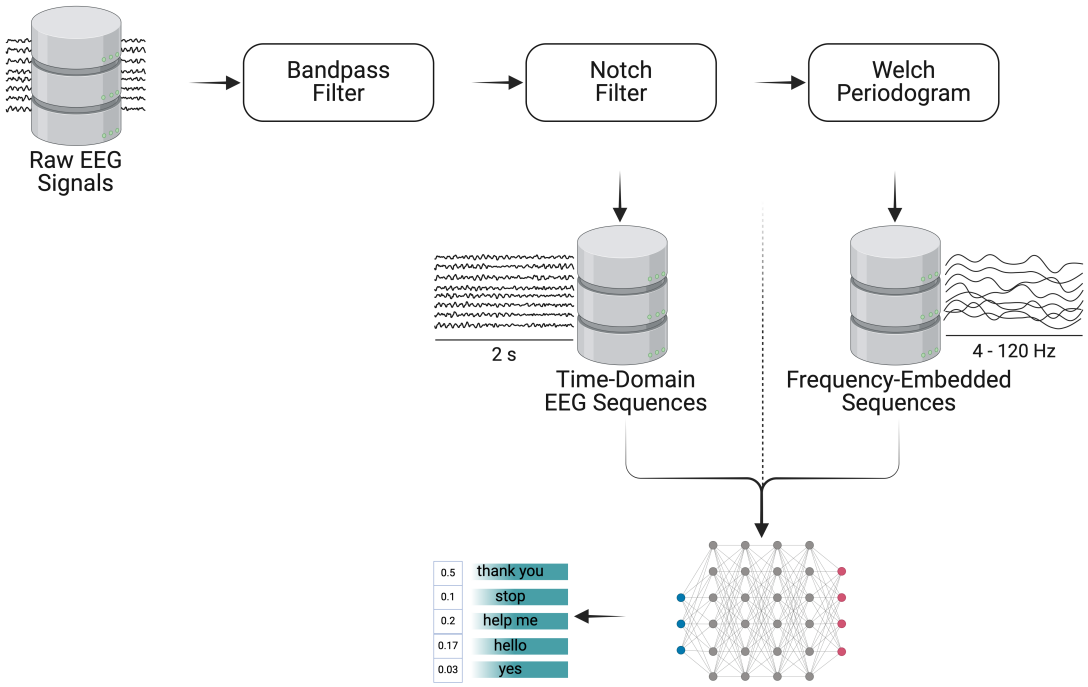

Figure 5.1. The block diagram of the proposed digital signal processing pipeline for EEG-to-Text interface. [The output probabilities are arbitrarily selected for schematic illustration only.]

imagined words/phrases. Figure 5.1 illustrates the overview of the proposed signal processing pipeline. The main contributions of this study can be summarized as follows:

- Proposing a lightweight and straightforward 1D-CNN architecture for multi-class EEG-to-Text interface.
- Comparing input feature representation for the 1D-CNN, *i.e.*, time-domain EEG signals versus frequency-embedded PSD sequences.
- Evaluating performance of intra-subject and fully zero-training inter-subject (pairwise and pooled) multi-class speech BCIs.

5.2 Materials and Method

5.2.1 About the dataset

In this study, we used a dataset from the 2020 International BCI Competition[3] (Track #3). The EEG signals were collected from 15 healthy participants. Each subject sat on a comfortable armchair in front of a computer screen, which was used to instruct the subject to imagine any of the five words or phrases, *i.e.*, 'hello', 'help me', 'stop', 'thank you' and

[3]https://osf.io/pq7vb/

'yes'. The subjects were instructed to imagine the silent pronounciation of words or phrases without articulating them or producing any sound.

The subjects were prohibited to generate any other task-specific brain activities other than the cued word or phrase and to minimize any movements and eye blinks when a cue appears or performing the task. An auditory cue corresponding to a class was presented for 2 s, followed by a cross mark on the computer screen for $0.8 - 1.2$ s. The subject then performed the given imagination task (2 s) as soon as the cross mark disappeared from the screen. Each trial initiated by a cross mark appearance on the screen and this was repeated for 4 consecutive trials followed by a rest period of 3 s.

The raw EEG signals were recorded using a BrainAmp amplifier, the BrainVision software (Brain Products GmbH, Germany) and MATLAB 2019a (The MathWorks Inc., USA). A 10-20 international configuration was used to place 64 EEG electrodes across the whole brain. While the ground electrode was placed on *Fpz*, the reference electrode was set at *FCz*. The impedance between a sensor and the skin was kept below 15 kΩ.

5.2.2 Time-domain signals versus frequency-embedded sequences

We trained the proposed 1D-CNN architecture using bandpass-filtered time-domain EEG signals and frequency-embedded PSD sequences in two different cases. We applied a Butterworth filter of order 4 with a passband of $4 - 120$ Hz. Then, we calculated PSD using the modified Welch periodogram with a 256-point discrete Fourier transform (Welch, 1967). The PSD approximates the per unit frequency-embedded power distribution of a time-domain EEG signal, and is defined as follows:

$$P_x(\omega) = \sum_{m=-\infty}^{\infty} x(m)e^{-j\omega m}. \tag{5.1}$$

Here, $x(m)$ is a time series. For M EEG channels, there were M time-domain filtered EEG signals or frequency-embedded PSD sequences as input to the 1D-CNN architecture.

5.2.3 The proposed 1-dimensional convolutional neural network architecture

A 1D-CNN can be used to learn local features from sequential data such as time-domain EEG signals or frequency-embedded PSD sequences (Kiranyaz *et al.*, 2021, 2015a,b).

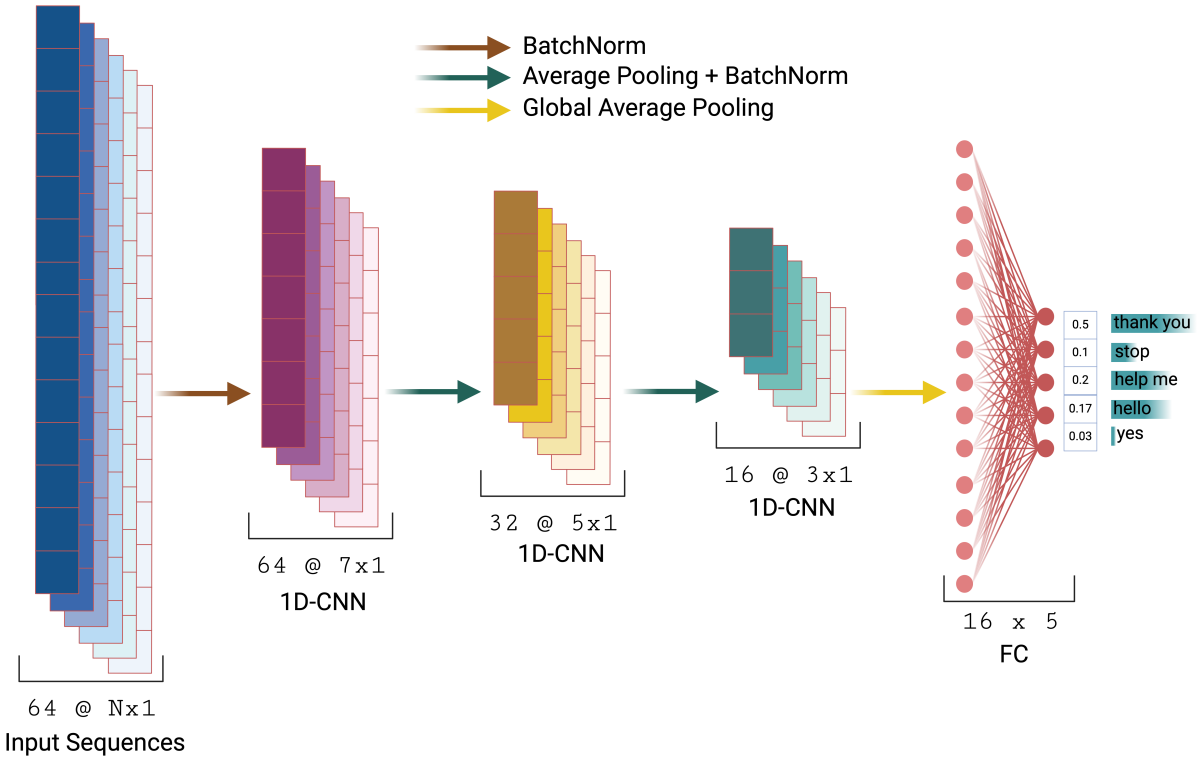

Figure 5.2. The proposed 1−dimensional convolutional neural network (1D-CNN). [N: number of input channels, FC: fully connected layer, the output probabilities are arbitrarily selected for schematic illustration only.]

Figure 5.2 illustrates the proposed 1D-CNN architecture. The multi-channel input data are passed through one or more convolutional layers. Each layer consists of $1D$ kernels with different lengths. The kernels are slid across each of the multi-channel input sequences while calculating the dot product at each point defined by the stride (number of points for moving kernels across the sequence data). The following equation refers to the convolution operation:

$$z_k = b_k + \sum_{n=0}^{M-1} y_n h_{k-n}. \tag{5.2}$$

Here, y is a 1D sequence, h is the kernel, b is a bias term, N is the number of elements in y, z is the output vector, and k defines the stride. The multi-channel data sequences are passed through all 1D-CNN layers sequentially while generating an output label. The learnable parameters such as bias and kernel weights are tuned by a backpropagation algorithm. The objective of backpropagation is to minimize a loss function, for example, the cross-entropy loss in this study.

To introduce nonlinearity into the convolutation operation (a linear function), we add a nonlinear activation function, *i.e.,* a rectified linear unit (ReLU) (Krizhevsky *et al.*, 2012). The following equation defines the ReLU operation for an input y.

$$f(y) = \begin{cases} y, & \text{if } y > 1 \\ 0, & \text{otherwise.} \end{cases} \tag{5.3}$$

For more details on 1D-CNN, please refer to (Kiranyaz *et al.*, 2021, 2015a,b).

For 64 EEG signals, we used either 64 bandpass-filtered EEG signals or 64 frequency-embedded PSD sequences as multi-channel input. We applied 64 kernels with the size of 7×1 and a stride of 1, followed by an average pooling layer with filter size of 7×1 and a stride of 3. Then, we employed 32 filters of size 5×1 and a stride of 1, followed by a second average pooling layer with kernel size 5×1 and stride of 2. In the final convolution layer, we used 16 filters of size 3×1 and a stride of 1. Finally, a global average pooling layer follows a fully connected layer of dimension 16×5 for classifying the words or phrases. Notably, a batch normalization layer was included before each convolution layer for the model's improved generalizability. We also included a dropout layer with a probability of 0.3 after each layer to reduce the chances of overfitting.

5.2.4 Intra- and inter-subject experimental settings

The dataset (5.2.1) consists of 400 trials for each subject. The objective of this study was to evaluate the proposed EEG-to-Text classification pipeline in both intra- and inter-subject settings. Figure 5.3 shows the distributions of training, validation and testing data splits. For intra-subject BCI, hold-out cross-validation settings as recommended by the BCI Competition 2020, *i.e.*, splitting subject-specific data into Training (75%), Validation (12.5%) and Testing (12.5%) sets, were used. We trained the proposed 1D-CNN using 300 trials from each subject and validated after each epoch using 50 trials from the same subject. We saved two models from each training session based on the best validation loss and accuracy, respectively. Then, we evaluated the subject-specific models on the testing trials from the corresponding subject and reported the best classification accuracy amongst that achieved by optimizing validation loss and accuracy. For inter-subject (pairwise) BCI, we applied the subject-specific models on the testing sets from all other subjects. We also proposed a 5-fold cross validation setup for evaluating inter-subject (pooled) EEG-to-Text

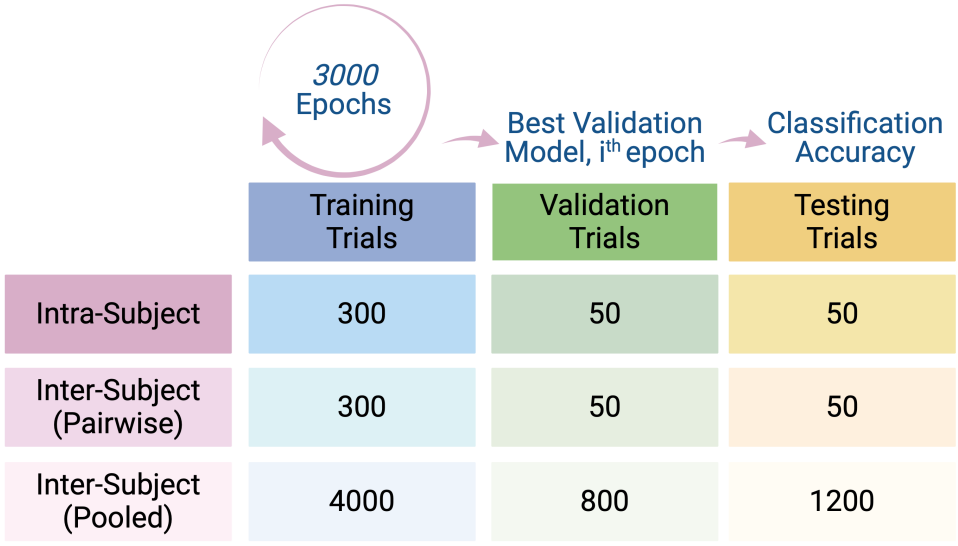

Figure 5.3. An overview of the data distributions for training, validation and testing sets for evaluating intra- and inter-subject BCI performances.

classification. The trials from all 15 subjects were dividied into 5 subsets. We kept one subset to evaluate the classification performance using the models trained and validated on the data from other 12 subjects. We shuffled the testing data for performance evaluation on every subset.

For both intra- and inter-subject experiments, we trained the models up to 3000 epochs with a set of learning rates, *i.e.*, $[1e^{-6}, 5e^{-6}, 1e^{-5}, 5e^{-5}, 1e^{-4}, 5e^{-4}, 1e^{-3}, 5e^{-3}, 1e^{-2}, 5e^{-2}, 1e^{-1}, 5e^{-1}]$. We used batch sizes $[8, 16, 32, 64, 128, 256]$ for intra-subject training while inter-subject batch sizes were $[64, 128, 256, 512, 1024, 2048]$. For each combination of learning rates and batch sizes, we ran each training session three times, totalling 216 models for each experiment.

5.2.5 Computational Resources

An AWS g5.12xlarge instance, which comprised of 48 AMD EPYC 7R32 vCPUs , 192 GB RAM and 4 NVIDIA A10 GPUs was used. Then, the intra- and inter-subject experiments were implemented using *Python* $3.9.19$ and *PyTorch* $2.3.1$ libraries. Due to a large number of trained models (*i.e.*, experiments), the training sessions were run in parallel utilising multiple GPUs.

5.3 Results and Implications

Tables 5.1 and 5.2 list the EEG-to-Text classification accuracies achieved using the subject-specific trained models. The main diagonals of the tables show intra-subject BCI performances while the remaining elements indicate inter-subject (pairwise) BCI performances. This chapter represents a classification accuracy (%) as $Acc(S_a \rightarrow S_b)$ when S_a refers to the training/validation subject and S_b is the testing subject. If $S_a = S_b$, the metric is an intra-subject accuracy. Unsurprisingly, all of the intra-subject classification accuracies but one ($S02$) were the best performing than their inter-subject (pairwise) counterparts using time-domain EEG signals. While using frequency-embedded PSD sequences, all intra-subject accuracies outperformed their inter-subject (pairwise) counterparts. When the maximum intra-subject accuracies achieved using EEG signals were $Acc(S03 \rightarrow S03) = 54$ and $Acc(S15 \rightarrow S15) = 54$, the highest accuracy using PSD sequences is $Acc(S08 \rightarrow S08) = 82$. For all subjects, the intra-subject accuracies using PSD sequences outperformed that achived using EEG signals. There were other notable intra-subject BCI performances in different cases, *i.e.*, $Acc(S03 \rightarrow S03) = 70$, $Acc(S05 \rightarrow S05) = 70$, $Acc(S07 \rightarrow S07) = 74$ and $Acc(S15 \rightarrow S15) = 72$ using the proposed PSD-based feature representation.

To benchmark the proposed EEG-to-Text classification pipeline with state-of-the-art studies, we highlighted recent studies that aimed primarily to classify imagined words or phrases in intra-subject BCI context (Table 5.3). Overall, the accuracy achived by the proposed frequency-embedded PSD sequences was 64.4 ± 8.3 that outperformed 46.1 ± 5.1 achieved using time-domain EEG signals. Lee *et al.* evaluated a CNN-based siamese neural network for EEG-to-Text classification on the same dataset used in this study. That study obtained a classification accuracy of 48.1 ± 3.9 (Lee *et al.*, 2021). There were some studies attempted to decode only two words from EEG signals and reached mean accuracies ≥ 80 (Kamble *et al.*, 2023b; Saha and Fels, 2019). Other studies used datasets comprising EEG signals associated with $3 - 15$ classes (Lopez-Bernal *et al.*, 2024; García-Salinas *et al.*, 2023; Pawar and Dhage, 2023; Cooney *et al.*, 2021; Einizade *et al.*, 2022; Nguyen *et al.*, 2017). As reported in Table 5.3, different signal processing and pattern recognition techniques were used in different studies and evaluated the classification performances on diverse datasets. There were different validation settings used in those studies; however, the results from state-of-the-art studies exhibited the overall progress in speech BCI field.

Training/Validation Subject	Testing Subject														
	$S01$	$S02$	$S03$	$S04$	$S05$	$S06$	$S07$	$S08$	$S09$	$S10$	$S11$	$S12$	$S13$	$S14$	$S15$
$S01$	**48**	30	28	34	30	30	36	30	28	36	34	34	28	28	32
$S02$	32	34	34	32	34	34	**38**	30	30	32	28	32	36	30	36
$S03$	34	34	**54**	34	36	30	30	36	32	30	30	36	36	34	34
$S04$	34	38	36	**44**	30	34	30	36	34	30	32	26	36	32	34
$S05$	28	30	38	32	**44**	34	40	30	30	32	32	38	42	32	34
$S06$	32	34	36	30	36	**48**	34	30	32	30	30	32	28	30	34
$S07$	32	34	36	32	34	32	**42**	32	32	32	32	30	30	28	32
$S08$	36	30	38	30	32	32	30	**46**	30	32	28	28	32	28	32
$S09$	26	30	28	30	26	32	28	30	**50**	32	28	30	30	34	34
$S10$	32	26	36	34	30	34	36	32	30	**42**	34	28	38	34	32
$S11$	30	34	42	28	36	34	34	34	30	34	**50**	30	36	32	36
$S12$	34	30	34	36	32	34	32	30	30	34	40	**48**	32	34	32
$S13$	34	32	34	34	40	36	36	34	30	32	32	34	**44**	32	36
$S14$	30	30	38	30	32	36	32	38	32	34	32	36	34	**44**	32
$S15$	30	30	32	32	32	34	32	28	30	36	32	36	38	38	**54**

Table 5.1. Intra- and inter-subject (pairwise) EEG-to-Text classification accuracies (%) achieved using time-domain EEG signals and the proposed 1−dimensional convolutional neural network.

Training/Validation Subject \ Testing Subject	$S01$	$S02$	$S03$	$S04$	$S05$	$S06$	$S07$	$S08$	$S09$	$S10$	$S11$	$S12$	$S13$	$S14$	$S15$
$S01$	**62**	26	34	36	28	28	28	34	36	30	30	38	32	28	30
$S02$	30	**50**	30	38	32	30	36	32	32	28	32	34	38	32	32
$S03$	30	32	**70**	32	32	30	32	32	36	34	34	36	34	32	34
$S04$	36	28	38	**60**	30	28	36	30	34	28	32	30	38	30	34
$S05$	36	26	42	36	**70**	30	28	30	32	38	30	36	34	28	34
$S06$	30	28	36	34	32	**64**	30	30	34	34	32	30	34	34	42
$S07$	32	26	28	28	36	30	**74**	34	28	30	32	30	32	28	30
$S08$	30	32	36	34	32	30	32	**82**	34	34	34	34	34	30	32
$S09$	32	28	34	28	40	34	26	28	**64**	28	26	30	30	28	36
$S10$	28	28	32	30	30	32	34	34	30	**60**	34	28	30	30	32
$S11$	32	34	38	36	32	32	30	38	30	34	**58**	34	36	34	28
$S12$	30	32	36	32	34	30	40	34	34	32	32	**62**	40	32	36
$S13$	28	30	40	34	32	32	36	38	30	34	36	32	**66**	32	34
$S14$	30	28	34	30	36	32	32	34	32	36	36	36	30	**52**	34
$S15$	38	30	38	34	32	32	30	32	34	32	32	34	36	32	**72**

Table 5.2. Intra- and inter-subject (pairwise) EEG-to-Text classification accuracies (%) achieved using frequency-embedded PSD sequences and the proposed $1-$dimensional convolutional neural network.

Study	# Classs	Methods	Validation Settings	Classification Accuracy (Mean±SD, %)
Proposed Method	5*	EEG, 1D-CNN PSD, 1D-CNN	Holdout (87.5%, 12.5%)	46.1 ± 5.1 64.4 ± 8.3
(Lopez-Bernal *et al.*, 2024)	4	WT, Inter-trial Coherence	5−Fold	61.6 ± 9.1
(García-Salinas *et al.*, 2023)	5 3	PSD, 2D-CNN	Holdout (80%, 20%)	44.0 ± 1.2 61.7 ± 3.2
(Pawar and Dhage, 2023)	5	WT, ELM	Holdout (70%, 30%)	63.7 ± 2.8
(Kamble *et al.*, 2023b)	2 15	SPWVD, 2D-CNN	10−fold	81.7 ± 4.9 51.4 ± 3.5
(Cooney *et al.*, 2021)	4	2D-CNN	5−fold	31.5 ± 4.1
(Einizade *et al.*, 2022)	4	Graph Fourier Transform	Holdout (90%, 10%)	49.1 ± 6.1
(Lee *et al.*, 2021)	6 5*	CNN-based Siamese Neural Network	5−Fold	45.0 ± 3.1 48.1 ± 3.9
(Li *et al.*, 2021a)	8	CNN	Holdout (80%, 20%)	54.3 ± 5.2
(Saha and Fels, 2019)	2#	2D-CNN, RNN, Autoencoders	Holdout (80%, 20%)	80.0 ± 7.6
(Nguyen *et al.*, 2017)	2# 3	CSP, RVM	10−fold	50.1 ± 3.5 66.2 ± 4.8

Table 5.3. A list of state-of-the-art studies where the primary objective was to classify imagined speech using EEG signals. (EEG: electroencephalography, PSD: power spectral density, 1D-CNN: 1−dimensional convolutional neural network, CSP: common spatial pattern, RVM: relevance vector machine, 2D-CNN: 2−dimensional convolutional neural network, RNN: recurrent neural network, WT: wavelet transform, ELM: extreme learning machine, SPWVD: smoothed pseudo-Wigner–Ville distribution; $*$ and # refer to two datasets used in different studies, respectively.)

5−Fold	EEG	PSD
Shuffle 1	22.7	24.4
Shuffle 2	23.8	24.6
Shuffle 3	23.0	24.5
Shuffle 4	22.3	23.9
Shuffle 5	24.8	25.1
Mean±SD	23.3 ± 1.0	24.5 ± 0.4

Table 5.4. Inter-subject (pooled) EEG-to-Text classification accuracies (%) in a 5−fold cross-validation settings.

For inter-subject (pairwise) BCI, the best classification accuracies achieved using EEG signals were $Acc(S05 \rightarrow S13) = 42$ and $Acc(S11 \rightarrow S03) = 42$ as shown in Table 5.1. Likewise, the highest inter-subject (pairwise) accuracy achieved using PSD sequences was $Acc(S05 \rightarrow S03) = 42$ as indicated in Table 5.2. Interestingly, the best inter-subject (pairwise) EEG-to-Text classification accuracies were the same using both feature representation techniques. The results from inter-subject (pairwise) experiments do not implicate any specific training-testing subject pairs showing consistent BCI performance using both feature representation techniques, and this study lacks quantification of inter-subject associativity when subject pairs share similar EEG characteristics associated with the imagined words/phrases (Saha *et al.*, 2017b, 2019b, 2017a). It is inconclusive in this study why the frequency-embedded PSD sequences do not outperform time-domain EEG signals like intra-subject BCI. In just one case, the inter-subject (pairwise) performance $Acc(S02 \rightarrow S07) = 38$ outperformed its intra-subject counterpart, $Acc(S02 \rightarrow S02) = 34$ when using time-domain EEG signals.

For inter-subject (pooled) experiements, the overall classification accuracies (Mean $\pm$ Standard Deviation) achieved using EEG signals and PSD sequences were 23.3 ± 1.0 and 24.5 ± 0.4, respectively (Table 5.3). Although a significantly larger dataset (4000 trials) was used to train the proposed 1D-CNN model as compared to subject-specific training (300 trials), the inter-subject (pooled) BCI demonstrated inferior performances than inter-subject (pairwise) experiments. The results might implicate inter-subject variablity is severe in this dataset, leading to insignificant performances in pooled experiments.

The dataset used in this study had balanced distributions of all classes in training, validation, and testing sets. Thus, classification accuracy was used as the primary metric to evaluate the performance of the proposed BCI. In addition, Figure 5.4 illustrates confusion matrices for the intra-subject BCI classification performances achieved using frequency-embedded

PSD sequences. The main diagonal of a confusion matrix represents the number of correctly predicted samples, while the remaining elements depict misclassified samples. The last two rows display the percentages of correctly and incorrectly classified observations for corresponding predicted classes. The rate of correct predictions represents class-wise precisions or positive predictive values. Similarly, the two right-most columns show the percentages of correctly and incorrectly classified observations for corresponding actual classes. The portion of correct classifications manifests class-wise recalls or true positive rates. The class-wise ('thank you') precision is 0% for subject $S02$, *i.e.*, the model did not predict any samples correctly for the phrase 'thank you'. For the best intra-subject performer, subject $S08$, the precision values are 100%, 100%, and 90% for 'help me', 'thank you', and 'yes,' respectively.

5.4 Discussion

5.4.1 Study Significance, Limitation and Future Outlook

This paper demonstrated a lightweight and straightforward 1D-CNN architecture for classifying multi-class speech utilizing time-domain bandpass-filtered EEG signals or their frequency-embedded PSD sequences. The compact structure, low computation complexity of 1D-CNN architectures compared to their $2D$ counterparts, and inherent capability to deal with sequence data make them appropriate for EEG classification (Kiranyaz *et al.*, 2021, 2015a,b). Many studies used 1D-CNN for EEG classification in various applications including identification of sleep stages (Yang *et al.*, 2021a) and classification of motor imagery tasks (Liu *et al.*, 2023b). Liu *et al.* utilized three parallel streams of $1D$ convolution filters (Liu *et al.*, 2023b), when this study illustrated only a series of three sets of $1D$ convolution filters. This study is the first proposition of 1D-CNN in the context of speech BCI while using frequency-embedded PSD sequences. García-Salinas *et al.* utilized PSD sequences to train 2D-CNN for speech classification and achieved an accuracy of 44.0 ± 1.2 in a $5-$class classification problem. This study used a different dataset and demonstrated that frequency-embedded PSD sequences showcased a higher classification accuracy of 64.4 ± 8.3 for classifying five words/phrases. Previous studies proposed frequency-embedded PSD sequences to identify different neurological conditions such as epilepsy and Parkinson's disease (Liu *et al.*, 2023a; Göker, 2023). Göker transformed time-domain EEG signals into frequency-embedded sequences using different methods such as

periodogram, Welch, and multitaper methods and fed spectral sequences into a bidirectional long short-term memory for differentiating between healthy and Parkinsonian groups (Göker, 2023). While the proposed frequency-embedded PSD sequences are compatible with 1D-CNN, this features a computationally efficient option than their $2D$ feature representation via short-time Fourier transform, wavelet transform, or smoothed pseudo-Wigner-Ville distribution to employ higher dimensional CNN architectures (Zhang *et al.*, 2024, 2021; Kamble *et al.*, 2023b). Task-related cortical modulations are frequency-specific (Sasai *et al.*, 2021; Klimesch, 2018), and thus, frequency-embedded features may be relevant for sensorimotor decoding from the brain's electrical activities. Moreover, unlike time-locked evoked potential, motor imagery or speech BCI may offer continuous neural decoding (Lopez-Bernal *et al.*, 2024; García-Salinas *et al.*, 2023; Pawar and Dhage, 2023; Kamble *et al.*, 2023b; Cooney *et al.*, 2022; Einizade *et al.*, 2022; Saha *et al.*, 2019b; Lee *et al.*, 2021; Li *et al.*, 2021a; Saha and Fels, 2019; Saha *et al.*, 2017b,a; Nguyen *et al.*, 2017; Saha *et al.*, 2016), in which frequency-embedded feature space may become more relevant than the time-domain attributes. Future studies are critical to understanding frequency-embedded features' applicability for the EEG-to-Text interface.

This study also promotes a fully zero-training speech BCI by featuring inter-subject (pairwise) and inter-subject (pooled) experiments. Due to inherent EEG signal variabilities across subjects, poor data quality may originate from diverse subjects who might share distant feature spaces, cause covariate shifts, and negatively impact the performance of deep learning methods. Thus, covariate shift adaptation techniques for inter-subject transfer learning are preamble to minimize or eliminate the tedious calibration sessions for user-specific training of a BCI. While most inter-subject BCIs require at least a few training samples (Jayaram *et al.*, 2016), this study demonstrated a good inter-subject (pairwise) classification accuracy (42%) without any training trial from the target subject, demonstrating the potential to develop a generalized multi-class EEG-to-Text interface. The best overall classification performance of the inter-subject (pooled) BCI is 24.5 ± 0.4 using frequency-embedded PSD sequences, which is above the chance level (*i.e.*, 20% for five classes) although inferior to inter-subject (pairwise) BCI. This study does not attribute any quantification of inter-subject associativity that could describe the poor performance of inter-subject (pooled) BCI. Recent studies have investigated if a subset of subjects shares similar EEG characteristics so that a proposed neural decoder can capture inter-subject associative task-related feature domains. Selecting data only from inter-subject associative subjects may attribute task-specific inter-subject generalizable features for increased BCI performance (Saha *et al.*, 2023b, 2019b; Fahimi *et al.*, 2019; Saha *et al.*, 2017b,a; Kang and

Choi, 2014; Kang *et al.*, 2009). Future studies may extend this work to quantify inter-subject associative subjects who can show increased EEG-to-Text classification performance.

5.4.2 Neural Mechanisms of Speech Imagination

Language is a complex skill that attributes to speech production and perception (Poeppel and Assaneo, 2020). They involve a diverse range of sensorimotor, cognitive and affective skills. For example, speech production involves articulatory muscle activations that refers to a motor task, comprising neural signatures associated with motor preparation and execution, respectively. There are substantial evicences for motor imagery as they share similar neural substrates to their corresponding actual motor actions (Jeannerod and Decety, 1995; Guillot *et al.*, 2012; Zich *et al.*, 2015). Likewise, speech imagery may share similar neural substrates as their actual articulation. However, their underlying neurophysiological mechanisms are still not well-understood (Chung *et al.*, 2023; Pratts *et al.*, 2023). Imagination can take different forms when a user imagining speech in their articulatory (production) or perception (hearing) form, and each form is associated with their distinct neural modulation patterns (Nalborczyk *et al.*, 2023). Lu *et al.* illustrated that imagery and perception of hearing showed functionally distinct neural substrates (Lu *et al.*, 2023). However, imagined speech may share the same neural oscillations as their articulated counterparts (Watanabe *et al.*, 2020). If true, imagined speech-based BCIBCI, like motor imagery-based ARTs, can benefit people with disabilities who are unable to produce speech (Bhatt and Sharma, 2024; Liu *et al.*, 2023b; Saha *et al.*, 2021, 2019b; Azab *et al.*, 2019; Zich *et al.*, 2015).

There are foundational elements of speech, such as phonemes, syllables, vocals and words. In automatic speech recognition, studies demonstrated various algorithms to understand the main components of speech signals and their impact on speech decoding (Benzeghiba *et al.*, 2007). Likewise, several BCI studies attempted to decode these fundamental parts of speech signals from EEG and demonstrated their potentiality in EEG-to-Text classification (Cooney *et al.*, 2022; Lopez-Bernal *et al.*, 2022; Deng *et al.*, 2010). While advanced signal processing and pattern recognition algorithms are essential to developing successful speech BCI, it is equally important to understand the underlying neural mechanisms associated with speech's critical elements (Fernyhough and Borghi, 2023; Nalborczyk *et al.*, 2023; Poeppel and Assaneo, 2020), mainly those contributed to state-of-the-art speech recognition algorithms (Benzeghiba *et al.*, 2007).

Figure 5.4. Confusion matrices for intra-subject BCIs when using frequency-embedded PSD sequences for classifying words/phrases.

5.5 Conclusion

This study demonstrated a modified Welch periodogram-based frequency-embedded PSD sequence representation for 1D-CNN in the intra- and inter-subject EEG-to-Text classification contexts. The results implicated that using PSD sequences outperformed EEG signals for the proposed method. This study further highlights the potential of imagined speech BCIs as alternative and state-of-the-art ARTs for people with disabilities.

Chapter Context:

This chapter demonstrated a modified version of the 1D-CNN architecture described in chapter 4 for classifying multi-class text classification tasks for intra- and inter-subject BCIs. Bandpass-filtered time-domain EEG signals and frequency-embedded PSD sequences were used as input for training the 1D-CNN model. The proposed BCI outperforms the state-of-the-art speech BCIs using non-invasive EEG signals.

The next chapter summarizes the overall contribution of this thesis with discussions on study limitations and future outlooks by reflecting on recent progress in BCI field.

Study Significance, Limitations and Future Outlook

6

THIS chapter summarizes the main contributions of this thesis, featuring a critical evaluation of brain-computer interfaces BCIs as state-of-the-art assistive and rehabilitative technologies (ARTs) and the propositions of inter-subject associative BCIs in the contexts of imagined movement and speech classification from the brain's electrical activities.

6.1 Study Significance

6.1.1 Personalized Assistive and Rehabilitative Technologies

A brain-computer interface (BCI) is an advanced human-computer interface featuring diverse assistive and rehabilitative technologies (ARTs) for people with disabilities (Willett *et al.*, 2023; Metzger *et al.*, 2023; Huggins *et al.*, 2022; Willett *et al.*, 2021; Flesher *et al.*, 2021; Moses *et al.*, 2021; Orlandi *et al.*, 2021; Saha *et al.*, 2021; Karlsson *et al.*, 2022). The first proposition of a BCI was for rehabilitation of impaired motor functions (Vidal, 1973); however, the recent evolution of BCI in diverse areas includes assistive and communication technologies. The beauty lies in BCI applications' eclectic nature for tailoring them to fulfill individual needs (French *et al.*, 2024; Huggins *et al.*, 2015; Nijboer *et al.*, 2014; Huggins *et al.*, 2011). People in post-neurological incidents suffer the burden of diverse types of disabilities, preventing them from accessing mainstream socioeconomic life (Metzger *et al.*, 2023; Bekteshi *et al.*, 2023; Monforte *et al.*, 2021; Makris *et al.*, 2021; Micera *et al.*, 2020; Goulet *et al.*, 2019; Milekovic *et al.*, 2018; Goldstein and Abrahams, 2013). This thesis attributes a critical discussion on BCI-based ARTs following a user-centric perspective. French *et al.* have discussed the importance of inclusive designs of ARTs, considering users' perspectives to subjective and objective evaluations such as BCI performance, user satisfaction and preferences, and accessibility (French *et al.*, 2024). It highlights essential ingredients of modern neural technologies driving notable BCI advancement as discussed in Chapter 2, a narrative (literature) review. There has been tremendous progress in developing neural sensors, leading to the BCI-based ARTs research directions. Noninvasive options are more scalable than invasive counterparts, such as microelectrode arrays, due to minimum or no risk factors for not requiring implantation but as plug-and-play gadgets (Edelman *et al.*, 2024; Saha *et al.*, 2021). Electroencephalography (EEG) is the most widely used neuroimaging technique, featuring a low-cost, easy-to-maintain, and portable option that promotes BCI-based ARTs for a diverse and large group of people, including those with disabilities.

6.1.2 Generalized Brain-Computer Interface Algorithms

While the diverse BCI applications offer unique support to each individual, fulfilling user needs through personalization, the decoding algorithms require individual calibration for each BCI use. Calibration is tedious and often frustrating for users, especially those with

limited communication abilities due to disabilities. The training and testing feature spaces differ because of inter-session and inter-subject variabilities in EEG signals, impacting BCI performance (Saha and Baumert, 2020; Saha *et al.*, 2019b, 2017b,a). Transfer learning strategies such as domain adaptation lessen the difference between feature spaces, demanding fewer training trials for calibration (Wei and Ding, 2023; Chen *et al.*, 2022; He and Wu, 2019; Azab *et al.*, 2019, 2018; Jayaram *et al.*, 2016). However, a fully zero-training BCI requiring no training trial benefits users when the model parameters are reproducible across sessions and subjects. Diversity in human neuroanatomical, neurophysiological, psychological, and cognitive characteristics contribute to EEG signal variabilities and, thus, developing inter-subject BCI is challenging (Saha *et al.*, 2021; Saha and Baumert, 2020). Predicting similarity across subjects may promote more generalized neural decoding algorithms; therefore, inter-subject associative BCI (Arı and Taçgın, 2024; Han *et al.*, 2024; Saha *et al.*, 2023b; Roy *et al.*, 2020; Saha *et al.*, 2019b, 2017b,a; Handiru and Prasad, 2016). This thesis presents a Bhattacharya distance-based predictor for intra- and inter-subject BCI performance as discussed in Chapter 3. Not all subjects share similar brain dynamics manifested in EEG signals; notwithstanding, studies demonstrated inter-subject associativity amongst some subjects. Hence, inter-subject associative BCIs correspond to pools of subjects when subjects in each pool showcase similar EEG features. The current literature does not provide substantial evidence for effectively measuring inter-subject associativity. The proposed predictor in chapter 3, along with other recent studies, proposed BCI performance predictors that utilized training samples for calculating the distance between inter-subject feature spaces (Saha *et al.*, 2023b, 2019b; Wronkiewicz *et al.*, 2015; Kang and Choi, 2014; Kang *et al.*, 2009).

6.1.3 Digital Signal Processing with Artificial Intelligence

EEG signals are nonlinear and nonstationary (Cohen, 2017); however, the primary objective of any neural decoding algorithm is to recognize intrinsic patterns associated with users' intentions or cognitive states. From a pattern recognition viewpoint, it is essential to transform EEG signals into intrinsic patterns that do not change due to the nonlinear and nonstationary nature of EEG signals. Significant advances in digital signal processing (DSP) algorithms have facilitated neural decoding algorithms for BCI (Lotte *et al.*, 2018, 2007; Bashashati *et al.*, 2007). Conventional handcrafted feature extraction from EEG signals may not sufficiently capture the changeable brain features. Nevertheless, recent developments in artificial intelligence AI techniques attribute built-in nonlinear activation

functions for directly learning more generic features from data (Zhang *et al.*, 2024; García-Salinas *et al.*, 2023; Bu *et al.*, 2023; Wang *et al.*, 2023b; Cooney *et al.*, 2021; Zhang *et al.*, 2021; Kiranyaz *et al.*, 2021; Roy *et al.*, 2020; Hua *et al.*, 2019; Pérez-Zapata *et al.*, 2018; Kiranyaz *et al.*, 2015b). There are preprocessing steps to augment and transform raw signals. Signal transformation by DSP techniques enhances signal quality or makes raw signals compatible with an AI architecture. Convolutional neural network (CNN) architectures, initially proposed for pattern recognition from $2-$dimensional ($2D$) data, *e.g.*, images, can apply for EEG classification tasks. The idea is to transform time-domain $1D$ multi-channel signals into $2D$ images by wavelet or short-term Fourier transform for time-frequency representation (Pawar and Dhage, 2023; Kamble *et al.*, 2022). This thesis demonstrates 1D-CNN architectures in Chapters 4 and 5 that can deal with multi-channel sequence data, such as time-domain EEG signals (Kiranyaz *et al.*, 2021, 2015a,b).

The proposed 1D-CNN DSP frameworks evaluate intra- and inter-subject BCI classification performance in imagined motor and speech recognition tasks, respectively. There are three different feature representation techniques, *i.e.*, bandpass filtered time-domain EEG signals, power spectral density (PSD), and bi-channel cross power spectral density (CPSD) sequences calculated using Welch periodogram (García-Salinas *et al.*, 2023; Welch, 1967) for training the proposed DSP frameworks. A previous study utilized PSD sequences for motor imagery classification (Herman *et al.*, 2008). Chapter 4 compares results achieved using time-domain bandpass filtered EEG signals, frequency-embedded PSD and CPSD sequences with 1D-CNN architectures for classifying two imagined movements. The proposed methods outperform common spatial pattern (CSP)-based methods, implicating the utility of 1D-CNN with different time/frequency input sequences. Then, chapter 5 extends the experiments to a speech BCI dataset for decoding multi-class imagined speech using time-domain EEG signals and frequency-embedded PSD sequences with a modified 1D-CNN architecture.

As proposed in Appendix A, other methods that can directly deal with sequence data include long short-term memory (LSTM) architectures. That study uses a time-embedded feature representation of EEG signals for predicting comatose patients' recovery (Saha *et al.*, 2023a). Although some AI techniques, such as 1D-CNN and LSTM architectures, can intrinsically deal with time-domain multi-channel EEG signals (Kiranyaz *et al.*, 2021; Saha *et al.*, 2023a), this thesis demonstrates that DSP-based spectral feature representation may perform better than that achieved using time-domain signals. Transformer is another deep learning architecture that readily deals with sequence data (Yenduri *et al.*, 2024). Although

it was initially proposed for natural language processing, it has shown promise for inter-subject BCI (Liu *et al.*, 2024). Recent studies have also applied generative AI techniques, such as generative adversarial networks, to develop sensorimotor BCI algorithms.

6.2 Study Limitations And Future Outlook

This thesis contributes to the field by proposing a novel inter-subject associativity predictor and DSP and AI-based neural decoding algorithms in the context of intra- and inter-subject BCI for decoding imagined movements or speech. The proposed methods, validated on two publicly available datasets, may require further investigations on larger datasets to evaluate the generalizability of the methods. The motor imagery (MI) dataset comprises 280 trials of EEG signals from only five subjects to classify only two MI tasks. However, the speech BCI dataset is more extensive, containing 400 samples collected from 15 subjects for classifying 5 words or phrases.

While the CSP-based neural decoding algorithms are computationally fast and do not require high training time, training 1D-CNN algorithms require high computational time. The $5-$fold cross-validation setup in Chapter 4 on MI dataset increased the required trained models for intra-dataset shuffling to produce robust results due to the optimization of hyperparameters such as learning rate and batch size, resulting in multiple training session for each model. The proposed speech BCI in chapter 5 used a holdout cross-validation setting for reducing the number of training sessions, which may limit the investigation of within-subject EEG signal variabilities and their impact on BCI performance.

Inter-subject associative BCI is an emerging research focus area as a parallel research direction on transfer learning strategies (Bu *et al.*, 2023; Chen *et al.*, 2022; Roy *et al.*, 2020; Saha *et al.*, 2019b; Azab *et al.*, 2019; Saha *et al.*, 2017b,a; Wronkiewicz *et al.*, 2015; Kang and Choi, 2014; Kang *et al.*, 2009; Hammer *et al.*, 2012). A myriad of studies carefully investigated the potential sources of inter-subject variabilities to identify predictors of BCI performance (Cueva *et al.*, 2025; Saha *et al.*, 2023b; Saha and Baumert, 2020; Saha *et al.*, 2019b; Wronkiewicz *et al.*, 2015; Kasahara *et al.*, 2015; Kang and Choi, 2014; Hammer *et al.*, 2012; Kang *et al.*, 2009). While these studies complement our understanding of variable EEG signals across users, more comprehensive studies may include an analysis of potential sources of these variabilities. This thesis included data-driven quantification of inter-subject variabilities or associativity in chapter 3 (Saha *et al.*, 2023b); however, the datasets used in the investigations do not have any secondary information regarding the

sources of these variabilities. Previous studies proposed inter-subject source localization techniques correlating projected MI cortical sources with BCI performance (Saha *et al.*, 2019b, 2017a; Wronkiewicz *et al.*, 2015). Similar to the proposed predictor discussed in Chapter 3, these techniques need training trials to calculate the inter-subject predictors. These are not ideal options when the requirement of training trials still exists when the aim is to develop a fully zero-training BCI. Recent studies have proposed resting EEG-based predictors for inter-subject associative BCI, which may utilize only $1-$minute of resting EEG signals for correcting inter-subject baselines for high performance BCIs (Park and Jun, 2024; Kwak *et al.*, 2023; Leeuwis *et al.*, 2021; Gu *et al.*, 2020; Li *et al.*, 2019; Deco *et al.*, 2011). This thesis does not present a practical solution to quantify inter-subject differences in EEG feature spaces. However, the proposed neural decoding algorithms demonstrate the feasibility of fully zero-training BCIs classifying imagined movement or speech.

6.3 Conclusion

Inter-subject associative BCI is a emerging area in the neural engineering field, which can benefit people with disabilities by promoting BCI-based ARTs as scalable and accessible options. Noninvasive signal acquisition is a preference, but intrinsic variabilities in brain dynamics reflected in EEG signals hinder the reproducibility of neural decoding algorithms demanding calibration sessions. In addition to the transfer learning strategies to compensate for the variabilities, quantifying inter-subject associativity that identifies pools of subjects showing similar brain signals can foster the development of generalized BCI decoding algorithms. This thesis has successfully demonstrated inter-subject associative BCI with small datasets and limited experimental flexibilities. However, the results implicates the feasibility of inter-subject associative BCI algorithms, motivating toward achieving completely zero-training BCI models. The proposed integration of AI architectures with DSP techniques highlights the relevance of conventional DSP algorithms in BCI research, both in intra- and inter-subject settings. In addition to generic feature learning using the proposed 1D-CNN architecture, results suggest that spectral representations of EEG signals, *i.e.*, PSD, and CPSD sequences are superior to temporal EEG signals for speech BCI. Nonetheless, a practical predictor of inter-subject associative BCI still needs to be found. Thus, future works should emphasize identifying a predictor that only requires no or negligible calibration efforts; for example, using only $1-$minute resting EEG looks like a practical solution (Kwak *et al.*, 2023).

A

Time-Embedded EEG Sequence Learning for Comatose Patients' Prognosis

In an intensive care unit (ICU), an accurate prognosis of comatose patients' recovery is critical for ongoing medical interventions. Patient prognosis guides decisions around continuation of care. Patients may recover from a coma despite poor initial prognosis; thus, more reliable predictors for recovery are needed. Electroencephalography (EEG)-based neurological markers may complement the current prognosis. The PhysioNet Challenge 2023 includes a dataset of EEG signals and clinical attributes from a total of 1020 adult patients in ICUs that remained in a coma after cardiac arrest, 607 of whom were dedicated to algorithmic training. We conceptualized a novel time-embedded feature space for continuous EEG followed by a bidirectional long short-term memory (LSTM) for learning any temporal patterns associated with comatose patients' recovery. We extracted EEG-related attributes: dynamic range, skewness, kurtosis, and subband (δ, θ, α and β) power after selecting 1 minute/hour EEG using a preprocessing algorithm. With a false positive rate < 0.05, the true positive rate (TPR) was the scoring metric at the 72^{nd} hour post cardiac arrest. Our team, USYD_BrainBuzz ranked 27^{th} and achieved scores of 0.26, 0.51 and 0.40 on the training, validation and testing sets, respectively. Results implicated that our approach has shown promise for continuous monitoring of comatose patients.

The contents of this chapter have been published in 2023 Computing in Cardiology (CinC) as:

Saha, S., Alam, R.U., Samore, A., Goodwin, A., Wong, M.L.S., McEwan, A. and Anderson, C., 2023, October. Time-Embedded EEG Sequence Learning for Comatose Patients' Prognosis. In *2023 Computing in Cardiology (CinC)* (Vol. 50, pp. 1-4). IEEE.

Author Contributions: SS led a team from the University of Sydney to participate in the Physionet Challenge for 2023. SS and RUA participated in discussions with other team members, independently worked on multiple implementations of diverse algorithms, and submitted them to the competition. This work presents the best-scored classification algorithm submitted by SS.

SS conceptualized the time-embedded feature representation for LSTM-based signal processing framework for predicting comatose patients' recovery in ICUs, implemented MATLAB codes, generated results, produced figures, wrote the original draft and edited the final version. RUA wokred on Python-based algorithms. All authors participated in the discussion and read and approved the final manuscript.

A.1 Introduction

Electroencephalography (EEG) is a clinical marker for investigating various neurological conditions, including predicting comatose patients' recovery after cardiac arrest (Reyna *et al.*, 2023; Saha *et al.*, 2021). Expert visual inspection of multi-day EEG signals is tedious. Results are often subjective, and inaccurate clinical assessment may lead to a catastrophic outcome. For example, the decision to continue life support depends on the accurate prognosis, but erroneously withdrawing life support can cause death (Kondziella *et al.*, 2023).

Advances in signal processing and artificial intelligence algorithms offer an alternative to manual clinical assessment of EEG signals (Zubler and Tzovara, 2023). Recent studies developed predictive models based on 1-dimensional convolutional neural network (1D-CNN), long short-term memory (LSTM) and transformer architectures for time-series or sequential data analysis (Hua *et al.*, 2019). Other methods include transforming data sequences into images to apply 2D-CNN for feature learning associated with coma and healthy states (Zubler and Tzovara, 2023). In this study, we have demonstrated a novel algorithm featuring signal-processing-based EEG feature extraction followed by LSTM-based time-embedded sequence analysis for predicting comatose patients' recovery.

A.2 The PhysioNet Challenge 2023

A.2.1 The Dataset

A group of researchers from the USA and Europe collected the data from seven different hospitals as part of the International Cardiac Arrest REsearch consortium (I-CARE) (Amorim *et al.*, 2023; Goldberger *et al.*, 2000; Reyna *et al.*, 2023). The dataset consists of 1020 patients who were in coma post cardiac arrest. The data were divided into three subsets: training, validation and testing. All participants had access to only the training set ($n = 607$) to develop their algorithms. The organizers then evaluated the submitted algorithms on the validation set, followed by the final evaluation on a testing set for selecting the competition winners.

Cerebral Performance Category (CPC) was used to classify the recovery on a scale of $1-5$. While scores 1 and 2 refer to good outcomes (good neurological functions to moderate disabilities), scores 3, 4 and 5 demonstrate poor recovery (severe neurological disabilities, coma or vegetative state to death). For this competition, the aim was to develop algorithms

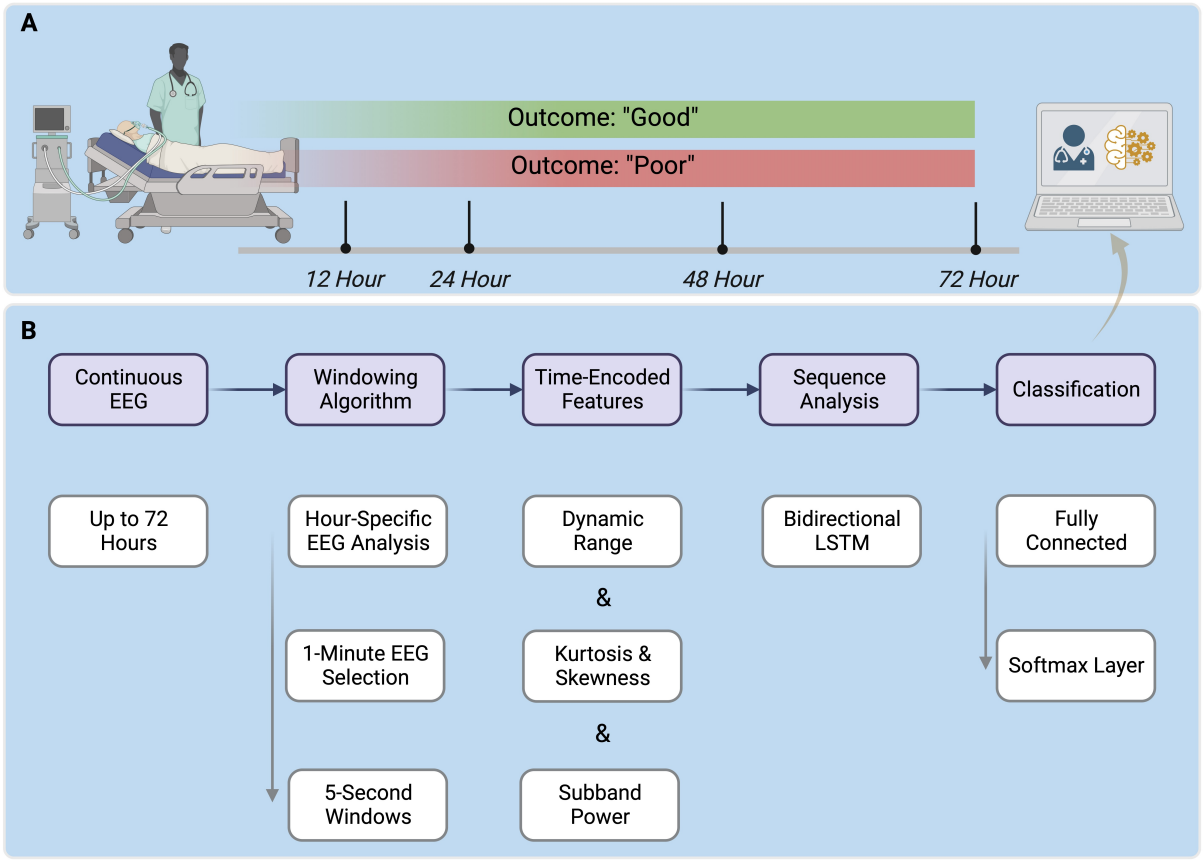

Figure A.1. A schematic illustration of (A) continuous monitoring in an intensive care unit and (B) the block diagram of the proposed EEG Sequence Learning Algorithm.

for predicting good versus poor outcomes. The number of patients with good and poor outcomes in the training set was 225 and 382, respectively.

A.2.2 The Proposed Algorithm

Figure A.1 illustrates the clinical environment and the block diagram of the proposed classification algorithm. Continuous EEG signals were collected up to several days, but for the competition we used data up to 72 hours. We utilized only 9 unipolar EEG to construct 12 bipolar EEG signals (*i.e.*, F3-C3, C3-P3, Fz-Cz, Cz-Pz, F4-C4, C4-P4, Fz-F3, Fz-F4, Cz-C3, Cz-C4, Pz-P3 and Pz-P4). The signals were resampled to a sample frequency $Fs = 100$ Hz followed by band pass filtering with corner frequencies 0.5 and 32 Hz. We used a zero-phase Butterworth filter with an order 4.

Windowing Algorithm and Features

We divided each hour data into 1-minute segments followed by calculating 99% power and corresponding bandwidth (bandwidth) for each segment. For each hour, the mean values were calculated for bandwidth and power. The Euclidian distance between each 1-minute segment's bandwidth and power, and mean bandwidth and power was then estimated. The distance metric was averaged over 12 bipolar channels. The segment with minimum distance was then selected. Finally, each 1-minute signal was further divided into 5-second windows for feature extraction.

Dynamic Range: Dynamic range was defined as the difference between 5^{th} and 95^{th} percentiles.

Skewness and Kurtosis: The skewness and kurtosis measure higher order statistical properties of a random signal and are defined as follows, respectively:

$$s = \frac{E(x-\mu)^3}{\sigma^3}, \tag{A.1}$$

$$k = \frac{E(x-\mu)^4}{\sigma^4}. \tag{A.2}$$

Here μ and σ are mean and standard deviation of x, and E refers to the expected value.

Subband Power: EEG signals were divided into four subbands, *i.e.*, δ $(0.5-4$ Hz), θ $(4-8$ Hz), α $(8-14$ Hz) and β $(14-30$ Hz). The power of each subband signal was then calculated as sum of the absolute squares of their time domain samples divided by the signal length.

We also utilized the clinical information such as age (in years), sex, time to return of spontaneous circulation from cardiac arrest, in-hospital or out of hospital cardiac arrest, targeted temperature (in Celsius). The clinical features were normalized to 0 to 1.

Time-Embedded Feature Space

All features were represented with time-embedding. For any feature, the first 12 values extracted from 5-second windows for any hour were embedded in chronological order, resulting a total of $12 \times 72 = 864$ attributes for each channel up to 72 hours. There were cases when no data were available for different hours contributing not a number (NaN) values. Data imputation, *i.e.*, NaN values were replaced with 0 to keep the feature space equal size for all patients while preserving temporal information.

Layer Type	Information
Input	Sequence data size 85×864
Bi-LSTM	No. of hidden units 128
Dropout	Probability 0.2
Bi-LSTM	No. of hidden units 64
Dropout	Probability 0.2
Bi-LSTM	No. of hidden units 32
Dropout	Probability 0.2
Fully-connected	No. of neurons 2
Softmax	Output

Table A.1. Specifications of the Bidirectional LSTM model.

Sequence Analysis for Classification

We then applied bidirectional LSTM for analyzing whether the time-embedded feature space depict any trends for differentiating between good and poor outcomes. LSTM is a recurrent neural network-based feature learning algorithm suitable for sequence data analysis. The output of our proposed LSTM model was fed into a fully-connected layer following classification with a softmax layer. Table A.1 lists specifications of the bidirectional LSTM architecture. The LSTM training options are optimizer - Adam, gradient threshold - 1, no of epochs - 250, learning rate - 0.001, $L2$ regularization - 0.1, shuffle - every epoch and environment - GPU. Dividing the training set ($n = 607$) into two subsets, features from only 500 patients (held-out subset of the training set) were used to train the model, and the remaining data from 107 patients (training set indices: $201 - 307$) were used for validation. The output network was evaluated on the training and unseen validation and testing sets.

A.2.3 Computational Resources

We implemented the proposed algorithm in MATLAB 2023a. The codes were then run on a g4dn.4xlarge instance on AWS featuring 16 vCPUs, 64 GB RAM (60 GB usable), 300 GB of local storage excluding the dataset, and an optional NVIDIA T4 GPU. For computing with GPU, we had a limit of 48 hours to train our proposed model followed by 24 hours for validation.

A.2.4 Performance Metrics

Assuming that poor outcome and good outcome represent positive and negative classes, respectively, the true positive rate (TPR) was calculated at a decision threshold using the

	Training	Validation	Testing
Score	0.26	0.51	0.40

Table A.2. Scores on training, validation and testing sets.

following equation:

$$TPR = \frac{TP}{FP + FN}. \tag{A.3}$$

The false positive rate (FPR) was calculated such that

$$FPR = \frac{FP}{FP + TN} < 0.05. \tag{A.4}$$

Here, TP, FP, TN and FN are the total number of true positives, false positives, true negatives and false negatives, respectively.

A.3 Results and Discussion

We achieved scores of 0.26, 0.51 and 0.40 on the training, validation and testing sets when constrained to FPR < 0.05 (Table A.2). The performance needs to be improved before an automated algorithm can be used in a clinical settings. Figure A.2 illustrates time-embedded representation of dynamics range, skewness , kurtosis and subband (δ, θ, α and β) powers. Further investigation is essential if the selected 1-minute data reflect associated physiological changes for differentiating comatose condition from healthy state.

There were missing data posing challenges for feature representation as input to the proposed sequence learning model. Imputing missing data streams, *i.e.*, replacing NaN values with zero may have biased the training of the proposed algorithm. In some cases, there were only a few hours of EEG signals available, which seems inadequate for learning useful temporal patterns as we hypothesized in our study.

Due to the time constraints of the PhysioNet Challenge 2023, there have been unexplored avenues of the dataset. For example, supplementary signals like electrocardiography (ECG) may offer complementary information to the proposed time-embedded feature representation. Future studies may include heart rate variability-related features extracted from ECG. The proposed time-embeddings of the EEG-extracted attributes demand further investigation into whether the sequence learning for predicting comatose patients' recovery is suitable in the clinical context. The training time limit of 48 hours restricted our opportunities

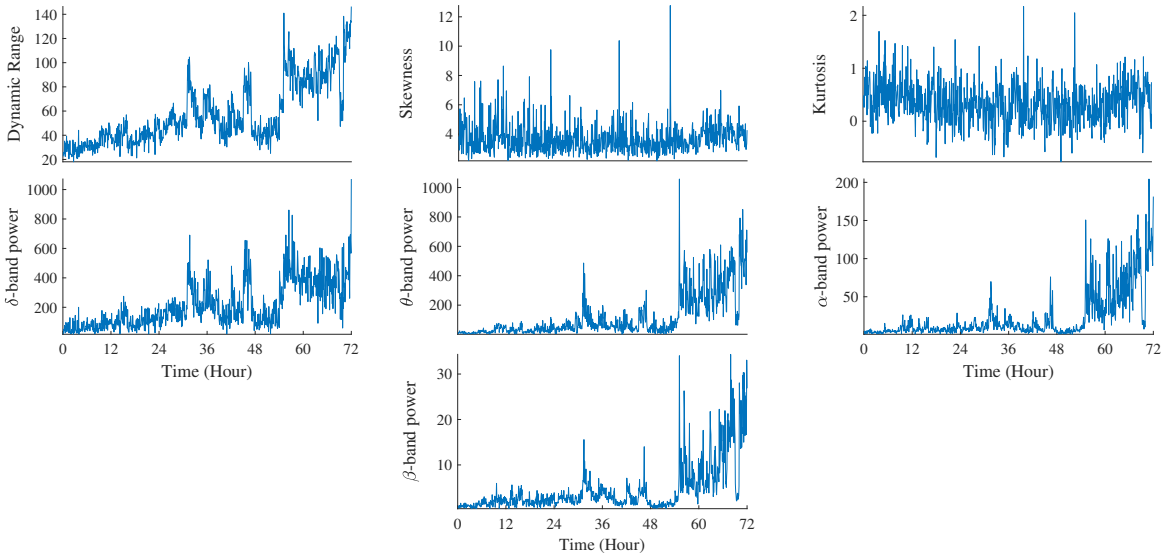

Figure A.2. The time-embedded feature representation extracted from bipolar C3-P3 channel for a subject (ID #0553).

to explore more complex artificial intelligence-based algorithms. A more extensive dataset than only 1 minute/hour EEG signals may accommodate training a complex model.

A.4 Conclusion

We ranked 27^{th} and achieved scores of 0.26, 0.51 and 0.40 on the training, validation and testing sets, suggesting that time-embedded feature representation enables recovery prediction based on EEG alterations over time. Further studies are needed to evaluate the clinical utility of our proposed algorithm and whether it is adaptable for real-time continuous monitoring of comatose patients' recovery in ICUs.

Overcoming Uncertainties in Electrogram-Based Atrial Fibrillation Mapping: A Review

B

In clinical rhythmology, intracardiac bipolar electrograms (EGMs) play a critical role in investigating the triggers and substrates inducing and perpetuating atrial fibrillation (AF). However, the interpretation of bipolar EGMs is ambiguous due to several aspects of electrodes, mapping algorithms and wave propagation dynamics, so it requires several variables to describe the effects of these uncertainties on EGM analysis. In this narrative review, we critically evaluate the potential impact of such uncertainties on the design of cardiac mapping tools on AF-related substrate characterization. Literature suggest uncertainties are due to several variables, including the wave propagation vector, the wave's incidence angle, inter-electrode spacing, electrode size and shape, and tissue contact. The preprocessing of the EGM signals and mapping density will impact the electro-anatomical representation and the features extracted from the local electrical activities. The superposition of multiple waves further complicates EGM interpretation. The inclusion of these uncertainties is a non-trivial problem but their consideration will yield a better interpretation of the intra-atrial dynamics in local activation patterns. From a translational perspective, this review provides a concise but complete overview of the critical variables for developing more precise cardiac mapping tools.

The contents of this chapter have been published in Cardiovascular Engineering and Technology as:

Saha, S., Linz, D., Saha, D., McEwan, A. and Baumert, M., 2024. Overcoming uncertainties in electrogram-based atrial fibrillation mapping: A review. *Cardiovascular Engineering and Technology*, 15(1), pp.52-64.

Author Contributions: SS conceived this review's idea, developed the initial proposal, prepared graphical illustrations, wrote the original draft, and edited and finalized the manuscript. DL, DS, MB, and AM reviewed the first draft and provided feedback. DS contributed to Figures B.1 and B.1 All authors read and approved the final manuscript.

B.1 Introduction

Atrial fibrillation (AF) is a global health burden that affects an estimated 60 million people worldwide (Elliott *et al.*, 2023; Essien *et al.*, 2021). It is the most common arrhythmia in humans, which occurs in the presence of irregular and disorganized electrical activities in the atrial conduction system (ACS) (Schotten *et al.*, 2021; Quah *et al.*, 2021; Roney *et al.*, 2019b; Wijesurendra and Casadei, 2019; Cheniti *et al.*, 2018; Nattel and Dobrev, 2017; Schotten *et al.*, 2011). An electrical signal passes rhythmically through specific (cardiac) conduction pathways and maintains the heart's pumping activity in sinus rhythm (SR) (Karki *et al.*, 2021; Padala *et al.*, 2021). However, structural remodeling of the arrhythmogenic substrates disrupts regular cardiac conduction dynamics in ACS, leading to AF.

Catheter-based isolation of the pulmonary veins represents the cornerstone of interventional AF treatment. Electro-anatomical mapping of local intracardiac bipolar electrograms (EGMs) is an established way to characterize the atrial substrate and identify potential ablation targets (Garcia and Wan, 2020; Ladas *et al.*, 2019; Issa *et al.*, 2009). Bipolar EGMs are constructed from unipolar EGMs to quantify the arrhythmogenic substrates because bipolar EGMs are less likely to be contaminated with far-field potentials, *i.e.*, ventricular artefacts (Ragot *et al.*, 2021; de Groot *et al.*, 2021; Frisch *et al.*, 2020; Saha *et al.*, 2019c; Ladas *et al.*, 2019; Issa *et al.*, 2009). However, multiple variables, including wave propagation direction relative to the bipolar electrode orientation, electrode size, inter-electrode spacing, electrode-tissue contact, filtering, mapping density, and mapping resolution, impact bipolar EGM (Kim *et al.*, 2020; Abdi *et al.*, 2021; Lydiard *et al.*, 2021; Anter and Josephson, 2016; Klemm *et al.*, 2007). This review aims to evaluate the effects of the variables on bipolar EGM-based AF mapping.

B.2 Cardiac Conduction Dynamics and Atrial Fibrillation

There are four fundamental characteristics of the cardiomyocyte cells, *i.e.*, contraction, autorhythmicity, intercellular conduction and electromechanical coupling (Del Corso *et al.*, 2022; Arshad and Atkinson, 2022; Anderson *et al.*, 2022; Karki *et al.*, 2021; Padala *et al.*, 2021; Prabhu and Sohaib, 2020; Zhang *et al.*, 2018; Pfeiffer *et al.*, 2014; Anderson *et al.*, 2009). The sinoatrial (SA) node is the natural pacemaker located in the upper region of the right atrium, which initiates each heartbeat. Electrical impulses from the SA node propagate through junctional fibers to the atrioventricular (AV) node in the right atrium and via the

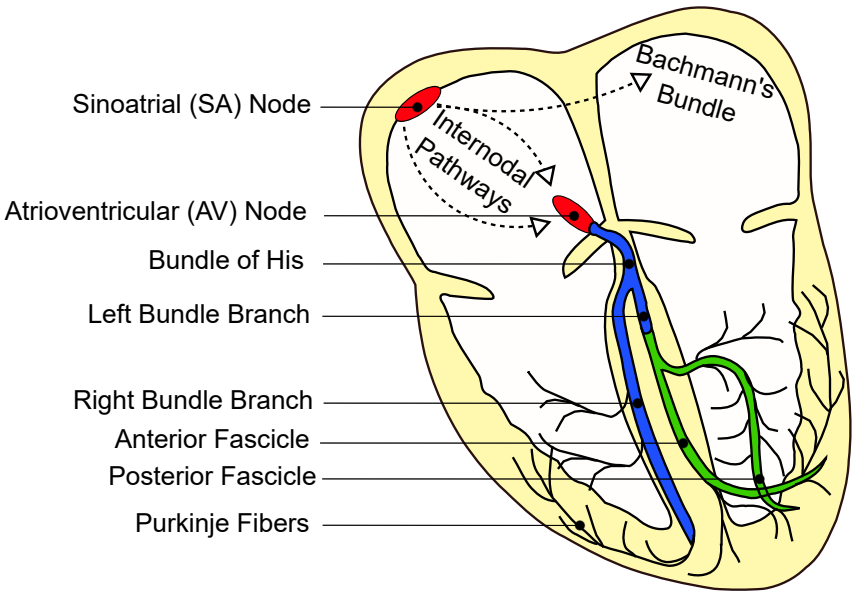

Figure B.1. Cardiac conduction system with its components.

inter-atrial Bachmann's bundle in the left atrium. With a delay in the AV node, impulses are then passed into the bundle of His where they bifurcate into right and left branches. Finally, the impulses proceed down to the Purkinje fibers throughout the ventricular walls. Figure B.1 illustrates the components and conduction pathways of the cardiac conduction system.

B.2.1 Mapping Intracardiac Ablation Target

The current intervention, intracardiac catheter ablation, is based on various hypotheses regarding AF initiation and perpetuation over time. Haissaguerre *et al.* have shown that ectopic electrical impulses coming from pulmonary veins could cause AF. Electrically isolating pulmonary veins may restore SR and has become a standard intervention for AF (Ramirez *et al.*, 2020; Haissaguerre *et al.*, 1998). A hypothesis of substrate-based AF characterization refers to ectopic source identification. The sources produce disruptive signals in the atrial anatomy and disturb regular cardiac conduction dynamics. Autonomic nervous system plays role in AF initiation and maintenance, and recent studies have identified ganglionated plexuses as ablation targets (Aksu *et al.*, 2023; Chen *et al.*, 2014; Coyle *et al.*, 2023). Other hypotheses include multiple wavelets, primary rotors and multiple functional re-entry circuits (Schotten *et al.*, 2021; Quah *et al.*, 2021; Roney *et al.*, 2019b; Wijesurendra and Casadei, 2019; Nattel and Dobrev, 2017; Narayan *et al.*, 2012b,a; Nattel, 2002) (Figure B.2).

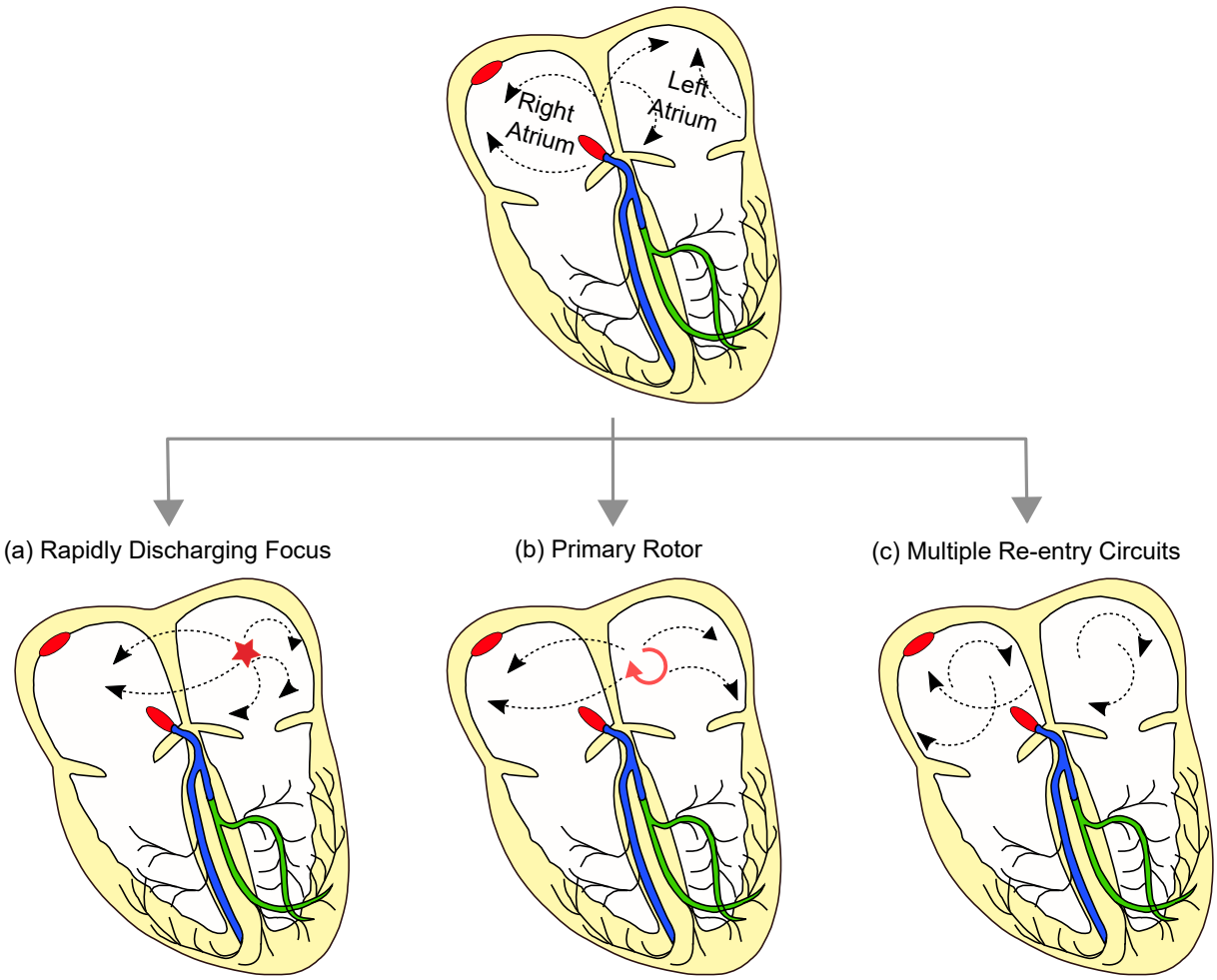

Figure B.2. Different hypotheses of atrial fibrillation genesis and maintenance.

Current ablation strategies depend on accurately identifying AF-related substrates (ablation targets) based on EGM characteristics. Structural changes associated with an electrical scar or diseased myocardium may introduce re-entry circuits within the ACS. Low voltage areas (bipolar peak-to-peak voltage < 0.5 mV) are assumed to be an indication of scar or structural defects (Nairn *et al.*, 2021; Linz *et al.*, 2019; Yamaguchi *et al.*, 2016; Harrison *et al.*, 2014; Badger *et al.*, 2010). Fractionated EGMs are sometimes the ablation targets (Baher *et al.*, 2019; van der Does and de Groot, 2017). According to Nademanee *et al.*, fractionated EGMs follow two criteria (Nademanee *et al.*, 2004). Atrial EGMs have two and more deflections and a variable baseline with complex atrial activation patterns, showing transient activities (*i.e.*, cycle length ≤ 120 ms) over a prolonged 10 s period. However, inconsistent definitions of EGM fractionation can impede success in clinical ablation (van der Does and de Groot, 2017; Almeida *et al.*, 2020). Local activation time and conduction velocity-based AF source mapping are potential alternatives in the clinical setting (Roney *et al.*, 2019a; Coveney *et al.*, 2020; Wong *et al.*, 2011). Recent studies

have proposed recurrent wave cycle length and their morphological similarity-based ablation target detection (Zaatari *et al.*, 2023; Ravelli *et al.*, 2014; Honarbakhsh *et al.*, 2018). Additional bipolar EGM-derived features such as dominant frequency and Shannon entropy have been clinically used to investigate the propagation of predominant waves and to identify the pivot of a rotor, respectively, which may guide substrate-based ablation (Li *et al.*, 2021b; Hwang *et al.*, 2016; Ganesan *et al.*, 2013).

B.2.2 Genesis of Focal Ectopic Source and Reentry Circuit

AF mechanisms manifest in ectopic firing, and various re-entry circuits in the ACS are assumed to occur due to atrial fibrotic substrates. Pathological fibrosis results from malfunctioning ion channels, unusual Ca^{2+} handling, autonomic neural regulation dysfunction, or structural remodeling. Extracellular matrix (ECM) triggers its regulatory protein cells to adjust for any changes during fibrosis to maintain cardiac homeostasis (Bianca J. J. M. Brundel and de Groot, 2022; Andersen *et al.*, 2021; Andrade *et al.*, 2014; Frangogiannis, 2019; Reese-Petersen *et al.*, 2020; Nguyen *et al.*, 2014; Pellman *et al.*, 2010; Burstein and Nattel, 2008). ECM provides structural support to cardiomyocytes, facilitates intra- and inter-cardiomyocyte cellular crosstalk, and transduces critical signals to vascular and interstitial cells (Reese-Petersen *et al.*, 2020). The essential components of ECM include transcriptionally active fibroblasts and endothelial cells (Pelouch *et al.*, 1993). When ECM starts synthesizing its proteins for fibrogenesis as a response to microenvironmental inflammatory and pro-fibrotic changes, increased fibroblasts and myofibroblasts may interfere with intra- and inter-cardiomyocyte electrical conduction. Fibroblasts and cardiomyocytes scarcely share similar intra- and inter-cellular conduction dynamics, and their complex interplay might cause disturbances in physiologic ACS (Andrade *et al.*, 2014; Frangogiannis, 2019; Reese-Petersen *et al.*, 2020). Recent studies implicated that asynchrony between endocardial and epicardial conduction causes AF initiation and maintenance (Bianca J. J. M. Brundel and de Groot, 2022; van der Does *et al.*, 2017; de Groot *et al.*, 2016; Verheule *et al.*, 2014; de Groot *et al.*, 2010; Ravelli *et al.*, 2023).

Complex cardiomyocyte-fibroblast interactions alter the electrophysiological properties of atrial cardiomyocytes (Pagani *et al.*, 2021; Andrade *et al.*, 2014; Frangogiannis, 2019; Reese-Petersen *et al.*, 2020; Nguyen *et al.*, 2014; Pellman *et al.*, 2010,?; Burstein and Nattel, 2008). For example, the shortening of action potential duration and effective refractory period due to ion channel dysfunction could cause the fibrotic substrates to develop

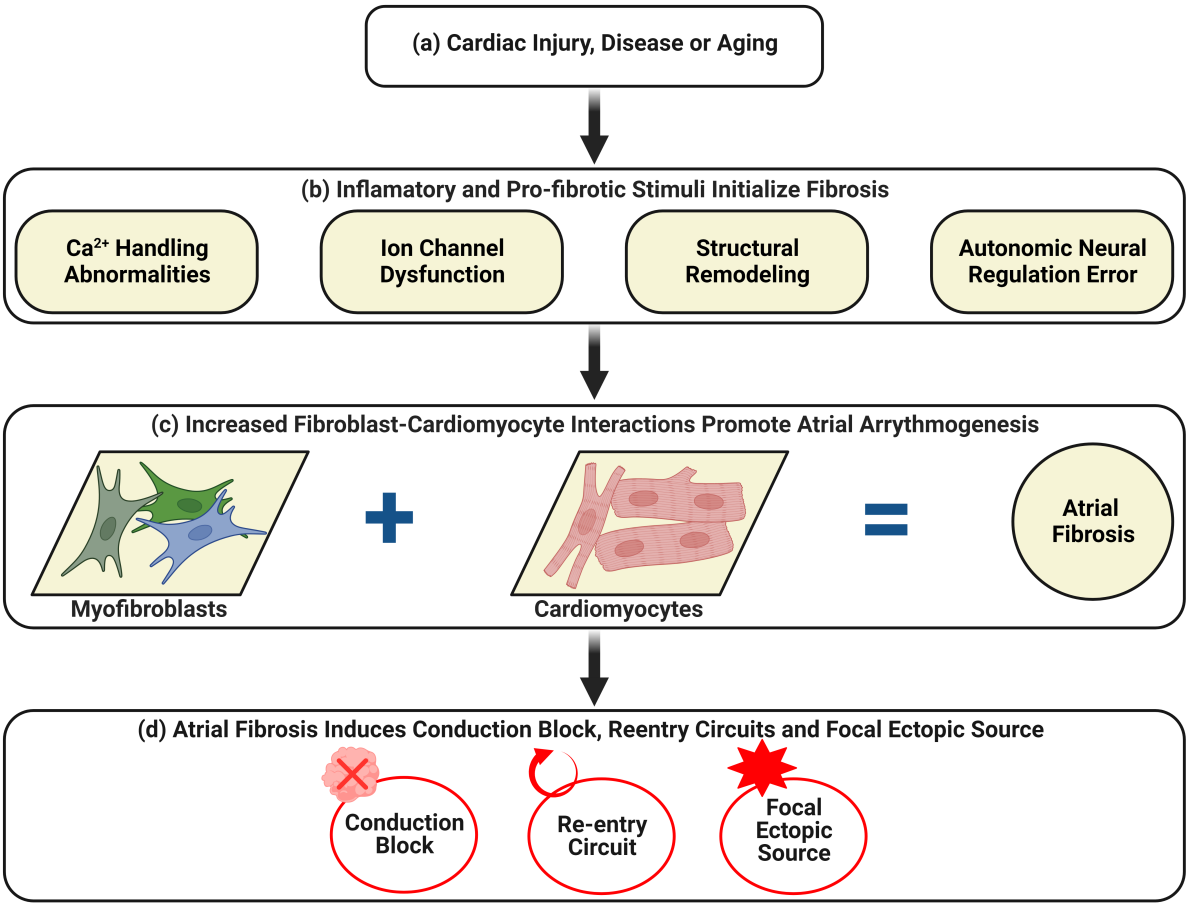

Figure B.3. Pathogenesis of atrial conduction block, focal ectopic source and re-entry circuit from a complex interplay between fibroblasts and cardiomyocytes.

spontaneous re-entry circuits. Ca^{2+} handling abnormalities and errors in autonomic neural regulation sometimes result in focal ectopic firing, which is a potential manifestation of AF-related substrates. Focal ectopic sources further trigger re-entry circuits. Ca^{2+} handling abnormalities can also contribute to structural remodeling leading to fibrotic or scar tissues and conduction blocks that induce re-entry circuits. Figure B.3 describes the complex interactions between the cardiomyocytes and ECM protein cells and the induction of AF. Takahashi *et al.* have studied that fibrosis, growth intercellular space, myofibrillar loss and reduced nuclear density are histological correlates of structural remodelling causing AF (Takahashi *et al.*, 2023).

B.3 Uncertainties Introduced by The Catheter

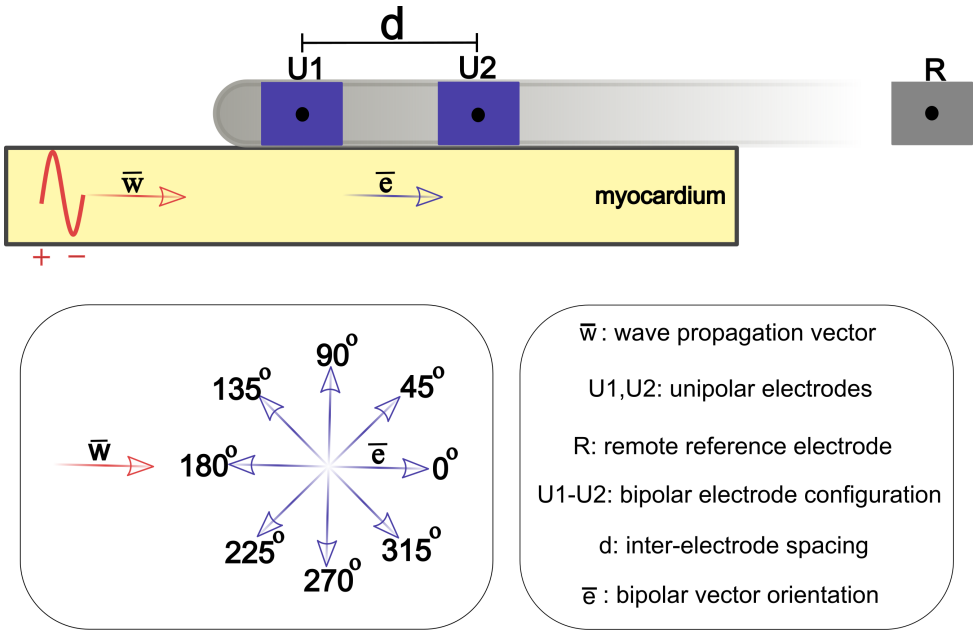

Figure B.4. A schematic illustration of unipolar and bipolar EGM signal acquisition system from myocardium surface.

B.3.1 Unipolar Versus Bipolar Signal Acquisition

For unipolar EGMs, an electrode is connected to the anodal (positive) input of the recording amplifier and the cathodal (negative) input is connected to a remote amplifier (reference electrode) (de Groot *et al.*, 2021; Baumert *et al.*, 2016; Tedrow and Stevenson, 2011). A bipolar EGM can then be constructed by subtracting two unipolar EGMs (de Groot *et al.*, 2021; Gaeta *et al.*, 2020; Baumert *et al.*, 2016). Figure B.4 shows unipolar and bipolar recording configurations from the myocardial surface. Both unipolar and bipolar EGM have specific advantages and disadvantages for AF-related substrate characterization. In unipolar mapping, only one electrode within the heart is used, with the second electrode located outside the heart. The anode can be Wilson's central terminal, which uses the extremity electrodes, an electrode located within the inferior vena, or an internal close unipolar reference electrode (Sroubek *et al.*, 2019). Unipolar mapping has a critical role, particularly during ablation; the signal of interest is obtained from the tip electrode rather than a combined signal from a distal and proximal electrode.

Because the reference electrode is placed at a distance from the heart, unipolar EGM is contaminated by far-field potentials, *e.g.*, ventricular artefacts (Ragot *et al.*, 2021; de Groot *et al.*, 2021; Frisch *et al.*, 2020; Saha *et al.*, 2019a; Ladas *et al.*, 2019; Issa *et al.*, 2009). Ventricular artefacts, *i.e.*, undesired signals originating from ventricles, are the dominant sources

that can be distinguished during SR. However, AF is characterized by chaotic and disorganized electrical activities within atria that may potentially corrupt local EGM morphology by the superposition of waves (Ragot *et al.*, 2021; Dalvi *et al.*, 2018). Constructing a bipolar EGM from a pair of unipolar electrodes may inherently reduce far-field artefacts (Saha *et al.*, 2019c). However, bipolar EGM is affected by several measurement uncertainties due to bipolar vector orientation, inter-electrode spacing, and tissue contact (Abdi *et al.*, 2021; Gaeta *et al.*, 2020; Anter and Josephson, 2016; Stinnett-Donnelly *et al.*, 2012).

B.3.2 Electrode Size and Inter-electrode Spacing

Electrode material, size, shape, thickness and inter-electrode spacing are catheter design specifications and impact EGM-derived features for substrate characterization, for example, when differentiating between healthy and scar tissues (Takigawa *et al.*, 2021, 2019; Stinnett-Donnelly *et al.*, 2012). An electrode's size, shape and thickness define the coverage area for signal acquisition and influence both unipolar and bipolar EGM (Beheshti *et al.*, 2018; Stinnett-Donnelly *et al.*, 2012; Takigawa *et al.*, 2021; de Groot *et al.*, 2021). Takigawa *et al.* have demonstrated that larger electrodes increase the amplitude and duration of unipolar and bipolar EGMs (Takigawa *et al.*, 2021). Thus, scar detection using a low-voltage threshold may be impacted. Inter-electrode spacing also affects substrate characterization. Closer inter-electrode spacing intrinsically reduces the contribution of far-field signals and better identifies the boundary between scar and healthy tissues (Takigawa *et al.*, 2019).

B.3.3 Relation between the Angle of Incidence and Bipolar EGM Vector

Bipolar EGMs are less prone to far-field artefacts and predominantly capture changes in local electrical activities; however, they depend highly on bipolar vector orientation. From a signal processing perspective, bipolar vector orientation could be exploited as a mapping tool for accurate identification of AF sources (Kuo *et al.*, 2022; Yavin *et al.*, 2022; Saha *et al.*, 2019c; Deno *et al.*, 2016; Massé *et al.*, 2016). Figure B.4 demonstrates the directional placement of electrodes (bipolar vector orientation) and wave propagation vector. Assuming a plannar wave propagating through a two-dimensional ($2D$) medium, a bipolar EGM measures either the maximum amplitude of a signal if the angle of incidence is $0°$ or the minimum of 0 mV if the angle of incidence is $90°$. Although variability in EGM measurement

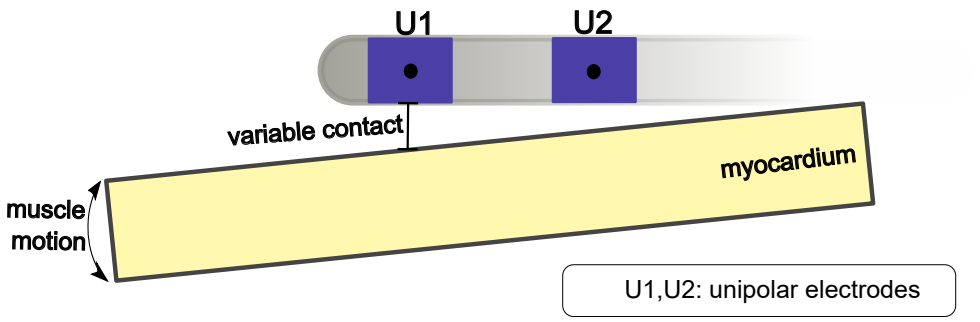

Figure B.5. Variable electrode-tissue contact due to continuous contraction of the heart.

using diverse bipolar vector orientations is obvious, the extent of uncertainty during AF-related substrate characterization requires rigorous clinical validation (Castells *et al.*, 2023; Kuo *et al.*, 2022; Yavin *et al.*, 2022; Gaeta *et al.*, 2020; Saha *et al.*, 2019c; Beheshti *et al.*, 2018; Deno *et al.*, 2016; Massé *et al.*, 2016). AF is a pathological condition delineating very complex and chaotic electrical wave propagation dynamics in a three-dimensional (3D) anatomical network of the atria. Thus, interpreting the impact of bipolar vector orientation on AF-related substrate characterization should not be straightforward.

B.3.4 Variable Tissue Contact

Identification of AF-related sources depends on the precise reconstruction of the atrial electro-anatomy and the spatiotemporal distribution of myocardial electrical potentials and associated features (Ladas *et al.*, 2019; Issa *et al.*, 2009). Continuous mechanical contraction of the complex atrial anatomy makes the positioning of catheter electrodes onerous (Lydiard *et al.*, 2021; Klemm *et al.*, 2007). Sometimes the electrodes are not in full contact with the surface, which may impact the EGM characteristics leading to some recording points being excluded from the analysis. If the distance between electrode and recording surface is too large to maintain acceptable signal quality, the corresponding EGMs are excluded. Figure B.5 illustrates variable electrode-tissue contact.

Nonetheless, the earlier cardiac mapping tools allow us to verify anatomical landmarks and atrial geometry with computed tomography or magnetic resonance scans, intracardiac echocardiographic and positron emission tomography imaging for guiding the ablation procedure (Ladas *et al.*, 2019; Shenasa *et al.*, 2019; Issa *et al.*, 2009; Klemm *et al.*, 2007). Registering the recording points with the corresponding atrial anatomy is key to

successful AF mapping. Notably, recent cardiac mapping systems (*e.g.*, CARTO^{TM}, EnSite Precision^{TM} and Rhythmia HDx^{TM}) use non-fluoroscopic, *i.e.*, magnetic- or impedance-based localization of electrodes (Ladas *et al.*, 2019). Inaccurate localization of the electrode postion (*i.e.*, EGM recording point) may mislead the electrophysiological interpretation of AF (Kim *et al.*, 2020).

B.4 Sources of Mapping Uncertainties

B.4.1 Preprocessing of EGM Signals

Constructing a bipolar EGM may reduce noise contents' dominance over local atrial signals intrinsically. However, further processing is essential to eliminate noise and artefacts while preserving local EGM morphology (Martinez-Iniesta *et al.*, 2017). Zero-phase band-pass filtering is typically applied to eliminate baseline shifts and high-frequency noise (Baumert *et al.*, 2016). The cut-off frequencies clinically used are 30 Hz and 300 Hz (Unger *et al.*, 2019; Saha *et al.*, 2019c). Botteron and Smith proposed band-pass filtering with cut-off frequencies of 40 Hz and 250 Hz, followed by rectification and low-pass filtering to discern the spatial organization of AF dynamics (Botteron and Smith, 1995). This filtering technique has also been utilized to extract dominant frequency mapping (Berenfeld *et al.*, 2000; Baumert *et al.*, 2016). Ciaccio *et al.* demonstrated the frequency range $3-12$ Hz associated with main atrial components. Bandpass filtering might distort the local EGM morphology by eliminating potential low-frequency signal of interest (Ciaccio *et al.*, 2013). Thus, there is a trade-off between noise or artefacts elimination and preserving local EGM morphology. Comprehensive retrospective clinical studies correlating substrate characterization with ablation outcomes can evaluate the efficacy of any signal processing method.

B.4.2 Electroanatomic Mapping System: Density and Resolution

Multimodal electroanatomic cardiac mapping systems such as CARTO^{TM}, EnSite Precision^{TM} and Rhythmia HDx^{TM} detect the electrode positions during EGM recording, which is represented by a 3D point cloud after matching each point with the corresponding atrial anatomy

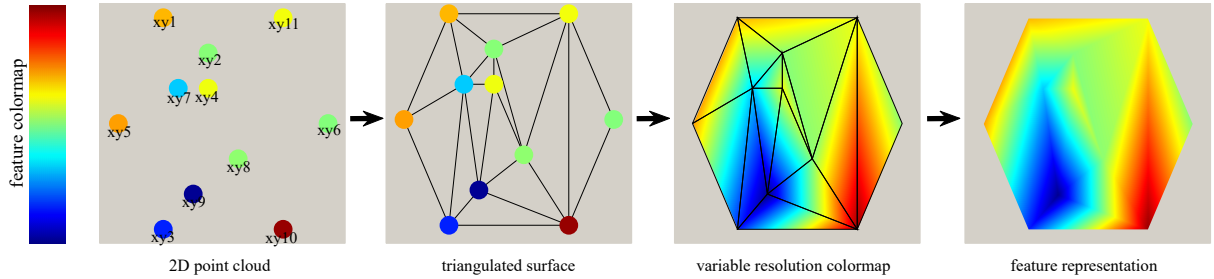

Figure B.6. A schematic illustration of surface reconstruction from irregularly sampled points (a 2D point cloud) and color rendering of an arbitrary feature set.

(Borlich and Sommer, 2019; Ladas *et al.*, 2019). The electrode position information is typically as accurate as 1 mm (Shenasa *et al.*, 2019), though the accuracy in electrode localization strongly depends on the mapping system in use. Mapping density refers to the tightness of point cloud (*i.e.*, recording sites) distribution. It depends on the inter-electrode spacing and sequential navigation of the catheter electrodes inside the atrial anatomy. Densely collected points may offer a better resolution of reconstructed atrial anatomy.

Once the 3D point cloud is approximated from the cardiac mapping system, the next step is to reconstruct the atrial anatomical surface with representations of spatio-temporal distributions of EGMs (Xiong *et al.*, 2022). Using methods derived from computational geometry (*e.g.*, Delaunay triangulation), first, the surface is reconstructed so that anatomically relevant information is preserved. Then, the surface is represented in colored maps (rendering by EGM-derived features) to investigate AF-related sources (Ladas *et al.*, 2019). Due to irregularly spaced points, the resolution of the reconstructed atrial anatomy is non-homogeneous. Figure B.6 shows an irregularly spaced $2D$ point cloud to illustrate surface reconstruction and color rendering.

B.5 Consequences of Uncertainties for Data Interpretation

Electro-anatomical mapping of AF requires a comprehensive clinical environment with multimodal electro-magnetic devices and medical instruments (Ladas *et al.*, 2019; Shenasa *et al.*, 2019). Cardiologists' skillful maneuvering of mapping catheters in the presence of mechanical contraction of the heart and continuous blood circulation further affects the quality of EGM signals. Innovation in the catheter design enables the navigation of electrodes inside the complex atrial anatomy and acquiring high-fidelity local EGM signals, potentially leading

to a successful AF source localization. From an engineering perspective, bipolar vector orientation, electrode size, inter-electrode spacing, electrode-tissue contact, filtering, mapping density and mapping resolution are essential variables to be included while constructing 3D electro-anatomical maps (Kuo *et al.*, 2022; Yavin *et al.*, 2022; Takigawa *et al.*, 2021; Lydiard *et al.*, 2021; Takigawa *et al.*, 2019; Borlich and Sommer, 2019; Beheshti *et al.*, 2018; Gaeta *et al.*, 2020; Ladas *et al.*, 2019; Saha *et al.*, 2019c; Deno *et al.*, 2016; Massé *et al.*, 2016; Shenasa *et al.*, 2019; Stinnett-Donnelly *et al.*, 2012; Martinez-Iniesta *et al.*, 2017; Baumert *et al.*, 2016; Ciaccio *et al.*, 2013). The extent of the impact of the variables above requires further clinical validation. Kim *et al.* have rigorously discussed the potential pitfalls of state-of-the-art cardiac mapping systems and highlighted the technological advances (Kim *et al.*, 2020).

Although ablation targets (AF sources) identification is sometimes onerous, various clinically accepted AF initiation and perpetuation hypotheses exist. Analyzing EGM signals to define clinically relevant features associated with the hypotheses for identifying AF sources is often ambiguous. Besides pulmonary vein isolation (Ramirez *et al.*, 2020; Haissaguerre *et al.*, 1998), a widely accepted precursor procedure, other substrate-based ablation strategies depend upon characterizing ectopic sources, re-entry, and rotational circuits. Fibrotic or scar tissues are supposedly responsible for re-entry and rotational circuits while obstructing common cardiac conduction pathways (Schotten *et al.*, 2021; Quah *et al.*, 2021; Roney *et al.*, 2019b; Wijesurendra and Casadei, 2019; Nattel and Dobrev, 2017; Narayan *et al.*, 2012b). Complex AF source identification in atrial anatomy is demanding, and uncertainties in EGM interpretation pose additional challenges. However, recent innovations in signal processing algorithms, including mutual information or artificial intelligence (AI)-based analysis of multi-electrode arrays, may offer complementary information to clinical decision-making (Sha *et al.*, 2022; Rodrigo *et al.*, 2022).

Voltage mapping enables defining low-voltage areas (peak-to-peak voltage < 0.5 mV) associated with the scar of fibrotic tissues (Nairn *et al.*, 2021; Linz *et al.*, 2019; Yamaguchi *et al.*, 2016; Harrison *et al.*, 2014; Badger *et al.*, 2010). Studies have implicated that bipolar vector orientation, inter-electrode spacing, and electrode-tissue contact directly impact the amplitude of EGM signals and thus voltage mapping (Takigawa *et al.*, 2021, 2019; Saha *et al.*, 2019c; Deno *et al.*, 2016; Massé *et al.*, 2016). Studies have demonstrated *in silico* that the diagnostic catheter shapes influence the EGM-derived markers for AF (Sánchez *et al.*, 2021; Bartolucci *et al.*, 2021; Heijman *et al.*, 2021; Aronis *et al.*, 2019). These variables also

impact other EGM-derived features such as local activation time, conduction velocity, fractionated EGM, dominant frequency and Shannon entropy (Li *et al.*, 2021b; Coveney *et al.*, 2020; Hwang *et al.*, 2016; Ganesan *et al.*, 2013; Wong *et al.*, 2011).

B.5.1 The State-of-The-Art Diagnostic Catheters

Multi-electrode array with innovative catheter design is at the forefront of cardiac mapping tool development, advancing personalized diagnostic and therapeutic interventions. Table B.6 lists some state-of-the-art diagnostic catheters with their specifications and design strengths (Berte *et al.*, 2020; Barkagan *et al.*, 2020; Sroubek *et al.*, 2019; *Octaray™ mapping catheter with trueref™ technology*, n.d.; Dodeja *et al.*, 2022; Deno *et al.*, 2016; Gaeta *et al.*, 2020; Kuo *et al.*, 2022; Linz *et al.*, 2019; Massé *et al.*, 2016; Saha *et al.*, 2019c; Stinnett-Donnelly *et al.*, 2012; Takigawa *et al.*, 2019, 2021; Yavin *et al.*, 2022; *Advisor HD Grid™ mapping catheter, sensor enabled™*, n.d.; Jiang *et al.*, 2020; Tan *et al.*, 2023; Yavin *et al.*, 2021). Recently introduced OctaRay™ mapping catheter attributes 48 electrodes, and their simultaneous recordings enable faster mapping of the whole atrium than its predecessor PentaRay™ mapping catheter (Barkagan *et al.*, 2020; Sroubek *et al.*, 2019; *Octaray™ mapping catheter with trueref™ technology*, n.d.; Dodeja *et al.*, 2022). OctaRay multi-electrode catheter with CARTO™ signal processing unit renders the atrial anatomy based on locally collected EGM features and assists clinicians in detecting ablation targets more accurately. HD Grid™ catheter has been another sought-after mapping tool in the clinical community because of its orthogonally arranged electrodes (Deno *et al.*, 2016; Gaeta *et al.*, 2020; Kuo *et al.*, 2022; Linz *et al.*, 2019; Massé *et al.*, 2016; Saha *et al.*, 2019c; Stinnett-Donnelly *et al.*, 2012; Takigawa *et al.*, 2019, 2021; Yavin *et al.*, 2022; *Advisor HD Grid™ mapping catheter, sensor enabled™*, n.d.; Jiang *et al.*, 2020). IntellaMap Orion™ and Constellation™ catheters are basket catheters having 64 electrodes and can cover a large area simultaneously (Ollitrault *et al.*, 2021; Pathik *et al.*, 2017; Oesterlein *et al.*, 2016). Notably, the constellation catheter is not on the market anymore, but the design showcases innovation in the cardiac mapping industry. The multi-electrode catheter technology has evolved significantly from single spline Decapolar™ (flexible) or Lasso™ (circular) catheters to multi-spline HD Grid™, OctaRay™ or Optrell™. Unlike grid-type catheters, Octaray™ and Pentaray™ are multi-spline catheters featuring flower shape open branch design. Simultaneous EGM from the electrode array can integrate advanced signal processing and AI-based algorithms for more accurate ablation target selection and, thus,

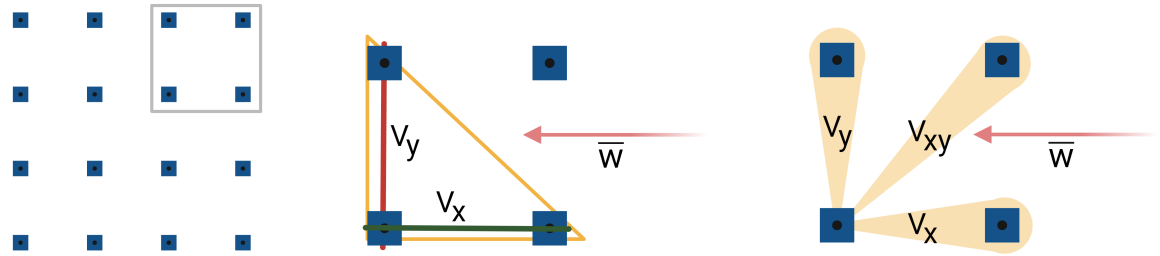

(a) Multi-Electrode Array (b) Omnipolar EGM Clique (c) Hypothetical Beamforming

Figure B.7. A schematic illustration of wavefront direction-aware EGM approximation concepts.

superior intervention outcome (Rodrigo *et al.*, 2022; Sánchez *et al.*, 2021; Baumert *et al.*, 2016).

B.5.2 The Principle of Wavefront Direction-Aware EGM

Innovation in multi-electrode mapping catheters, especially grid-type HD Grid™ and Optrell™ catheters, enable integrating multiple bipolar electrode orientations into a wavefront direction-aware omnipolar technology (Dittrich *et al.*, 2023; Ruiperez-Campillo *et al.*, 2023a; Castells *et al.*, 2023; Iacopino *et al.*, 2023; Van Schie *et al.*, 2022; Yeo *et al.*, 2022; Karatela *et al.*, 2022; Burg *et al.*, 2022; van Schie *et al.*, 2021; Deno *et al.*, 2020; Haldar *et al.*, 2017; Deno *et al.*, 2016). Deno *et al.* proposed the construction of omnipolar EGM from multiple bipolar EGM considering specific alignments of the electrodes, called as clique (Deno *et al.*, 2020, 2016). Assuming four unipolar electrodes arranged in a square area and $\overline{W}$ is a propagating wavefront passing through locally (Figure B.7), omnipolar technology exploits the wavefront characteristics such as propagation direction . Then, bipolar EGMs from orthogonally placed bipolar electrode pairs can be calculated without maneuvering the catheter. If V_x and V_y are voltages captured by two mutually orthogonal bipolar orientations using a triangular clique, omnipolar technology features the maximum measurable voltages using a particular mapping catheter. Notably, the type of clique formation can vary using different sets of bipolar orientations (Ruipérez-Campillo *et al.*, 2023b). For a more detailed calculation of the omnipolar voltage, please refer to (Deno *et al.*, 2016, 2020). Omnipolar EGM explicitly reduces the impact of the directionality of bipolar orientations (Dittrich *et al.*, 2023; Ruiperez-Campillo *et al.*, 2023a; Castells *et al.*, 2023; Iacopino *et al.*, 2023; Van Schie *et al.*, 2022; Yeo *et al.*, 2022; Karatela *et al.*, 2022; Burg *et al.*, 2022; van Schie *et al.*, 2021; Deno *et al.*, 2020; Haldar *et al.*, 2017; Deno *et al.*, 2016).

Saha *et al.* proposed a beamforming-inspired spatial filtering technique for minimizing the impact of directionality while utilizing the diversity gain from multiple bipolar electrode orientations (Saha *et al.*, 2019c). Current grid-type mapping catheters, such as HD Grid™ and Optrell™, offer special arrangements of the electrodes, allowing the simultaneous processing of various EGMs. Array signal processing is a popular topic in the wireless or cellular communication industry (Jeong *et al.*, 2015; Wang *et al.*, 2019), and the advancements may contribute to current cardiac mapping tools after adequate clinical validation. Figure B.7 schematically compares the concepts of omnipolar and beamforming EGM constructions for reducing the effect of directionality.

B.6 Future Perspectives and Conclusion

There are still scopes for improvement while considering the uncertainties of bipolar EGM-based cardiac mapping tools, as discussed in the review. Three factors could be vital for the next frontier of AF mapping technologies, *i.e.*, the user-centric design of catheter electrodes, the precision of electrode localization, and the integration of AI (Kim *et al.*, 2020; Ladas *et al.*, 2019; Shenasa *et al.*, 2019; Issa *et al.*, 2009; Klemm *et al.*, 2007; Trayanova *et al.*, 2021; Alhusseini *et al.*, 2020; Corrado *et al.*, 2021; Berte *et al.*, 2020; Barkagan *et al.*, 2020; Sroubek *et al.*, 2019; *Octaray™ mapping catheter with trueref™ technology*, n.d.; Dodeja *et al.*, 2022; Deno *et al.*, 2016; Gaeta *et al.*, 2020; Kuo *et al.*, 2022; Linz *et al.*, 2019; Massé *et al.*, 2016; Saha *et al.*, 2019c; Stinnett-Donnelly *et al.*, 2012; Takigawa *et al.*, 2019, 2021; Yavin *et al.*, 2022; *Advisor HD Grid™ mapping catheter, sensor enabled™*, n.d.; Jiang *et al.*, 2020). The intrinsic nonlinearity in the AI-based algorithm may capture the time-variant and nonstationary EGM dynamics for AF source mapping utilizing multi-electrode catheters. The *in silico* simulation is a precursor for validating novel algorithms while quantifying their differences in AF source selection (Sánchez *et al.*, 2021; Bartolucci *et al.*, 2021; Heijman *et al.*, 2021; Aronis *et al.*, 2019).

Cardiologists' feedback on the existing state-of-the-art cardiac mapping tools concerning maneuverability, ease-of-use and accuracy in ablation target identification can revise the problem statement for engineers, prompting them to develop catheter electrodes fulfilling user needs. Then, increasing the accuracy of electrode localization (registering electrodes in the atrial anatomy) tools could play an essential role in AF target selection. Finally, how effectively we could integrate AI in the mapping system, from surface reconstruction to AF-related source localization, is crucial.

Appendix B

Comprehensive studies from engineering perspectives are critical for demonstrating the effects of the variables reviewed in this paper and the clinical implications of detecting unsuitable ablation targets (AF-related sources). Recent advances in multielectrode catheter design provide high-density acquisition of spatially distributed atrial electrical activities. Retrospective investigation of the collected data and clinically annotated AF-related targets could be a precursor to exploiting the power of advanced signal processing and AI to identify the AF sources accurately.

Diagnostic Catheter	Manufacturer	No. of Splines	No. of Electrodes	Electrode Size (mm)	Inter-Electrode Distance (Centre-to-Centre, mm)	Design Strength
Optrell™	Biosense Webster	6	48	~ 0.9	2.4	Orthogonal electrode orientations
OctaRay™	Biosense Webster	8	48	~ 0.5	2	Electrodes in circular formation
HD Grid™	Abbott	4	16	1	4	Orthogonal electrode orientations
PentaRay™	Biosense Webster	5	20	1	1	Electrodes in circular formation
IntellaMap Orion™	Boston Scientific	8	64	2.82	2.5	Flexible basket covering broad area
Constellation™ ($60mm$)	Boston Scientific	8	64	2.66	6.5	Flexible basket covering broad area
Decapolar™	Biosense Webster	1	10	1	3	Electrodes on a flexible spline
Lasso™ (Circular)	Biosense Webster	1	20	1	3	Electrodes on a circular spline

Table B.1. A list of some state-of-the-art diagnostic catheters featuring multi-electrode.

Bibliography

Abdi, B., van Schie, M. S., de Groot, N. M., and Hendriks, R. C. (2021). 'Analyzing the effect of electrode size on electrogram and activation map properties', *Computers in Biology and Medicine*, **134**, 104467.

Acı, Ç. İ., Kaya, M., and Mishchenko, Y. (2019). 'Distinguishing mental attention states of humans via an eeg-based passive bci using machine learning methods', *Expert Systems with Applications*, **134**, pp. 153–166.
Advisor HD Grid™ mapping catheter, sensor enabled™

Advisor HD Grid™ mapping catheter, sensor enabled™ (n.d.). Accessed February 21, 2023 [Online].

Ahn, H.-J., Lee, D.-H., Jeong, J.-H., and Lee, S.-W. (2022). 'Multiscale convolutional transformer for eeg classification of mental imagery in different modalities', IEEE Transactions on Neural Systems and Rehabilitation Engineering, **31***, pp. 646–656.*

Ajrawi, S., Rao, R., and Sarkar, M. (2021). 'Cybersecurity in brain-computer interfaces: Rfid-based design-theoretical framework', Informatics in Medicine Unlocked, **22***, 100489.*

Aksu, T., Skeete, J. R., and Huang, H. H. (2023). 'Ganglionic plexus ablation: A step-by-step guide for electrophysiologists and review of modalities for neuromodulation for the management of atrial fibrillation', Arrhythmia & Electrophysiology Review, **12**.

Alhusseini, M. I., Abuzaid, F., Rogers, A. J., Zaman, J. A., Baykaner, T., Clopton, P., Bailis, P., Zaharia, M., Wang, P. J., Rappel, W.-J etxxxxx al.. (2020). 'Machine learning to classify intracardiac electrical patterns during atrial fibrillation: machine learning of atrial fibrillation', Circulation: Arrhythmia and Electrophysiology, **13***(8), e008160.*

Allert, N., Cheeran, B., Deuschl, G., Barbe, M. T., Csoti, I., Ebke, M., Glaser, M., Kang, J.-S., Kelm, S., Krack, P etxxxxx al.. (2018). 'Postoperative rehabilitation after deep brain stimulation surgery for movement disorders', Clinical Neurophysiology, **129***(3), pp. 592–601.*

Almeida, T. P., Soriano, D. C., Mase, M., Ravelli, F., Bezerra, A. S., Li, X., Chu, G. S., Salinet, J., Stafford, P. J., Ng, G. A etxxxxx al.. (2020). 'Unsupervised classification of

atrial electrograms for electroanatomic mapping of human persistent atrial fibrillation', Ieee Transactions on Biomedical Engineering, **68***(4), pp. 1131–1141.*

Amorim, E., Zheng, W.-L., Ghassemi, M. M., Aghaeeaval, M., Kandhare, P., Karukonda, V., Lee, J. W., Herman, S. T., Sivaraju, A., Gaspard, N., Hofmeijer, J., van Putten, M. J., Sameni, R., Reyna, M. A., Clifford, G. D., and Westover, M. B. (2023). 'The international cardiac arrest research (i-care) consortium electroencephalography database', Critical Care Medicine, **doi:10.1097/CCM.0000000000006074***.*

Andersen, J. H., Andreasen, L., and Olesen, M. S. (2021). 'Atrial fibrillation—a complex polygenetic disease', European Journal of Human Genetics, **29***(7), pp. 1051–1060.*

Anderson, R. H., Sánchez-Quintana, D., Spicer, D. E., Farré, J., and Sternick, E. B. (2022). 'How does the cardiac impulse pass from the sinus to the atrioventricular node?', Heart Rhythm, .

Anderson, R. H., Yanni, J., Boyett, M. R., Chandler, N. J., and Dobrzynski, H. (2009). 'The anatomy of the cardiac conduction system', Clinical Anatomy: The Official Journal of the American Association of Clinical Anatomists and the British Association of Clinical Anatomists, **22***(1), pp. 99–113.*

Andrade, J., Khairy, P., Dobrev, D., and Nattel, S. (2014). 'The clinical profile and pathophysiology of atrial fibrillation: relationships among clinical features, epidemiology, and mechanisms', Circulation research, **114***(9), pp. 1453–1468.*

Andresen, E. M., Fried-Oken, M., Peters, B., and Patrick, D. L. (2016). 'Initial constructs for patient-centered outcome measures to evaluate brain–computer interfaces', Disability and Rehabilitation: Assistive Technology, **11***(7), pp. 548–557.*

Antal, A., and Herrmann, C. S. (2016). 'Transcranial alternating current and random noise stimulation: possible mechanisms', Neural plasticity, **2016***(1), 3616807.*

Anter, E., and Josephson, M. E. (2016). 'Bipolar voltage amplitude: what does it really mean?', Heart Rhythm, **13***(1), pp. 326–327.*

Arı, E., and Taçgın, E. (2024). 'Nf-eeg: A generalized cnn model for multi class eeg motor imagery classification without signal preprocessing for brain computer interfaces', Biomedical Signal Processing and Control, **92***, 106081.*

Aricò, P., Borghini, G., Di Flumeri, G., Sciaraffa, N., and Babiloni, F. (2018). 'Passive bci beyond the lab: current trends and future directions', Physiological measurement, **39***(8), 08TR02.*

Armengol-Urpi, A., Kovacs, R., and Sarma, S. E. (2023). 'Brain-hack: Remotely injecting false brain-waves with rf to take control of a brain-computer interface', Proceedings of the 5th Workshop on CPS&IoT Security and Privacy, pp. 53–66.

Aronis, K. N., Ali, R., and Trayanova, N. A. (2019). 'The role of personalized atrial modeling in understanding atrial fibrillation mechanisms and improving treatment', International journal of cardiology, **287***, pp. 139–147.*

Arshad, A., and Atkinson, A. J. (2022). 'A 21st century view of the anaotmy of the cardiac conduction system', Translational Research in Anatomy, 100204.

Azab, A. M., Mihaylova, L., Ang, K. K., and Arvaneh, M. (2019). 'Weighted transfer learning for improving motor imagery-based brain–computer interface', IEEE Transactions on Neural Systems and Rehabilitation Engineering, **27***(7), pp. 1352–1359.*

Azab, A. M., Toth, J., Mihaylova, L. S., and Arvaneh, M. (2018). 'A review on transfer learning approaches in brain–computer interface', Signal processing and machine learning for brain-machine interfaces, pp. 81–98.

Badger, T. J., Daccarett, M., Akoum, N. W., Adjei-Poku, Y. A., Burgon, N. S., Haslam, T. S., Kalvaitis, S., Kuppahally, S., Vergara, G., McMullen, L etxxxxx al.. (2010). 'Evaluation of left atrial lesions after initial and repeat atrial fibrillation ablation: lessons learned from delayed-enhancement mri in repeat ablation procedures', Circulation: Arrhythmia and Electrophysiology, **3***(3), pp. 249–259.*

Baher, A., Buck, B., Fanarjian, M., Paul Mounsey, J., Gehi, A., Chung, E., Akar, F. G., Webber Jr, C. L., Akar, J. G., and Hummel, J. P. (2019). 'Recurrence quantification analysis of complex-fractionated electrograms differentiates active and passive sites during atrial fibrillation', Journal of cardiovascular electrophysiology, **30***(11), pp. 2229–2238.*

Bamdadian, A., Guan, C., Ang, K. K., and Xu, J. (2015). 'Towards improvement of mi-bci performance of subjects with bci deficiency', 2015 7th International IEEE/EMBS Conference on Neural Engineering (NER), IEEE, pp. 17–20.

Barkagan, M., Sroubek, J., Shapira-Daniels, A., Yavin, H., Jang, J., Nezafat, R., and Anter, E. (2020). 'A novel multielectrode catheter for high-density ventricular mapping: electrogram characterization and utility for scar mapping', EP Europace, **22***(3), pp. 440–449.*

Barmpas, K., Panagakis, Y., Bakas, S., Adamos, D. A., Laskaris, N., and Zafeiriou, S. (2023). 'Improving generalization of cnn-based motor-imagery eeg decoders via dynamic convolutions', IEEE Transactions on Neural Systems and Rehabilitation Engineering, **31***, pp. 1997–2005.*

Bartolucci, C., Fabbri, C., Tomasi, C., Sabbatani, P., Severi, S., and Corsi, C. (2021). 'Computational analysis of mapping catheter geometry and contact quality effects on rotor detection in atrial fibrillation', Frontiers in Physiology, **12***, 732161.*

Bashashati, A., Fatourechi, M., Ward, R. K., and Birch, G. E. (2007). 'A survey of signal processing algorithms in brain–computer interfaces based on electrical brain signals', Journal of Neural engineering, **4***(2), R32.*

Baumert, M., Sanders, P., and Ganesan, A. (2016). 'Quantitative-electrogram-based methods for guiding catheter ablation in atrial fibrillation', Proceedings of the IEEE, **104***(2), pp. 416–431.*

Beheshti, M., Magtibay, K., Massé, S., Porta-Sanchez, A., Haldar, S., Bhaskaran, A., Nayyar, S., Glover, B., Deno, D. C., Vigmond, E. J etxxxxx al.. (2018). 'Determinants of atrial bipolar voltage: Inter electrode distance and wavefront angle', Computers in biology and medicine, **102***, pp. 449–457.*

Bekteshi, S., Monbaliu, E., McIntyre, S., Saloojee, G., Hilberink, S. R., Tatishvili, N., and Dan, B. (2023). 'Towards functional improvement of motor disorders associated with cerebral palsy', The Lancet Neurology, **22***(3), pp. 229–243.*

Benaroch, C., Yamamoto, M. S., Roc, A., Dreyer, P., Jeunet, C., and Lotte, F. (2022). 'When should mi-bci feature optimization include prior knowledge, and which one?', Brain-Computer Interfaces, **9***(2), pp. 115–128.*

Benzeghiba, M., De Mori, R., Deroo, O., Dupont, S., Erbes, T., Jouvet, D., Fissore, L., Laface, P., Mertins, A., Ris, C etxxxxx al.. (2007). 'Automatic speech recognition and speech variability: A review', Speech communication, **49***(10-11), pp. 763–786.*

Berenfeld, O., Mandapati, R., Dixit, S., Skanes, A. C., Chen, J., Mansour, M., and Jalife, J. (2000). 'Spatially distributed dominant excitation frequencies reveal hidden organization

in atrial fibrillation in the langendorff-perfused sheep heart', Journal of cardiovascular electrophysiology, **11***(8), pp. 869–879.*

Bergeron, D., Iorio-Morin, C., Bonizzato, M., Lajoie, G., Orr Gaucher, N., Racine, É., and Weil, A. G. (2023). 'Use of invasive brain-computer interfaces in pediatric neurosurgery: technical and ethical considerations', Journal of Child Neurology, **38***(3-4), pp. 223–238.*

Bernal, S. L., Celdrán, A. H., and Pérez, G. M. (2023). 'Eight reasons to prioritize brain-computer interface cybersecurity', Communications of the ACM, **66***(4), pp. 68–78.*

Berte, B., Zeppenfeld, K., and Tung, R. (2020). 'Impact of micro-, mini-and multi-electrode mapping on ventricular substrate characterisation', Arrhythmia & electrophysiology review, **9***(3), 128.*

Bethlehem, R. A., Seidlitz, J., White, S. R., Vogel, J. W., Anderson, K. M., Adamson, C., Adler, S., Alexopoulos, G. S., Anagnostou, E., Areces-Gonzalez, A etxxxxx al.. (2022). 'Brain charts for the human lifespan', Nature, **604***(7906), pp. 525–533.*

Bhatt, M. W., and Sharma, S. (2024). 'Multi-scale self-attention approach for analysing motor imagery signals in brain-computer interfaces', Journal of Neuroscience Methods, 110182.

Bhattacharyya, S., Clerc, M., and Hayashibe, M. (2019). 'Augmenting motor imagery learning for brain–computer interfacing using electrical stimulation as feedback', IEEE Transactions on Medical Robotics and Bionics, **1***(4), pp. 247–255.*

Bianca J. J. M. Brundel, Xun Ai, M. T. H. M. F. K. G. Y. H. L., and de Groot, N. M. S. (2022). 'Atrial fibrillation', Nature Reviews Disease Primers, **8***(21), pp. 2056–676X.*

Blanco Mora, D. A., Van Hoornweder, S., van Dun, K., Verstraelen, S., Cuypers, K., Bermúdez i Badia, S., and Meesen, R. (2024). 'Toward methodologies for motor imagery enhancement: a tdcs-bci study', Brain-Computer Interfaces, pp. 1–15.

Borlich, M., and Sommer, P. (2019). 'Cardiac mapping systems: rhythmia, topera, ensite precision, and carto', Cardiac Electrophysiology Clinics, **11***(3), pp. 449–458.*

Botteron, G. W., and Smith, J. M. (1995). 'A technique for measurement of the extent of spatial organization of atrial activation during atrial fibrillation in the intact human heart', IEEE Transactions on Biomedical Engineering, **42***(6), pp. 579–586.*

Branco, M. P., Pels, E. G., Nijboer, F., Ramsey, N. F., and Vansteensel, M. J. (2023). 'Brain-computer interfaces for communication: preferences of individuals with locked-in syndrome, caregivers and researchers', Disability and Rehabilitation: Assistive Technology, **18***(6), pp. 963–973.*

Brown, R. E., and Milner, P. M. (2003). 'The legacy of donald o. hebb: more than the hebb synapse', Nature Reviews Neuroscience, **4***(12), pp. 1013–1019.*

Brown, T. T., and Jernigan, T. L. (2012). 'Brain development during the preschool years', Neuropsychology review, **22***, pp. 313–333.*

Brunner, C., Birbaumer, N., Blankertz, B., Guger, C., Kübler, A., Mattia, D., Millán, J. d. R., Miralles, F., Nijholt, A., Opisso, E etxxxxx al.. (2015). 'Bnci horizon 2020: towards a roadmap for the bci community', Brain-computer interfaces, **2***(1), pp. 1–10.*

Brunner, I., Lundquist, C. B., Pedersen, A. R., Spaich, E. G., Dosen, S., and Savic, A. (2024). 'Brain computer interface training with motor imagery and functional electrical stimulation for patients with severe upper limb paresis after stroke: a randomized controlled pilot trial', Journal of NeuroEngineering and Rehabilitation, **21***(1), 10.*

Bu, Y., Harrington, D. L., Lee, R. R., Shen, Q., Angeles-Quinto, A., Ji, Z., Hansen, H., Hernandez-Lucas, J., Baumgartner, J., Song, T etxxxxx al.. (2023). 'Magnetoencephalogram-based brain–computer interface for hand-gesture decoding using deep learning', Cerebral Cortex, **33***(14), pp. 8942–8955.*

Burg, M. R., Anderson, R. D., Massé, S., and Nanthakumar, K. (2022). 'Cardiac mapping with irreverence to time: Replacing isochrones with omnipolar vectors', Heart Rhythm, **19***(11), pp. 1802–1803.*

Burstein, B., and Nattel, S. (2008). 'Atrial fibrosis: mechanisms and clinical relevance in atrial fibrillation', Journal of the American College of Cardiology, **51***(8), pp. 802–809.*

Cao, L., Li, J., Ji, H., and Jiang, C. (2014). 'A hybrid brain computer interface system based on the neurophysiological protocol and brain-actuated switch for wheelchair control', Journal of neuroscience methods, **229***, pp. 33–43.*

Card, N. S., Wairagkar, M., Iacobacci, C., Hou, X., Singer-Clark, T., Willett, F. R., Kunz, E. M., Fan, C., Vahdati Nia, M., Deo, D. R etxxxxx al.. (2024). 'An accurate and rapidly calibrating speech neuroprosthesis', New England Journal of Medicine, **391***(7), pp. 609–618.*

Castells, F., Ruipérez-Campillo, S., Segarra, I., Cervigón, R., Casado-Arroyo, R., Merino, J. L., and Millet, J. (2023). 'Performance assessment of electrode configurations for the estimation of omnipolar electrograms from high density arrays', Computers in Biology and Medicine, 106604.

Chandler, J. A., Van der Loos, K. I., Boehnke, S., Beaudry, J. S., Buchman, D. Z., and Illes, J. (2022). 'Brain computer interfaces and communication disabilities: Ethical, legal, and social aspects of decoding speech from the brain', Frontiers in human neuroscience, **16***, 841035.*

Chen, P.-S., Chen, L. S., Fishbein, M. C., Lin, S.-F., and Nattel, S. (2014). 'Role of the autonomic nervous system in atrial fibrillation: pathophysiology and therapy', Circulation research, **114***(9), pp. 1500–1515.*

Chen, Y., Yang, R., Huang, M., Wang, Z., and Liu, X. (2022). 'Single-source to single-target cross-subject motor imagery classification based on multisubdomain adaptation network', IEEE Transactions on Neural Systems and Rehabilitation Engineering, **30***, pp. 1992–2002.*

Cheniti, G., Vlachos, K., Pambrun, T., Hooks, D., Frontera, A., Takigawa, M., Bourier, F., Kitamura, T., Lam, A., Martin, C etxxxxx al.. (2018). 'Atrial fibrillation mechanisms and implications for catheter ablation', Frontiers in physiology, **9***, 1458.*

Chung, L. K., Jack, B. N., Griffiths, O., Pearson, D., Luque, D., Harris, A. W., Spencer, K. M., Le Pelley, M. E., So, S. H., and Whitford, T. J. (2023). 'Neurophysiological evidence of motor preparation in inner speech and the effect of content predictability', Cerebral Cortex, **33***(24), pp. 11556–11569.*

Ciaccio, E. J., Biviano, A. B., and Garan, H. (2013). 'Computational method for high resolution spectral analysis of fractionated atrial electrograms', Computers in Biology and Medicine, **43***(10), pp. 1573–1582.*

Cohen, M. X. (2017). 'Where does eeg come from and what does it mean?', Trends in neurosciences, **40***(4), pp. 208–218.*

Coin, A., and Dubljević, V. (2023). 'An introduction to policy, identity, and neurotechnology: The neuroethics of brain–computer interfaces', Policy, Identity, and Neurotechnology: The Neuroethics of Brain-Computer Interfaces, Springer, pp. 1–7.

Cooney, C., Folli, R., and Coyle, D. (2021). 'A bimodal deep learning architecture for eeg-fnirs decoding of overt and imagined speech', IEEE Transactions on Biomedical Engineering, **69***(6), pp. 1983–1994.*

Cooney, C., Folli, R., and Coyle, D. (2022). 'Opportunities, pitfalls and trade-offs in designing protocols for measuring the neural correlates of speech', Neuroscience & Biobehavioral Reviews, **140***, 104783.*

Corrado, C., Williams, S., Roney, C., Plank, G., O'Neill, M., and Niederer, S. (2021). 'Using machine learning to identify local cellular properties that support re-entrant activation in patient-specific models of atrial fibrillation', EP Europace, **23***(Supplement_1), pp. i12–i20.*

Coveney, S., Corrado, C., Roney, C. H., O'Hare, D., Williams, S. E., O'Neill, M. D., Niederer, S. A., Clayton, R. H., Oakley, J. E., and Wilkinson, R. D. (2020). 'Gaussian process manifold interpolation for probabilistic atrial activation maps and uncertain conduction velocity', Philosophical Transactions of the Royal Society A, **378***(2173), 20190345.*

Coyle, C., Koutsoftidis, S., Kim, M.-Y., Porter, B., Keene, D., Luther, V., Handa, B., Kay, J., Lim, E., Malcolme-Lawes, L etxxxxx al.. (2023). 'Feasibility of mapping and ablating ectopy-triggering ganglionated plexus reproducibly in persistent atrial fibrillation', Journal of Interventional Cardiac Electrophysiology, pp. 1–8.

Craik, A., He, Y., and Contreras-Vidal, J. L. (2019). 'Deep learning for electroencephalogram (eeg) classification tasks: a review', Journal of neural engineering, **16***(3), 031001.*

Cueva, V. M., Bougrain, L., Lotte, F., and Rimbert, S. (2025). 'Reliable predictor of bci motor imagery performance using median nerve stimulation', Journal of Neural Engineering, .

Dalvi, R., Nayyar, S., Suszko, A., and Chauhan, V. S. (2018). 'A least squares approach to estimation of far-field voltage in unipolar electrograms in atrial fibrillation', 2018 52nd Asilomar Conference on Signals, Systems, and Computers, IEEE, pp. 1230–1233.

Darvishi, S., Gharabaghi, A., Ridding, M. C., Abbott, D., and Baumert, M. (2018). 'Reaction time predicts brain–computer interface aptitude', IEEE journal of translational engineering in health and medicine, **6***, pp. 1–11.*

de Groot, N. M., Houben, R. P., Smeets, J. L., Boersma, E., Schotten, U., Schalij, M. J., Crijns, H., and Allessie, M. A. (2010). 'Electropathological substrate of longstanding persistent atrial fibrillation in patients with structural heart disease: epicardial breakthrough', Circulation, **122***(17), pp. 1674–1682.*

de Groot, N., Shah, D., Boyle, P. M., Anter, E., Clifford, G. D., Deisenhofer, I., Deneke, T., van Dessel, P., Doessel, O., Dilaveris, P etxxxxx al.. (2021). 'Critical appraisal of technologies to assess electrical activity during atrial fibrillation: a position paper from the european heart rhythm association and european society of cardiology working group on ecardiology in collaboration with the heart rhythm society, asia pacific heart rhythm society, latin american heart rhythm society and computing in cardiology', EP Europace, .

de Groot, N., Van Der Does, L., Yaksh, A., Lanters, E., Teuwen, C., Knops, P., van de Woestijne, P., Bekkers, J., Kik, C., Bogers, A etxxxxx al.. (2016). 'Direct proof of endo-epicardial asynchrony of the atrial wall during atrial fibrillation in humans', Circulation: Arrhythmia and Electrophysiology, **9***(5), e003648.*

Deco, G., Jirsa, V. K., and McIntosh, A. R. (2011). 'Emerging concepts for the dynamical organization of resting-state activity in the brain', Nature reviews neuroscience, **12***(1), pp. 43–56.*

Del Corso, G., Verzicco, R., and Viola, F. (2022). 'A fast computational model for the electrophysiology of the whole human heart', Journal of computational physics, **457***, 111084.*

Deng, S., Srinivasan, R., Lappas, T., and D'Zmura, M. (2010). 'Eeg classification of imagined syllable rhythm using hilbert spectrum methods', Journal of neural engineering, **7***(4), 046006.*

Deno, D. C., Balachandran, R., Morgan, D., Ahmad, F., Massé, S., and Nanthakumar, K. (2016). 'Orientation-independent catheter-based characterization of myocardial activation', IEEE transactions on biomedical engineering, **64***(5), pp. 1067–1077.*

Deno, D. C., Bhaskaran, A., Morgan, D. J., Goksu, F., Batman, K., Olson, G. K., Magtibay, K., Nayyar, S., Porta-Sánchez, A., Laflamme, M. A etxxxxx al.. (2020). 'High-resolution, live, directional mapping', Heart Rhythm, **17***(9), pp. 1621–1628.*

Dittrich, S., Scheurlen, C., van den Bruck, J.-H., Filipovic, K., Wörmann, J., Erlhöfer, S., Schipper, J.-H., Lüker, J., Steven, D., and Sultan, A. (2023). 'The omnipolar mapping technology—a new mapping tool to overcome "bipolar blindness" resulting in true high-density maps', Journal of Interventional Cardiac Electrophysiology, pp. 1–10.

Dobkin, B. H. (2007). 'Brain–computer interface technology as a tool to augment plasticity and outcomes for neurological rehabilitation', The Journal of physiology, **579***(3), pp. 637–642.*

Dodeja, A. K., Tan, Y., Ackley, T., Russell, J., Kertesz, N., Daniels, C. J., and Kamp, A. (2022). 'Pentaray® multielectrode mapping catheter for atrial tachyarrhythmia in adults with congenital heart disease', Texas Heart Institute Journal, **49***(5), e207535.*

Dreyer, P., Roc, A., Pillette, L., Rimbert, S., and Lotte, F. (2023). 'A large eeg database with users' profile information for motor imagery brain-computer interface research', Scientific Data, **10***(1), 580.*

Dunlap, C. F., Colachis IV, S. C., Meyers, E. C., Bockbrader, M. A., and Friedenberg, D. A. (2020). 'Classifying intracortical brain-machine interface signal disruptions based on system performance and applicable compensatory strategies: a review', Frontiers in Neurorobotics, **14***, 558987.*

Duun-Henriksen, J., Baud, M., Richardson, M. P., Cook, M., Kouvas, G., Heasman, J. M., Friedman, D., Peltola, J., Zibrandtsen, I. C., and Kjaer, T. W. (2020). 'A new era in electroencephalographic monitoring? subscalp devices for ultra–long-term recordings', Epilepsia, **61***(9), pp. 1805–1817.*

Edelman, B. J., Meng, J., Suma, D., Zurn, C., Nagarajan, E., Baxter, B. S., Cline, C. C., and He, B. (2019). 'Noninvasive neuroimaging enhances continuous neural tracking for robotic device control', Science robotics, **4***(31), eaaw6844.*

Edelman, B. J., Zhang, S., Schalk, G., Brunner, P., Müller-Putz, G., Guan, C., and He, B. (2024). 'Non-invasive brain-computer interfaces: State of the art and trends', IEEE Reviews in Biomedical Engineering, .

Edughele, H. O., Zhang, Y., Muhammad-Sukki, F., Vien, Q.-T., Morris-Cafiero, H., and Agyeman, M. O. (2022). 'Eye-tracking assistive technologies for individuals with amyotrophic lateral sclerosis', IEEE Access, **10***, pp. 41952–41972.*

Einizade, A., Mozafari, M., Jalilpour, S., Bagheri, S., and Sardouie, S. H. (2022). 'Neural decoding of imagined speech from eeg signals using the fusion of graph signal processing and graph learning techniques', Neuroscience Informatics, **2***(3), 100091.*

Elliott, A. D., Middeldorp, M. E., Van Gelder, I. C., Albert, C. M., and Sanders, P. (2023). 'Epidemiology and modifiable risk factors for atrial fibrillation', Nature Reviews Cardiology, pp. 1–14.

Essien, U. R., Kornej, J., Johnson, A. E., Schulson, L. B., Benjamin, E. J., and Magnani, J. W. (2021). 'Social determinants of atrial fibrillation', Nature Reviews Cardiology, pp. 1–11.

Faezmehr, A., Foodeh, R., Shalchyan, V., and Daliri, M. R. (2024). 'Improving mean covariance matrix estimation by minimizing within-class dissimilarities using asymmetry of kullback-leibler divergence in mi-based bci', IEEE Transactions on Industrial Informatics, .

Fahimi, F., Zhang, Z., Goh, W. B., Lee, T.-S., Ang, K. K., and Guan, C. (2019). 'Inter-subject transfer learning with an end-to-end deep convolutional neural network for eeg-based bci', Journal of neural engineering, **16***(2), 026007.*

Ferguson, M., Sharma, D., Ross, D., and Zhao, F. (2019). 'A critical review of microelectrode arrays and strategies for improving neural interfaces', Advanced healthcare materials, **8***(19), 1900558.*

Fernyhough, C., and Borghi, A. M. (2023). 'Inner speech as language process and cognitive tool', Trends in cognitive sciences, .

Ferrero, L., Quiles, V., Ortiz, M., Iáñez, E., Gil-Agudo, Á., and Azorín, J. M. (2023). 'Brain-computer interface enhanced by virtual reality training for controlling a lower limb exoskeleton', Iscience, **26***(5).*

Flesher, S. N., Downey, J. E., Weiss, J. M., Hughes, C. L., Herrera, A. J., Tyler-Kabara, E. C., Boninger, M. L., Collinger, J. L., and Gaunt, R. A. (2021). 'A brain-computer interface that evokes tactile sensations improves robotic arm control', Science, **372***(6544), pp. 831–836.*

Foysal, K. R., and Baker, S. N. (2020). 'Induction of plasticity in the human motor system by motor imagery and transcranial magnetic stimulation', The Journal of Physiology, **598***(12), pp. 2385–2396.*

Frangogiannis, N. G. (2019). 'The extracellular matrix in ischemic and nonischemic heart failure', Circulation research, **125***(1), pp. 117–146.*

French, J., Anderson, K. D., Welden, J., Axelson, P., Bayes, B., and Burkhart, I. (2024). 'Inclusive rehabilitation and assistive technologies development: An exploration of considerations, principles, and stakeholder engagement'.

Frisch, D., Oesterlein, T. G., Unger, L. A., Lenis, G., Wakili, R., Schmitt, C., Luik, A., Dössel, O., and Loewe, A. (2020). 'Mapping and removing the ventricular far field component in unipolar atrial electrograms', IEEE Transactions on Biomedical Engineering, **67***(10), pp. 2905–2915.*

Fry, A., Breyman, E., LaGrassa, E., Oxley, T., and Putrino, D. (2023). 'Ethical considerations of endovascular brain–computer interfaces', Policy, Identity, and Neurotechnology: The Neuroethics of Brain-Computer Interfaces, Springer, pp. 43–63.

Gaeta, S., Bahnson, T. D., and Henriquez, C. (2020). 'Mechanism and magnitude of bipolar electrogram directional sensitivity: Characterizing underlying determinants of bipolar amplitude', Heart rhythm, **17***(5), pp. 777–785.*

Ganesan, A. N., Kuklik, P., Lau, D. H., Brooks, A. G., Baumert, M., Lim, W. W., Thanigaimani, S., Nayyar, S., Mahajan, R., Kalman, J. M etxxxxx al.. (2013). 'Bipolar electrogram shannon entropy at sites of rotational activation: implications for ablation of atrial fibrillation', Circulation: Arrhythmia and Electrophysiology, **6***(1), pp. 48–57.*

Gao, Z., Pang, Z., Chen, Y., Lei, G., Zhu, S., Li, G., Shen, Y., and Xu, W. (2022). 'Restoring after central nervous system injuries: neural mechanisms and translational applications of motor recovery', Neuroscience Bulletin, **38***(12), pp. 1569–1587.*

Garcia, J. V., and Wan, D. K. (2020). 'The kit: Access, catheter placement, transeptal puncture, ablation technology, 3d mapping', Decoding Cardiac Electrophysiology: Understanding the Techniques and Defining the Jargon, pp. 21–39.

García-Salinas, J. S., Torres-García, A. A., Reyes-Garćia, C. A., and Villaseñor-Pineda, L. (2023). 'Intra-subject class-incremental deep learning approach for eeg-based imagined speech recognition', Biomedical Signal Processing and Control, **81***, 104433.*

Göker, H. (2023). 'Automatic detection of parkinson's disease from power spectral density of electroencephalography (eeg) signals using deep learning model', Physical and engineering sciences in medicine, **46***(3), pp. 1163–1174.*

Goldberger, A. L., Amaral, L. A., Glass, L., Hausdorff, J. M., Ivanov, P. C., Mark, R. G., Mietus, J. E., Moody, G. B., Peng, C.-K., and Stanley, H. E. (2000). 'PhysioBank, PhysioToolkit, and PhysioNet: Components of a new research resource for complex physiologic signals', Circulation, **101***(23), pp. e215–e220.*

Goldstein, L. H., and Abrahams, S. (2013). 'Changes in cognition and behaviour in amyotrophic lateral sclerosis: nature of impairment and implications for assessment', The Lancet Neurology, **12***(4), pp. 368–380.*

Goodman, H. B., and Rowland, P. (2021). 'Deficiencies of compliancy for data and storage: Isolating the cia triad components to identify gaps to security', National Cyber Summit (NCS) Research Track 2020, Springer, pp. 170–192.

Göransson, N., Johansson, J. D., Wårdell, K., and Zsigmond, P. (2021). 'Postoperative lead movement after deep brain stimulation surgery and the change of stimulation volume', Stereotactic and functional neurosurgery, **99***(3), pp. 221–229.*

Goulet, J., Richard-Denis, A., Thompson, C., and Mac-Thiong, J.-M. (2019). 'Relationships between specific functional abilities and health-related quality of life in chronic traumatic spinal cord injury', American Journal of Physical Medicine & Rehabilitation, **98***(1), pp. 14–19.*

Grami, F., de Marco, G., Bodranghien, F., Manto, M., and Habas, C. (2022). 'Cerebellar transcranial direct current stimulation reconfigures brain networks involved in motor execution and mental imagery', The Cerebellum, **21***(4), pp. 665–680.*

Gu, L., Yu, Z., Ma, T., Wang, H., Li, Z., and Fan, H. (2020). 'Eeg-based classification of lower limb motor imagery with brain network analysis', Neuroscience, **436***, pp. 93–109.*

Guillot, A., Di Rienzo, F., MacIntyre, T., Moran, A., and Collet, C. (2012). 'Imagining is not doing but involves specific motor commands: a review of experimental data related to motor inhibition', Frontiers in human neuroscience, **6***, 247.*

Haissaguerre, M., Jaïs, P., Shah, D. C., Takahashi, A., Hocini, M., Quiniou, G., Garrigue, S., Le Mouroux, A., Le Métayer, P., and Clémenty, J. (1998). 'Spontaneous initiation of atrial fibrillation by ectopic beats originating in the pulmonary veins', New England Journal of Medicine, **339***(10), pp. 659–666.*

Haldar, S. K., Magtibay, K., Porta-Sanchez, A., Massé, S., Mitsakakis, N., Lai, P. F., Azam, M. A., Asta, J., Kusha, M., Dorian, P etxxxxx al.. (2017). 'Resolving bipolar electrogram voltages during atrial fibrillation using omnipolar mapping', Circulation: Arrhythmia and Electrophysiology, **10***(9), e005018.*

Hallett, M., Aybek, S., Dworetzky, B. A., McWhirter, L., Staab, J. P., and Stone, J. (2022). 'Functional neurological disorder: new subtypes and shared mechanisms', The Lancet Neurology, **21***(6), pp. 537–550.*

Hammer, E. M., Halder, S., Blankertz, B., Sannelli, C., Dickhaus, T., Kleih, S., Müller, K.-R., and Kübler, A. (2012). 'Psychological predictors of smr-bci performance', Biological psychology, **89***(1), pp. 80–86.*

Han, J.-W., Bak, S., Kim, J.-M., Choi, W., Shin, D.-H., Son, Y.-H., and Kam, T.-E. (2024). 'Meta-eeg: Meta-learning-based class-relevant eeg representation learning for zero-calibration brain–computer interfaces', Expert Systems with Applications, **238***, 121986.*

Handiru, V. S., and Prasad, V. A. (2016). 'Optimized bi-objective eeg channel selection and cross-subject generalization with brain–computer interfaces', IEEE Transactions on Human-Machine Systems, **46***(6), pp. 777–786.*

Harrison, J. L., Jensen, H. K., Peel, S. A., Chiribiri, A., Grøndal, A. K., Bloch, L. Ø., Pedersen, S. F., Bentzon, J. F., Kolbitsch, C., Karim, R etxxxxx al.. (2014). 'Cardiac magnetic resonance and electroanatomical mapping of acute and chronic atrial ablation injury: a histological validation study', European heart journal, **35***(22), pp. 1486–1495.*

He, H., and Wu, D. (2019). 'Transfer learning for brain–computer interfaces: A euclidean space data alignment approach', IEEE Transactions on Biomedical Engineering, **67***(2), pp. 399–410.*

Hedman, A. M., van Haren, N. E., Schnack, H. G., Kahn, R. S., and Hulshoff Pol, H. E. (2012). 'Human brain changes across the life span: a review of 56 longitudinal magnetic resonance imaging studies', Human brain mapping, **33***(8), pp. 1987–2002.*

Heijman, J., Sutanto, H., Crijns, H. J., Nattel, S., and Trayanova, N. A. (2021). 'Computational models of atrial fibrillation: Achievements, challenges, and perspectives for improving clinical care', Cardiovascular Research, **117***(7), pp. 1682–1699.*

Herman, P., Prasad, G., McGinnity, T. M., and Coyle, D. (2008). 'Comparative analysis of spectral approaches to feature extraction for eeg-based motor imagery classification', IEEE Transactions on Neural Systems and Rehabilitation Engineering, **16***(4), pp. 317–326.*

Hill, K., Kovacs, T., and Shin, S. (2015). 'Critical issues using brain-computer interfaces for augmentative and alternative communication', Archives of Physical Medicine and Rehabilitation, **96***(3), pp. S8–S15.*

Honarbakhsh, S., Schilling, R. J., Providencia, R., Keating, E., Chow, A., Sporton, S., Lowe, M., Earley, M. J., Lambiase, P. D., and Hunter, R. J. (2018). 'Characterization of drivers maintaining atrial fibrillation: correlation with markers of rapidity and organization on spectral analysis', Heart Rhythm, **15***(9), pp. 1296–1303.*

Hosseini, M.-P., Hosseini, A., and Ahi, K. (2020). 'A review on machine learning for eeg signal processing in bioengineering', IEEE reviews in biomedical engineering, **14***, pp. 204–218.*

Hua, Y., Zhao, Z., Li, R., Chen, X., Liu, Z., and Zhang, H. (2019). 'Deep learning with long short-term memory for time series prediction', IEEE Communications Magazine, **57***(6), pp. 114–119.*

Huggins, J. E., Karlsson, P., and Warschausky, S. A. (2022). 'Challenges of brain-computer interface facilitated cognitive assessment for children with cerebral palsy', Frontiers in Human Neuroscience, **16***, 977042.*

Huggins, J. E., Moinuddin, A. A., Chiodo, A. E., and Wren, P. A. (2015). 'What would brain-computer interface users want: opinions and priorities of potential users with spinal cord injury', Archives of physical medicine and rehabilitation, **96***(3), pp. S38–S45.*

Huggins, J. E., Wren, P. A., and Gruis, K. L. (2011). 'What would brain-computer interface users want? opinions and priorities of potential users with amyotrophic lateral sclerosis', Amyotrophic Lateral Sclerosis, **12***(5), pp. 318–324.*

Hwang, M., Song, J.-S., Lee, Y.-S., Li, C., Shim, E. B., and Pak, H.-N. (2016). 'Electrophysiological rotor ablation in in-silico modeling of atrial fibrillation: comparisons with dominant frequency, shannon entropy, and phase singularity', PloS one, **11***(2), e0149695.*

Iacopino, S., Cecchini, F., Tripodi, A., Sorrenti, P., Fabiano, G., and Petretta, A. (2023). 'Epicardial multisite conduction blocks detected by equispaced electrode array and omnipolar technology in brugada syndrome', HeartRhythm Case Reports, **9***(1), pp. 12–16.*

Ienca, M., and Haselager, P. (2016). 'Hacking the brain: brain–computer interfacing technology and the ethics of neurosecurity', Ethics and information technology, **18***, pp. 117–129.*

Ioffe, S., and Szegedy, C. (2015). 'Batch normalization: accelerating deep network training by reducing internal covariate shift', Proceedings of the 32nd International Conference on International Conference on Machine Learning - Volume 37, ICML'15, JMLR.org, 448–456.

Issa, Z. F., Miller, J. M., and Zipes, D. P. (2009). 'Chapter 3 - mapping and navigation modalities', in Z. F. Issa., J. M. Miller., and D. P. Zipes. (eds.), Clinical Arrhythmology and Electrophysiology, W.B. Saunders, Philadelphia, pp. 57–99.

Jadavji, Z., Zewdie, E., Kelly, D., Kinney-Lang, E., Robu, I., and Kirton, A. (2022). 'Establishing a clinical brain-computer interface program for children with severe neurological disabilities', Cureus, **14***(6).*

Jayaram, V., Alamgir, M., Altun, Y., Scholkopf, B., and Grosse-Wentrup, M. (2016). 'Transfer learning in brain-computer interfaces', IEEE Computational Intelligence Magazine, **11***(1), pp. 20–31.*

Jeannerod, M., and Decety, J. (1995). 'Mental motor imagery: a window into the representational stages of action', Current opinion in neurobiology, **5***(6), pp. 727–732.*

Jeong, C., Park, J., and Yu, H. (2015). 'Random access in millimeter-wave beamforming cellular networks: issues and approaches', IEEE Communications Magazine, **53***(1), pp. 180–185.*

Jiang, R., Beaser, A. D., Aziz, Z., Upadhyay, G. A., Nayak, H. M., and Tung, R. (2020). 'High-density grid catheter for detailed mapping of sinus rhythm and scar-related ventricular tachycardia: comparison with a linear duodecapolar catheter', Clinical Electrophysiology, **6***(3), pp. 311–323.*

Jovanovic, L. I., Kapadia, N., Zivanovic, V., Rademeyer, H. J., Alavinia, M., McGillivray, C., Kalsi-Ryan, S., Popovic, M. R., and Marquez-Chin, C. (2021). 'Brain–computer interface-triggered functional electrical stimulation therapy for rehabilitation of reaching and grasping after spinal cord injury: a feasibility study', Spinal Cord Series and Cases, **7***(1), 24.*

Kamble, A., Ghare, P. H., and Kumar, V. (2022). 'Deep-learning-based bci for automatic imagined speech recognition using spwvd', IEEE Transactions on Instrumentation and Measurement, **72***, pp. 1–10.*

Kamble, A., Ghare, P. H., and Kumar, V. (2023a). 'Optimized rational dilation wavelet transform for automatic imagined speech recognition', IEEE Transactions on Instrumentation and Measurement, **72***, pp. 1–10.*

Kamble, A., Ghare, P. H., Kumar, V., Kothari, A., and Keskar, A. G. (2023b). 'Spectral analysis of eeg signals for automatic imagined speech recognition', IEEE Transactions on Instrumentation and Measurement, **72***, pp. 1–9.*

Kang, H., and Choi, S. (2014). 'Bayesian common spatial patterns for multi-subject eeg classification', Neural Networks, **57***, pp. 39–50.*

Kang, H., Nam, Y., and Choi, S. (2009). 'Composite common spatial pattern for subject-to-subject transfer', IEEE Signal Processing Letters, **16***(8), pp. 683–686.*

Kaongoen, N., Choi, J., Choi, J. W., Kwon, H., Hwang, C., Hwang, G., Kim, B. H., and Jo, S. (2023). 'The future of wearable eeg: A review of ear-eeg technology and its applications', Journal of neural engineering, .

Karatela, M. F., Dowell, R. S., Friedman, D., Jackson, K. P., and Piccini, J. P. (2022). 'Omnipolar versus bipolar electrode mapping in patients with atrial fibrillation undergoing catheter ablation', Clinical Electrophysiology, **8***(12), pp. 1539–1552.*

Karikari, E., and Koshechkin, K. A. (2023). 'Review on brain-computer interface technologies in healthcare', Biophysical Reviews, **15***(5), pp. 1351–1358.*

Karki, R., Raina, A., Ezzeddine, F. M., Bois, M. C., and Asirvatham, S. J. (2021). 'Anatomy and pathology of the cardiac conduction system', Cardiac Electrophysiology Clinics, **13***(4), pp. 569–584.*

Karlsson, P., Orlandi, S., Zhao, H., and McEwan, A. (2022). 'Brain–computer interface as a potential access method for communication in non-verbal children with cerebral palsy: a state-of-the-art review', Wearable/Personal Monitoring Devices Present to Future, pp. 61–85.

Kasahara, K., DaSalla, C. S., Honda, M., and Hanakawa, T. (2015). 'Neuroanatomical correlates of brain–computer interface performance', Neuroimage, **110***, pp. 95–100.*

Kelly, D., Rowley, D., Floreani, E. D., Kinney-Lang, E., Robu, I., and Kirton, A. (2023). 'Think big: brain-computer interface goals for children with quadriplegic cerebral palsy', 2023 IEEE International Conference on Systems, Man, and Cybernetics (SMC), IEEE, pp. 3323–3328.

Keser, Z., Buchl, S. C., Seven, N. A., Markota, M., Clark, H. M., Jones, D. T., Lanzino, G., Brown Jr, R. D., Worrell, G. A., and Lundstrom, B. N. (2022). 'Electroencephalogram (eeg) with or without transcranial magnetic stimulation (tms) as biomarkers for post-stroke recovery: a narrative review', Frontiers in neurology, **13***, 827866.*

Kim, Y.-H., Chen, S.-A., Ernst, S., Guzman, C. E., Han, S., Kalarus, Z., Labadet, C., Lin, Y.-J., Lo, L.-W., Nogami, A etxxxxx al.. (2020). '2019 aphrs expert consensus statement on three-dimensional mapping systems for tachycardia developed in collaboration with hrs, ehra, and lahrs', Journal of arrhythmia, **36***(2), 215.*

Kiranyaz, S., Avci, O., Abdeljaber, O., Ince, T., Gabbouj, M., and Inman, D. J. (2021). '1d convolutional neural networks and applications: A survey', Mechanical systems and signal processing, **151***, 107398.*

Kiranyaz, S., Ince, T., and Gabbouj, M. (2015a). 'Real-time patient-specific ecg classification by 1-d convolutional neural networks', IEEE transactions on biomedical engineering, **63***(3), pp. 664–675.*

Kiranyaz, S., Ince, T., Hamila, R., and Gabbouj, M. (2015b). 'Convolutional neural networks for patient-specific ecg classification', 2015 37th Annual International Conference of the IEEE Engineering in Medicine and Biology Society (EMBC), IEEE, pp. 2608–2611.

Kleih-Dahms, S. C., Botrel, L., and Kübler, A. (2021). 'The influence of motivation and emotion on sensorimotor rhythm-based brain–computer interface performance', Psychophysiology, **58***(8), e13832.*

Klein, E., and Ojemann, J. (2016). 'Informed consent in implantable bci research: identification of research risks and recommendations for development of best practices', Journal of Neural Engineering, **13***(4), 043001.*

Klemm, H. U., Steven, D., Johnsen, C., Ventura, R., Rostock, T., Lutomsky, B., Risius, T., Meinertz, T., and Willems, S. (2007). 'Catheter motion during atrial ablation due to the beating heart and respiration: Impact on accuracy and spatial referencing in three-dimensional mapping', Heart Rhythm, **4***(5), pp. 587–592.*

Klimesch, W. (2018). 'The frequency architecture of brain and brain body oscillations: an analysis', European Journal of Neuroscience, **48***(7), pp. 2431–2453.*

Kondziella, D., Amiri, M., Othman, M. H., Jakobsen, E. W., Jansen, T., and Møller, K. (2023). 'Understanding, detecting, and stimulating consciousness recovery in the icu', Acta Neurochirurgica, **165***(4), pp. 809–828.*

Krizhevsky, A., Sutskever, I., and Hinton, G. E. (2012). 'Imagenet classification with deep convolutional neural networks', Advances in neural information processing systems, **25***.*

Krusienski, D. J., Grosse-Wentrup, M., Galán, F., Coyle, D., Miller, K. J., Forney, E., and Anderson, C. W. (2011). 'Critical issues in state-of-the-art brain–computer interface signal processing', Journal of neural engineering, **8***(2), 025002.*

Kübler, A., Holz, E. M., Riccio, A., Zickler, C., Kaufmann, T., Kleih, S. C., Staiger-Sälzer, P., Desideri, L., Hoogerwerf, E.-J., and Mattia, D. (2014). 'The user-centered design as novel perspective for evaluating the usability of bci-controlled applications', PloS one, **9***(12), e112392.*

Kumar, S., Alawieh, H., Racz, F. S., Fakhreddine, R., and Millán, J. d. R. (2024). 'Transfer learning promotes acquisition of individual bci skills', PNAS nexus, **3***(2), pgae076.*

Kuo, M.-J., Lo, L.-W., Lin, Y.-J., Chang, S.-L., Hu, Y.-F., Chung, F.-P., Tuan, T.-C., Chao, T.-F., Liao, J.-N., Chang, T.-Y etxxxxx al.. (2022). 'Low voltage zones detected by omnipolar vmax map accurately identifies the potential atrial substrate and predicts the af ablation outcome after pv isolation', International journal of cardiology, **351***, pp. 42–47.*

Kwak, Y., Kong, K., Song, W.-J., and Kim, S.-E. (2023). 'Subject-invariant deep neural networks based on baseline correction for eeg motor imagery bci', IEEE Journal of Biomedical and Health Informatics, **27***(4), pp. 1801–1812.*

Kwon, M., Cho, H., Won, K., Ahn, M., and Jun, S. C. (2020). 'Use of both eyes-open and eyes-closed resting states may yield a more robust predictor of motor imagery bci performance', Electronics, **9***(4), 690.*

Ladas, T. P., Sugrue, A., Nan, J., Vaidya, V. R., Padmanabhan, D., Venkatachalam, K., and Asirvatham, S. J. (2019). 'Fundamentals of cardiac mapping', Card Electrophysiol Clin, **11***(3), pp. 433–48.*

LaFleur, K., Cassady, K., Doud, A., Shades, K., Rogin, E., and He, B. (2013). 'Quadcopter control in three-dimensional space using a noninvasive motor imagery-based brain–computer interface', Journal of neural engineering, **10***(4), 046003.*

Lee, D.-Y., Lee, M., and Lee, S.-W. (2021). 'Decoding imagined speech based on deep metric learning for intuitive bci communication', IEEE Transactions on Neural Systems and Rehabilitation Engineering, **29***, pp. 1363–1374.*

Lee, M., Yoon, J.-G., and Lee, S.-W. (2020). 'Predicting motor imagery performance from resting-state eeg using dynamic causal modeling', Frontiers in human neuroscience, **14***, 321.*

Leeuwis, N., Yoon, S., and Alimardani, M. (2021). 'Functional connectivity analysis in motor-imagery brain computer interfaces', Frontiers in Human Neuroscience, **15***, 732946.*

Leuthardt, E. C., Moran, D. W., and Mullen, T. R. (2021). 'Defining surgical terminology and risk for brain computer interface technologies', Frontiers in Neuroscience, **15***, 599549.*

Li, F., Chao, W., Li, Y., Fu, B., Ji, Y., Wu, H., and Shi, G. (2021a). 'Decoding imagined speech from eeg signals using hybrid-scale spatial-temporal dilated convolution network', Journal of neural engineering, **18***(4), 0460c4.*

Li, F., Yi, C., Song, L., Jiang, Y., Peng, W., Si, Y., Zhang, T., Zhang, R., Yao, D., Zhang, Y etxxxxx al.. (2019). 'Brain network reconfiguration during motor imagery revealed by a large-scale network analysis of scalp eeg', Brain topography, **32***, pp. 304–314.*

Li, H., Ding, M., Zhang, R., and Xiu, C. (2022). 'Motor imagery eeg classification algorithm based on cnn-lstm feature fusion network', Biomedical signal processing and control, **72***, 103342.*

Li, X., Chu, G. S., Almeida, T. P., Vanheusden, F. J., Salinet, J., Dastagir, N., Mistry, A. R., Vali, Z., Sidhu, B., Stafford, P. J etxxxxx al.. (2021b). 'Automatic extraction of recurrent patterns of high dominant frequency mapping during human persistent atrial fibrillation', Frontiers in physiology, **12***.*

Li, Y., and Nam, C. S. (2016). 'Collaborative brain-computer interface for people with motor disabilities [research frontier]', IEEE Computational Intelligence Magazine, **11***(3), pp. 56–66.*

Li, Y., Kambara, H., Koike, Y., and Sugiyama, M. (2010). 'Application of covariate shift adaptation techniques in brain–computer interfaces', IEEE Transactions on Biomedical Engineering, **57***(6), pp. 1318–1324.*

Linz, D., Saha, S., Kutieleh, R., Kadhim, K., Lau, D., Baumert, M., and Sanders, P. (2019). 'Impact of bipolar vector orientation and inter-electrode spacing on electrograms during human atrial fibrillation', European Heart Journal, **40***(Supplement_1), pp. ehz748–1153.*

Liu, J., Wang, R., Yang, Y., Zong, Y., Leng, Y., Zheng, W., and Ge, S. (2024). 'Convolutional transformer-based cross subject model for ssvep-based bci classification', IEEE Journal of Biomedical and Health Informatics, .

Liu, S., Wang, J., Li, S., and Cai, L. (2023a). 'Epileptic seizure detection and prediction in eegs using power spectra density parameterization', IEEE Transactions on Neural Systems and Rehabilitation Engineering, **31***, pp. 3884–3894.*

Liu, S., Zhang, J., Wang, A., Wu, H., Zhao, Q., and Long, J. (2022). 'Subject adaptation convolutional neural network for eeg-based motor imagery classification', Journal of Neural Engineering, **19***(6), 066003.*

Liu, X., Xiong, S., Wang, X., Liang, T., Wang, H., and Liu, X. (2023b). 'A compact multi-branch 1d convolutional neural network for eeg-based motor imagery classification', Biomedical Signal Processing and Control, **81***, 104456.*

Liv, N., and Greenbaum, D. (2023). 'Cyberneurosecurity', Policy, Identity, and Neurotechnology: The Neuroethics of Brain-Computer Interfaces, Springer, pp. 233–251.

Lopez-Bernal, D., Balderas, D., Ponce, P., and Molina, A. (2022). 'A state-of-the-art review of eeg-based imagined speech decoding', Frontiers in human neuroscience, **16***, 867281.*

Lopez-Bernal, D., Balderas, D., Ponce, P., and Molina, A. (2024). 'Exploring inter-trial coherence for inner speech classification in eeg-based brain–computer interface', Journal of Neural Engineering, **21***(2), 026048.*

Lorach, H., Galvez, A., Spagnolo, V., Martel, F., Karakas, S., Intering, N., Vat, M., Faivre, O., Harte, C., Komi, S etxxxxx al.. (2023). 'Walking naturally after spinal cord injury using a brain–spine interface', Nature, **618***(7963), pp. 126–133.*

Lotte, F., Bougrain, L., Cichocki, A., Clerc, M., Congedo, M., Rakotomamonjy, A., and Yger, F. (2018). 'A review of classification algorithms for eeg-based brain–computer interfaces: a 10 year update', Journal of neural engineering, **15***(3), 031005.*

Lotte, F., Congedo, M., Lécuyer, A., Lamarche, F., and Arnaldi, B. (2007). 'A review of classification algorithms for eeg-based brain–computer interfaces', Journal of neural engineering, **4***(2), R1.*

Lu, H., Eng, H.-L., Guan, C., Plataniotis, K. N., and Venetsanopoulos, A. N. (2010). 'Regularized common spatial pattern with aggregation for eeg classification in small-sample setting', IEEE transactions on Biomedical Engineering, **57***(12), pp. 2936–2946.*

Lu, L., Han, M., Zou, G., Zheng, L., and Gao, J.-H. (2023). 'Common and distinct neural representations of imagined and perceived speech', Cerebral Cortex, **33***(10), pp. 6486–6493.*

Lumsden, D. E., Ashmore, J., Charles-Edwards, G., Selway, R., Lin, J.-P., and Ashkan, K. (2015). 'Observation and modeling of deep brain stimulation electrode depth in the pallidal target of the developing brain', World Neurosurgery, **83***(4), pp. 438–446.*

Lydiard, S., Pontré, B., Lowe, B. S., Ball, H., Sasso, G., and Keall, P. (2021). 'Cardiac radioablation for atrial fibrillation: Target motion characterization and treatment delivery considerations', Medical Physics, **48***(3), pp. 931–941.*

Makris, T., Dorstyn, D., and Crettenden, A. (2021). 'Quality of life in children and adolescents with cerebral palsy: a systematic review with meta-analysis', Disability and rehabilitation, **43***(3), pp. 299–308.*

Martin, S., Armstrong, E., Thomson, E., Vargiu, E., Solà, M., Dauwalder, S., Miralles, F., and Daly Lynn, J. (2018). 'A qualitative study adopting a user-centered approach to design and validate a brain computer interface for cognitive rehabilitation for people with brain injury', Assistive Technology, **30***(5), pp. 233–241.*

Martinez-Iniesta, M., Ródenas, J., Alcaraz, R., and Rieta, J. J. (2017). 'Waveform integrity in atrial fibrillation: The forgotten issue of cardiac electrophysiology', Annals of biomedical engineering, **45***(8), pp. 1890–1907.*

Martini, M. L., Oermann, E. K., Opie, N. L., Panov, F., Oxley, T., and Yaeger, K. (2020). 'Sensor modalities for brain-computer interface technology: a comprehensive literature review', Neurosurgery, **86***(2), pp. E108–E117.*

Massé, S., Magtibay, K., Jackson, N., Asta, J., Kusha, M., Zhang, B., Balachandran, R., Radisic, M., Deno, D. C., and Nanthakumar, K. (2016). 'Resolving myocardial activation with novel omnipolar electrograms', Circulation: Arrhythmia and Electrophysiology, **9***(7), e004107.*

Metzger, S. L., Littlejohn, K. T., Silva, A. B., Moses, D. A., Seaton, M. P., Wang, R., Dougherty, M. E., Liu, J. R., Wu, P., Berger, M. A etxxxxx al.. (2023). 'A high-performance

neuroprosthesis for speech decoding and avatar control', Nature, **620***(7976), pp. 1037–1046.*

Micera, S., Caleo, M., Chisari, C., Hummel, F. C., and Pedrocchi, A. (2020). 'Advanced neurotechnologies for the restoration of motor function', Neuron, **105***(4), pp. 604–620.*

Miinalainen, T., Rezaei, A., Us, D., Nüßing, A., Engwer, C., Wolters, C. H., and Pursiainen, S. (2019). 'A realistic, accurate and fast source modeling approach for the eeg forward problem', NeuroImage, **184***, pp. 56–67.*

Milekovic, T., Sarma, A. A., Bacher, D., Simeral, J. D., Saab, J., Pandarinath, C., Sorice, B. L., Blabe, C., Oakley, E. M., Tringale, K. R etxxxxx al.. (2018). 'Stable long-term bci-enabled communication in als and locked-in syndrome using lfp signals', Journal of neurophysiology, **120***(7), pp. 343–360.*

Min, B.-K., Marzelli, M. J., and Yoo, S.-S. (2010). 'Neuroimaging-based approaches in the brain–computer interface', Trends in biotechnology, **28***(11), pp. 552–560.*

Moghimi, S., Kushki, A., Marie Guerguerian, A., and Chau, T. (2013). 'A review of eeg-based brain-computer interfaces as access pathways for individuals with severe disabilities', Assistive Technology, **25***(2), pp. 99–110.*

Mohammadi, M., Knoche, H., Thøgersen, M., Bengtson, S. H., Kobbelgaard, F. V., Gull, M. A., Bentsen, B., Severinsen, K. E., Khan, B. Y. A., and Struijk, L. N. A. (2023). 'Tongue control of a five-dof upper-limb exoskeleton rehabilitates drinking and eating for individuals with severe disabilities', International Journal of Human-Computer Studies, **170***, 102962.*

Monforte, J., Smith, B., and Pérez-Samaniego, V. (2021). "it's not a part of me, but it is what it is': the struggle of becoming en-wheeled after spinal cord injury', Disability and Rehabilitation, **43***(17), pp. 2447–2453.*

Morishita, T., Hilliard, J. D., Okun, M. S., Neal, D., Nestor, K. A., Peace, D., Hozouri, A. A., Davidson, M. R., Bova, F. J., Sporrer, J. M etxxxxx al.. (2017). 'Postoperative lead migration in deep brain stimulation surgery: incidence, risk factors, and clinical impact', PLoS One, **12***(9), e0183711.*

Moses, D. A., Metzger, S. L., Liu, J. R., Anumanchipalli, G. K., Makin, J. G., Sun, P. F., Chartier, J., Dougherty, M. E., Liu, P. M., Abrams, G. M etxxxxx al.. (2021). 'Neuroprosthesis for decoding speech in a paralyzed person with anarthria', New England Journal of Medicine, **385***(3), pp. 217–227.*

Motamedi-Fakhr, S., Moshrefi-Torbati, M., Hill, M., Hill, C. M., and White, P. R. (2014). 'Signal processing techniques applied to human sleep eeg signals—a review', Biomedical Signal Processing and Control, **10***, pp. 21–33.*

Mrachacz-Kersting, N., Ibáñez, J., and Farina, D. (2021). 'Towards a mechanistic approach for the development of non-invasive brain-computer interfaces for motor rehabilitation', The Journal of physiology, **599***(9), pp. 2361–2374.*

Mrachacz-Kersting, N., Jiang, N., Stevenson, A. J. T., Niazi, I. K., Kostic, V., Pavlovic, A., Radovanovic, S., Djuric-Jovicic, M., Agosta, F., Dremstrup, K etxxxxx al.. (2016). 'Efficient neuroplasticity induction in chronic stroke patients by an associative brain-computer interface', Journal of neurophysiology, **115***(3), pp. 1410–1421.*

Nademanee, K., McKenzie, J., Kosar, E., Schwab, M., Sunsaneewitayakul, B., Vasavakul, T., Khunnawat, C., and Ngarmukos, T. (2004). 'A new approach for catheter ablation of atrial fibrillation: mapping of the electrophysiologic substrate', Journal of the American College of Cardiology, **43***(11), pp. 2044–2053.*

Nairn, D., Nagel, C., Mueller-Edenborn, B., Lehrmann, H., Jadidi, A., and Loewe, A. (2021). 'Spatial and quantitative assessment of the correlation between sinus rhythm and atrial fibrillation voltage mapping to identify low voltage substrate in persistent atrial fibrillation', EP Europace, **23***(Supplement_3), pp. euab116–163.*

Nalborczyk, L., Longcamp, M., Bonnard, M., Serveau, V., Spieser, L., and Alario, F.-X. (2023). 'Distinct neural mechanisms support inner speaking and inner hearing', Cortex, **169***, pp. 161–173.*

Narayan, S. M., Krummen, D. E., and RAPPEL, W.-J. (2012a). 'Clinical mapping approach to diagnose electrical rotors and focal impulse sources for human atrial fibrillation', Journal of cardiovascular electrophysiology, **23***(5), pp. 447–454.*

Narayan, S. M., Krummen, D. E., Shivkumar, K., Clopton, P., Rappel, W.-J., and Miller, J. M. (2012b). 'Treatment of atrial fibrillation by the ablation of localized sources: Confirm (conventional ablation for atrial fibrillation with or without focal impulse and rotor modulation) trial', Journal of the American College of Cardiology, **60***(7), pp. 628–636.*

Naseer, N., and Hong, K.-S. (2015). 'fnirs-based brain-computer interfaces: a review', Frontiers in human neuroscience, **9***, 3.*

Naser, M. Y., and Bhattacharya, S. (2023). 'Towards practical bci-driven wheelchairs: a systematic review study', IEEE Transactions on Neural Systems and Rehabilitation Engineering, **31***, pp. 1030–1044.*

Nattel, S. (2002). 'New ideas about atrial fibrillation 50 years on', Nature, **415***(6868), pp. 219–226.*

Nattel, S., and Dobrev, D. (2017). 'Controversies about atrial fibrillation mechanisms: aiming for order in chaos and whether it matters', Circulation research, **120***(9), pp. 1396–1398.*

Naufel, S., and Klein, E. (2020). 'Brain–computer interface (bci) researcher perspectives on neural data ownership and privacy', Journal of Neural Engineering, **17***(1), 016039.*

Nguyen, C. H., Karavas, G. K., and Artemiadis, P. (2017). 'Inferring imagined speech using eeg signals: a new approach using riemannian manifold features', Journal of neural engineering, **15***(1), 016002.*

Nguyen, T. P., Qu, Z., and Weiss, J. N. (2014). 'Cardiac fibrosis and arrhythmogenesis: the road to repair is paved with perils', Journal of molecular and cellular cardiology, **70***, pp. 83–91.*

Nijboer, F., Clausen, J., Allison, B. Z., and Haselager, P. (2013). 'The asilomar survey: Stakeholders' opinions on ethical issues related to brain-computer interfacing', Neuroethics, **6***, pp. 541–578.*

Nijboer, F., Plass-Oude Bos, D., Blokland, Y., van Wijk, R., and Farquhar, J. (2014). 'Design requirements and potential target users for brain-computer interfaces–recommendations from rehabilitation professionals', Brain-Computer Interfaces, **1***(1), pp. 50–61.*
Octaray™ mapping catheter with trueref™ technology

Octaray™ mapping catheter with trueref™ technology (n.d.). Accessed February 21, 2023 [Online].

Oesterlein, T., Frisch, D., Loewe, A., Seemann, G., Schmitt, C., Dössel, O., and Luik, A. (2016). 'Basket-type catheters: diagnostic pitfalls caused by deformation and limited coverage', BioMed research international, **2016***.*

Ollitrault, P., Champ-Rigot, L., Ferchaud, V., Pellissier, A., Coffin, O., and Milliez, P. (2021). 'Vascular entrapment of a multipolar basket catheter (oriontm) during catheter ablation', Journal of Cardiovascular Electrophysiology, **32***(2), pp. 545–546.*

Organization, W. H etxxxxx al.. (2002). 'Towards a common language for functioning, disability, and health: Icf', The international classification of functioning, disability and health, .

Orlandi, S., House, S. C., Karlsson, P., Saab, R., and Chau, T. (2021). 'Brain-computer interfaces for children with complex communication needs and limited mobility: a systematic review', Frontiers in Human Neuroscience, **15***, 643294.*

Orsborn, A. L., Moorman, H. G., Overduin, S. A., Shanechi, M. M., Dimitrov, D. F., and Carmena, J. M. (2014). 'Closed-loop decoder adaptation shapes neural plasticity for skillful neuroprosthetic control', Neuron, **82***(6), pp. 1380–1393.*

Ortiz, M., Iáñez, E., Gaxiola-Tirado, J. A., Gutiérrez, D., and Azorín, J. M. (2020). 'Study of the functional brain connectivity and lower-limb motor imagery performance after transcranial direct current stimulation', International Journal of Neural Systems, **30***(08), 2050038.*

Oxley, T. J., Opie, N. L., John, S. E., Rind, G. S., Ronayne, S. M., Wheeler, T. L., Judy, J. W., McDonald, A. J., Dornom, A., Lovell, T. J etxxxxx al.. (2016). 'Minimally invasive endovascular stent-electrode array for high-fidelity, chronic recordings of cortical neural activity', Nature biotechnology, **34***(3), pp. 320–327.*

Padala, S. K., Cabrera, J.-A., and Ellenbogen, K. A. (2021). 'Anatomy of the cardiac conduction system', Pacing and Clinical Electrophysiology, **44***(1), pp. 15–25.*

Pagani, S., Dede', L., Frontera, A., Salvador, M., Limite, L., Manzoni, A., Lipartiti, F., Tsitsinakis, G., Hadjis, A., Della Bella, P etxxxxx al.. (2021). 'A computational study of the electrophysiological substrate in patients suffering from atrial fibrillation', Frontiers in Physiology, **12***, 673612.*

Park, H., and Jun, S. C. (2024). 'Connectivity study on resting-state eeg between motor imagery bci-literate and bci-illiterate groups', Journal of Neural Engineering, **21***(4), 046042.*

Park, W., Kwon, G. H., Kim, Y.-H., Lee, J.-H., and Kim, L. (2016). 'Eeg response varies with lesion location in patients with chronic stroke', Journal of neuroengineering and rehabilitation, **13***, pp. 1–10.*

Park, Y., and Chung, W. (2020). 'Optimal channel selection using correlation coefficient for csp based eeg classification', IEEE Access, **8***, pp. 111514–111521.*

Pathik, B., Lee, G., Sacher, F., Haïssaguerre, M., Jaïs, P., Massoullié, G., Derval, N., Sanders, P., Kistler, P., and Kalman, J. M. (2017). 'Epicardial-endocardial breakthrough during stable atrial macroreentry: evidence from ultra–high-resolution 3-dimensional mapping', Heart Rhythm, **14***(8), pp. 1200–1207.*

Patrick-Krueger, K. M., Burkhart, I., and Contreras-Vidal, J. L. (2024). 'The state of clinical trials of implantable brain–computer interfaces', Nature Reviews Bioengineering, pp. 1–18.

Pawar, D., and Dhage, S. (2023). 'Eeg-based covert speech decoding using random rotation extreme learning machine ensemble for intuitive bci communication', Biomedical Signal Processing and Control, **80***, 104379.*

Pellman, J., Lyon, R. C., and Sheikh, F. (2010). 'Extracellular matrix remodeling in atrial fibrosis: mechanisms and implications in atrial fibrillation', Journal of molecular and cellular cardiology, **48***(3), pp. 461–467.*

Pelouch, V., Dixon, I., Golfman, L., Beamish, R. E., and Dhalla, N. S. (1993). 'Role of extracellular matrix proteins in heart function', Molecular and cellular biochemistry, **129***(2), pp. 101–120.*

Pérez-Velasco, S., Marcos-Martínez, D., Santamaría-Vázquez, E., Martínez-Cagigal, V., and Hornero, R. (2025). 'Bridging motor execution and motor imagery bci paradigms: An inter-task transfer learning approach', Biomedical Signal Processing and Control, **107***, 107834.*

Pérez-Zapata, A., Cardona-Escobar, A. F., Jaramillo-Garzón, J. A., and Díaz, G. M. (2018). 'Deep convolutional neural networks and power spectral density features for motor imagery classification of eeg signals', Augmented Cognition: Intelligent Technologies: 12th International Conference, AC 2018, Held as Part of HCI International 2018, Las Vegas, NV, USA, July 15-20, 2018, Proceedings, Part I, Springer, pp. 158–169.

Peters, R. (2006). 'Ageing and the brain', Postgraduate medical journal, **82***(964), pp. 84–88.*

Pfeiffer, E. R., Tangney, J. R., Omens, J. H., and McCulloch, A. D. (2014). 'Biomechanics of cardiac electromechanical coupling and mechanoelectric feedback', Journal of biomechanical engineering, **136***(2), 021007.*

Phan, H., Lorenzen, K. P., Heremans, E., Chén, O. Y., Tran, M. C., Koch, P., Mertins, A., Baumert, M., Mikkelsen, K. B., and De Vos, M. (2023). 'L-seqsleepnet: Whole-cycle long sequence modelling for automatic sleep staging', IEEE Journal of Biomedical and Health Informatics, .

Poeppel, D., and Assaneo, M. F. (2020). 'Speech rhythms and their neural foundations', Nature reviews neuroscience, **21***(6), pp. 322–334.*

Prabhu, S., and Sohaib, A. (2020). 'The basic language of cardiac electrophysiology—an introduction to intracardiac electrograms and electrophysiology studies', Decoding Cardiac Electrophysiology: Understanding the Techniques and Defining the Jargon, pp. 3–19.

Pratts, J., Pobric, G., and Yao, B. (2023). 'Bridging phenomenology and neural mechanisms of inner speech: Ale meta-analysis on egocentricity and spontaneity in a dual-mechanistic framework', NeuroImage, **282***, 120399.*

Quah, J. X., Dharmaprani, D., Tiver, K., Lahiri, A., Hecker, T., Perry, R., Selvanayagam, J. B., Joseph, M. X., McGavigan, A., and Ganesan, A. (2021). 'Atrial fibrosis and substrate based characterization in atrial fibrillation: Time to move forwards', Journal of Cardiovascular Electrophysiology, **32***(4), pp. 1147–1160.*

Ragot, D., Nayyar, S., Massin, S. Z., Ha, A. C., Singh, S. M., Labos, C., Suszko, A., Dalvi, R., and Chauhan, V. S. (2021). 'Unipolar electrogram-based voltage mapping with far-field cancellation to improve detection of abnormal atrial substrate during atrial fibrillation', Journal of Cardiovascular Electrophysiology, **32***(6), pp. 1572–1583.*

Ramirez, F. D., Reddy, V. Y., Viswanathan, R., Hocini, M., and Jaïs, P. (2020). 'Emerging technologies for pulmonary vein isolation', Circulation Research, **127***(1), pp. 170–183.*

Ramoser, H., Muller-Gerking, J., and Pfurtscheller, G. (2000). 'Optimal spatial filtering of single trial eeg during imagined hand movement', IEEE transactions on rehabilitation engineering, **8***(4), pp. 441–446.*

Rao, R. P., Stocco, A., Bryan, M., Sarma, D., Youngquist, T. M., Wu, J., and Prat, C. S. (2014). 'A direct brain-to-brain interface in humans', PloS one, **9***(11), e111332.*

Ravelli, F., Masè, M., Cristoforetti, A., Avogaro, L., D'Amato, E., Tessarolo, F., Piccoli, F., and Graffigna, A. (2023). 'Quantitative assessment of transmural fibrosis profile in the human atrium: evidence for a three-dimensional arrhythmic substrate by slice-to-slice histology', Europace, **25***(2), pp. 739–747.*

Ravelli, F., Mase, M., Cristoforetti, A., Marini, M., and Disertori, M. (2014). 'The logical operator map identifies novel candidate markers for critical sites in patients with atrial fibrillation', Progress in Biophysics and Molecular Biology, **115***(2-3), pp. 186–197.*

Reese-Petersen, A. L., Olesen, M. S., Karsdal, M. A., Svendsen, J. H., and Genovese, F. (2020). 'Atrial fibrillation and cardiac fibrosis: A review on the potential of extracellular matrix proteins as biomarkers', Matrix biology, **91***, pp. 188–203.*

Reyna, M. A., Amorim, E., Sameni, R., Weigle, J., Elola, A., Bahrami Rad, A., Seyedi, S., Kwon, H., Zheng, W.-L., Ghassemi, M., van Putten., J.A.M., M., Hofmeijer, J., Gaspard, N., Sivaraju, A., Herman, S., Lee, J. W., Westover, M. B., and Clifford, G. D. (2023). 'Predicting neurological recovery from coma after cardiac arrest: The George B. Moody PhysioNet Challenge 2023', Computing in Cardiology, **50***, pp. 1–4.*

Rimbert, S., Gayraud, N., Bougrain, L., Clerc, M., and Fleck, S. (2019). 'Can a subjective questionnaire be used as brain-computer interface performance predictor?', Frontiers in human neuroscience, **12***, 529.*

Roberts, J. W., Wood, G., and Wakefield, C. J. (2020). 'Examining the equivalence between imagery and execution within the spatial domain–does motor imagery account for signal-dependent noise?', Experimental Brain Research, **238***(12), pp. 2983–2992.*

Rodrigo, M., Alhusseini, M. I., Rogers, A. J., Krittanawong, C., Thakur, S., Feng, R., Ganesan, P., and Narayan, S. M. (2022). 'Atrial fibrillation signatures on intracardiac electrograms identified by deep learning', Computers in Biology and Medicine, **145***, 105451.*

Roney, C. H., Whitaker, J., Sim, I., O'Neill, L., Mukherjee, R. K., Razeghi, O., Vigmond, E. J., Wright, M., O'Neill, M. D., Williams, S. E etxxxxx al.. (2019a). 'A technique for measuring anisotropy in atrial conduction to estimate conduction velocity and atrial fibre direction', Computers in biology and medicine, **104***, pp. 278–290.*

Roney, C. H., Wit, A. L., and Peters, N. S. (2019b). 'Challenges associated with interpreting mechanisms of af', Arrhythmia & Electrophysiology Review, **8***(4), 273.*

Roy, S., Chowdhury, A., McCreadie, K., and Prasad, G. (2020). 'Deep learning based inter-subject continuous decoding of motor imagery for practical brain-computer interfaces', Frontiers in Neuroscience, **14***, 918.*

Rubin, D. B., Ajiboye, A. B., Barefoot, L., Bowker, M., Cash, S. S., Chen, D., Donoghue, J. P., Eskandar, E. N., Friehs, G., Grant, C etxxxxx al.. (2023). 'Interim safety profile

from the feasibility study of the braingate neural interface system', Neurology, **100***(11), pp. e1177–e1192.*

Ruiperez-Campillo, S., Castells, F., Crespo, M., Pancorbo, L., Guill, A., Chorro, F., Merino, J., Casado-Arroyo, R., and Millet, J. (2023a). 'Study of the omnipolar egm reconstruction for robustness against wavefront propagation in epicardial signals', Europace, **25***(Supplement_1), pp. euad122–662.*

Ruipérez-Campillo, S., Crespo, M., Tormos, Á., Guill, A., Cebrián, A., Alberola, A., Heimer, J., Chorro, F. J., Millet, J., and Castells, F. (2023b). 'Evaluation and assessment of clique arrangements for the estimation of omnipolar electrograms in high density electrode arrays: an experimental animal model study', Physical and Engineering Sciences in Medicine, pp. 1–12.

Saha, P., and Fels, S. (2019). 'Hierarchical deep feature learning for decoding imagined speech from eeg', Proceedings of the AAAI Conference on Artificial Intelligence, Vol. 33, pp. 10019–10020.

Saha, S., Ahmed, K. I., and Mostafa, R. (2016). 'Wavelet coherence based channel selection for classifying single trial motor imagery', 2016 9th International Conference on Electrical and Computer Engineering (ICECE), IEEE, pp. 467–470.

Saha, S., Ahmed, K. I., Mostafa, R., Khandoker, A. H., and Hadjileontiadis, L. (2017a). 'Enhanced inter-subject brain computer interface with associative sensorimotor oscillations', Healthcare technology letters, **4***(1), pp. 39–43.*

Saha, S., Ahmed, K. I. U., Mostafa, R., Hadjileontiadis, L., and Khandoker, A. (2017b). 'Evidence of variabilities in eeg dynamics during motor imagery-based multiclass brain–computer interface', IEEE Transactions on Neural Systems and Rehabilitation Engineering, **26***(2), pp. 371–382.*

Saha, S., Alam, R.-u., Samore, A., Goodwin, A., Wong, M. L.-S., McEwan, A., and Anderson, C. (2023a). 'Time-embedded eeg sequence learning for comatose patients' prognosis', 2023 Computing in Cardiology (CinC), Vol. 50, IEEE, pp. 1–4.

Saha, S., and Baumert, M. (2020). 'Intra-and inter-subject variability in eeg-based sensorimotor brain computer interface: a review', Frontiers in computational neuroscience, **13***, 87.*

Saha, S., Baumert, M., and McEwan, A. (2023b). 'Can inter-subject associativity predict data-driven bci performance?', 2023 45th Annual International Conference of the IEEE Engineering in Medicine & Biology Society (EMBC), IEEE, pp. 1–4.

Saha, S., Hartmann, S., Linz, D., Sanders, P., and Baumert, M. (2019a). 'A ventricular far-field artefact filtering technique for atrial electrograms', 2019 Computing in Cardiology (CinC), IEEE, pp. Page–1.

Saha, S., Hossain, M. S., Ahmed, K., Mostafa, R., Hadjileontiadis, L., Khandoker, A., and Baumert, M. (2019b). 'Wavelet entropy-based inter-subject associative cortical source localization for sensorimotor bci', Frontiers in Neuroinformatics, **13***, 47.*

Saha, S., Linz, D., Sanders, P., and Baumert, M. (2019c). 'Beamforming-inspired spatial filtering technique for intracardiac electrograms', 2019 41st Annual International Conference of the IEEE Engineering in Medicine and Biology Society (EMBC), IEEE, pp. 4254–4257.

Saha, S., Mamun, K. A., Ahmed, K., Mostafa, R., Naik, G. R., Darvishi, S., Khandoker, A. H., and Baumert, M. (2021). 'Progress in brain computer interface: Challenges and opportunities', Frontiers in Systems Neuroscience, **15***, 578875.*

Sample, M., Aunos, M., Blain-Moraes, S., Bublitz, C., Chandler, J. A., Falk, T. H., Friedrich, O., Groetzinger, D., Jox, R. J., Koegel, J etxxxxx al.. (2019). 'Brain–computer interfaces and personhood: interdisciplinary deliberations on neural technology', Journal of Neural Engineering, **16***(6), 063001.*

Sánchez, J., Luongo, G., Nothstein, M., Unger, L. A., Saiz, J., Trenor, B., Luik, A., Dössel, O., and Loewe, A. (2021). 'Using machine learning to characterize atrial fibrotic substrate from intracardiac signals with a hybrid in silico and in vivo dataset', Frontiers in Physiology, 1000.

Sannelli, C., Vidaurre, C., Müller, K.-R., and Blankertz, B. (2016). 'Ensembles of adaptive spatial filters increase bci performance: an online evaluation', Journal of neural engineering, **13***(4), 046003.*

Sannelli, C., Vidaurre, C., Müller, K.-R., and Blankertz, B. (2019). 'A large scale screening study with a smr-based bci: Categorization of bci users and differences in their smr activity', PloS one, **14***(1), e0207351.*

Sasai, S., Koike, T., Sugawara, S. K., Hamano, Y. H., Sumiya, M., Okazaki, S., Takahashi, H. K., Taga, G., and Sadato, N. (2021). 'Frequency-specific task modulation of human brain functional networks: A fast fmri study', NeuroImage, **224***, 117375.*

Schmitz-Luhn, B., Katzenmeier, C., and Woopen, C. (2012). 'Law and ethics of deep brain stimulation', International Journal of Law and Psychiatry, **35***(2), pp. 130–136.*

Schotten, U., Lee, S., Zeemering, S., and Waldo, A. L. (2021). 'Paradigm shifts in electrophysiological mechanisms of atrial fibrillation', EP Europace, **23***(Supplement_2), pp. ii9–ii13.*

Schotten, U., Verheule, S., Kirchhof, P., and Goette, A. (2011). 'Pathophysiological mechanisms of atrial fibrillation: a translational appraisal', Physiological reviews, **91***(1), pp. 265–325.*

Seghier, M. L., and Price, C. J. (2018). 'Interpreting and utilising intersubject variability in brain function', Trends in cognitive sciences, **22***(6), pp. 517–530.*

Sha, Q., Elliott, L., Zhang, X., Levy, T., Sharma, T., and Abdelaal, A. (2022). 'Atrial fibrillation driver identification through regional mutual information networks: a modeling perspective', Journal of Interventional Cardiac Electrophysiology, **64***(3), pp. 649–660.*

Shenasa, M., Razavi, S.-M., Shenasa, H., and Al-Ahmad, A. (2019). 'The ideal cardiac mapping system', Cardiac electrophysiology clinics, **11***(4), pp. 739–748.*

Sierra-Mercado, D., Zuk, P., Beauchamp, M. S., Sheth, S. A., Yoshor, D., Goodman, W. K., McGuire, A. L., and Lázaro-Muñoz, G. (2019). 'Device removal following brain implant research', Neuron, **103***(5), pp. 759–761.*

Silversmith, D. B., Abiri, R., Hardy, N. F., Natraj, N., Tu-Chan, A., Chang, E. F., and Ganguly, K. (2021). 'Plug-and-play control of a brain–computer interface through neural map stabilization', Nature biotechnology, **39***(3), pp. 326–335.*

Sitaram, R., Ros, T., Stoeckel, L., Haller, S., Scharnowski, F., Lewis-Peacock, J., Weiskopf, N., Blefari, M. L., Rana, M., Oblak, E etxxxxx al.. (2017). 'Closed-loop brain training: the science of neurofeedback', Nature Reviews Neuroscience, **18***(2), pp. 86–100.*

Sitaram, R., Weiskopf, N., Caria, A., Veit, R., Erb, M., and Birbaumer, N. (2007). 'fmri brain-computer interfaces', IEEE Signal processing magazine, **25***(1), pp. 95–106.*

Soekadar, S., Witkowski, M., Gómez, C., Opisso, E., Medina, J., Cortese, M., Cempini, M., Carrozza, M. C., Cohen, L., Birbaumer, N etxxxxx al.. (2016). 'Hybrid eeg/eog-based brain/neural hand exoskeleton restores fully independent daily living activities after quadriplegia', Science Robotics, **1***(1), eaag3296.*

Soldado-Magraner, J., Antonietti, A., French, J., Higgins, N., Young, M. J., Larrivee, D., and Monteleone, R. (2024). 'Applying the ieee brain neuroethics framework to intra-cortical brain-computer interfaces', Journal of Neural Engineering, **21***(2), 022001.*

Song, Y., Zheng, Q., Liu, B., and Gao, X. (2022). 'Eeg conformer: Convolutional transformer for eeg decoding and visualization', IEEE Transactions on Neural Systems and Rehabilitation Engineering, **31***, pp. 710–719.*

Sponheim, C., Papadourakis, V., Collinger, J. L., Downey, J., Weiss, J., Pentousi, L., Elliott, K., and Hatsopoulos, N. G. (2021). 'Longevity and reliability of chronic unit recordings using the utah, intracortical multi-electrode arrays', Journal of neural engineering, **18***(6), 066044.*

Sroubek, J., Rottmann, M., Barkagan, M., Leshem, E., Shapira-Daniels, A., Brem, E., Fuentes-Ortega, C., Malinaric, J., Basu, S., Bar-Tal, M etxxxxx al.. (2019). 'A novel octaray multielectrode catheter for high-resolution atrial mapping: Electrogram characterization and utility for mapping ablation gaps', Journal of Cardiovascular Electrophysiology, **30***(5), pp. 749–757.*

Stamford, J. A., Schmidt, P. N., and Friedl, K. E. (2015). 'What engineering technology could do for quality of life in parkinson's disease: a review of current needs and opportunities', IEEE journal of biomedical and health informatics, **19***(6), pp. 1862–1872.*

Stefano Filho, C. A., Attux, R., and Castellano, G. (2024). 'Motor imagery neurofeedback: From system conceptualization to neural correlates', Current Behavioral Neuroscience Reports, pp. 1–21.

Steinert, S., and Friedrich, O. (2020). 'Wired emotions: Ethical issues of affective brain–computer interfaces', Science and engineering ethics, **26***(1), pp. 351–367.*

Stinnett-Donnelly, J. M., Thompson, N., Habel, N., Petrov-Kondratov, V., de Sa, D. D. C., Bates, J. H., and Spector, P. S. (2012). 'Effects of electrode size and spacing on the resolution of intracardiac electrograms', Coronary artery disease, **23***(2), pp. 126–132.*

Sunny, M. S. H., Zarif, M. I. I., Rulik, I., Sanjuan, J., Rahman, M. H., Ahamed, S. I., Wang, I., Schultz, K., and Brahmi, B. (2021). 'Eye-gaze control of a wheelchair mounted 6dof assistive robot for activities of daily living', Journal of NeuroEngineering and Rehabilitation, **18***, pp. 1–12.*

Takahashi, Y., Yamaguchi, T., Otsubo, T., Nakashima, K., Shinzato, K., Osako, R., Shichida, S., Kawano, Y., Fukui, A., Kawaguchi, A etxxxxx al.. (2023). 'Histological validation of atrial structural remodelling in patients with atrial fibrillation', European Heart Journal, ehad396.

Takigawa, M., Kitamura, T., Basu, S., Bartal, M., Martin, C. A., Martin, R., Cheniti, G., Vlachos, K., Pillois, X., Frontera, A etxxxxx al.. (2021). 'Effect of electrode size and spacing on electrograms: Optimized electrode configuration for near-field electrogram characterization', Heart Rhythm, .

Takigawa, M., Relan, J., Martin, R., Kim, S., Kitamura, T., Cheniti, G., Vlachos, K., Pillois, X., Frontera, A., Massoullié, G etxxxxx al.. (2019). 'Detailed analysis of the relation between bipolar electrode spacing and far-and near-field electrograms', JACC: Clinical Electrophysiology, **5***(1), pp. 66–77.*

Tan, J. L., Guandalini, G. S., Hyman, M. C., Arkles, J., Santangeli, P., Schaller, R. D., Garcia, F., Supple, G., Frankel, D. S., Nazarian, S etxxxxx al.. (2023). 'Substrate and arrhythmia characterization using the multi-electrode optrell mapping catheter for ventricular arrhythmia ablation—a single-center experience', Journal of Interventional Cardiac Electrophysiology, pp. 1–11.

Tedrow, U. B., and Stevenson, W. G. (2011). 'Recording and interpreting unipolar electrograms to guide catheter ablation', Heart Rhythm, **8***(5), pp. 791–796.*

Tran, P., Jeong, S., Wolf, S. L., and Desai, J. P. (2020). 'Patient-specific, voice-controlled, robotic flexotendon glove-ii system for spinal cord injury', IEEE Robotics and Automation Letters, **5***(2), pp. 898–905.*

Trayanova, N. A., Popescu, D. M., and Shade, J. K. (2021). 'Machine learning in arrhythmia and electrophysiology', Circulation research, **128***(4), pp. 544–566.*

Unger, L. A., Oesterlein, T. G., Loewe, A., and Dössel, O. (2019). 'Noise quantification and noise reduction for unipolar and bipolar electrograms', 2019 Computing in Cardiology (CinC), IEEE, pp. Page–1.

van der Does, L. J., and de Groot, N. M. (2017). 'Inhomogeneity and complexity in defining fractionated electrograms', Heart Rhythm, **14***(4), pp. 616–624.*

van der Does, L., Kik, C., Allessie, M., and de Groot, N. (2017). 'Endo–epicardial dissociation in conduction', European Heart Journal, **38***(22), pp. 1775–1775.*

Van der Groen, O., Potok, W., Wenderoth, N., Edwards, G., Mattingley, J. B., and Edwards, D. (2022). 'Using noise for the better: The effects of transcranial random noise stimulation on the brain and behavior', Neuroscience & Biobehavioral Reviews, **138***, 104702.*

van Schie, M. S., Kharbanda, R. K., Houck, C. A., Lanters, E. A., Taverne, Y. J., Bogers, A. J., and de Groot, N. M. (2021). 'Identification of low-voltage areas: a unipolar, bipolar, and omnipolar perspective', Circulation: Arrhythmia and Electrophysiology, **14***(7), e009912.*

Van Schie, M. S., Knops, P., Zhang, L., Van Schaagen, F., Taverne, Y. J., and De Groot, N. (2022). 'Detection of endo-epicardial atrial low-voltage areas using unipolar and omnipolar voltage mapping', Frontiers in Physiology, 2154.

Vansteensel, M. J., Leinders, S., Branco, M. P., Crone, N. E., Denison, T., Freudenburg, Z. V., Geukes, S. H., Gosselaar, P. H., Raemaekers, M., Schippers, A etxxxxx al.. (2024). 'Longevity of a brain–computer interface for amyotrophic lateral sclerosis', New England Journal of Medicine, **391***(7), pp. 619–626.*

Vansteensel, M. J., Pels, E. G., Bleichner, M. G., Branco, M. P., Denison, T., Freudenburg, Z. V., Gosselaar, P., Leinders, S., Ottens, T. H., Van Den Boom, M. A etxxxxx al.. (2016). 'Fully implanted brain–computer interface in a locked-in patient with als', New England Journal of Medicine, **375***(21), pp. 2060–2066.*

Verheule, S., Eckstein, J., Linz, D., Maesen, B., Bidar, E., Gharaviri, A., and Schotten, U. (2014). 'Role of endo-epicardial dissociation of electrical activity and transmural conduction in the development of persistent atrial fibrillation', Progress in biophysics and molecular biology, **115***(2-3), pp. 173–185.*

Viana, P. F., Remvig, L. S., Duun-Henriksen, J., Glasstetter, M., Dümpelmann, M., Nurse, E. S., Martins, I. P., Schulze-Bonhage, A., Freestone, D. R., Brinkmann, B. H etxxxxx al.. (2021). 'Signal quality and power spectrum analysis of remote ultra long-term subcutaneous eeg', Epilepsia, **62***(8), pp. 1820–1828.*

Vidal, J. J. (1973). 'Toward direct brain-computer communication', Annual review of Biophysics and Bioengineering, **2***(1), pp. 157–180.*

Vidaurre, C., and Blankertz, B. (2010). 'Towards a cure for bci illiteracy', Brain topography, **23***, pp. 194–198.*

Vidaurre, C., Haufe, S., Jorajuría, T., Müller, K.-R., and Nikulin, V. V. (2020). 'Sensorimotor functional connectivity: a neurophysiological factor related to bci performance', Frontiers in Neuroscience, **14***, 575081.*

Wang, H., Sun, Y., Wang, F., Cao, L., Zhou, W., Wang, Z., and Chen, S. (2021). 'Cross-subject assistance: Inter-and intra-subject maximal correlation for enhancing the performance of ssvep-based bcis', IEEE Transactions on Neural Systems and Rehabilitation Engineering, **29***, pp. 517–526.*

Wang, J., Cheng, S., Tian, J., and Gao, Y. (2023a). 'A 2d cnn-lstm hybrid algorithm using time series segments of eeg data for motor imagery classification', Biomedical Signal Processing and Control, **83***, 104627.*

Wang, M., Gao, F., Jin, S., and Lin, H. (2019). 'An overview of enhanced massive mimo with array signal processing techniques', IEEE Journal of Selected Topics in Signal Processing, **13***(5), pp. 886–901.*

Wang, R., Wang, J., Yu, H., Wei, X., Yang, C., and Deng, B. (2015). 'Power spectral density and coherence analysis of alzheimer's eeg', Cognitive neurodynamics, **9***, pp. 291–304.*

Wang, X., Wang, Y., Liu, D., Wang, Y., and Wang, Z. (2023b). 'Automated recognition of epilepsy from eeg signals using a combining space–time algorithm of cnn-lstm', Scientific Reports, **13***(1), 14876.*

Watanabe, H., Tanaka, H., Sakti, S., and Nakamura, S. (2020). 'Synchronization between overt speech envelope and eeg oscillations during imagined speech', Neuroscience research, **153***, pp. 48–55.*

Wei, Q., and Ding, X. (2023). 'Intra-and inter-subject common spatial pattern for reducing calibration effort in mi-based bci', IEEE Transactions on Neural Systems and Rehabilitation Engineering, **31***, pp. 904–916.*

Welch, P. (1967). 'The use of fast fourier transform for the estimation of power spectra: a method based on time averaging over short, modified periodograms', IEEE Transactions on audio and electroacoustics, **15***(2), pp. 70–73.*

Wijesurendra, R. S., and Casadei, B. (2019). 'Mechanisms of atrial fibrillation', Heart, **105***(24), pp. 1860–1867.*

Willett, F. R., Avansino, D. T., Hochberg, L. R., Henderson, J. M., and Shenoy, K. V. (2021). 'High-performance brain-to-text communication via handwriting', Nature, **593***(7858), pp. 249–254.*

Willett, F. R., Kunz, E. M., Fan, C., Avansino, D. T., Wilson, G. H., Choi, E. Y., Kamdar, F., Glasser, M. F., Hochberg, L. R., Druckmann, S etxxxxx al.. (2023). 'A high-performance speech neuroprosthesis', Nature, **620***(7976), pp. 1031–1036.*

Wimpff, M., Gizzi, L., Zerfowski, J., and Yang, B. (2024). 'Eeg motor imagery decoding: A framework for comparative analysis with channel attention mechanisms', Journal of Neural Engineering, **21***(3), 036020.*

Woeppel, K., Hughes, C., Herrera, A. J., Eles, J. R., Tyler-Kabara, E. C., Gaunt, R. A., Collinger, J. L., and Cui, X. T. (2021). 'Explant analysis of utah electrode arrays implanted in human cortex for brain-computer-interfaces', Frontiers in Bioengineering and Biotechnology, **9***, 759711.*

Wojciuk, M., Swiderska-Chadaj, Z., Siwek, K., and Gertych, A. (2024). 'Improving classification accuracy of fine-tuned cnn models: Impact of hyperparameter optimization', Heliyon, **10***(5).*

Wong, K. C., Sadarmin, P. P., De Bono, J., Qureshi, N., Jones, M., Rajappan, K., Bashir, Y., and Betts, T. R. (2011). 'Local activation times at the high posterior wall of the left atrium during left atrial appendage pacing predict roof line block with high specificity and sensitivity', Europace, **13***(9), pp. 1243–1249.*

Wronkiewicz, M., Larson, E., and Lee, A. K. (2015). 'Leveraging anatomical information to improve transfer learning in brain–computer interfaces', Journal of neural engineering, **12***(4), 046027.*

Xiong, Z., Stiles, M. K., Yao, Y., Shi, R., Nalar, A., Hawson, J., Lee, G., and Zhao, J. (2022). 'Automatic 3d surface reconstruction of the left atrium from clinically mapped point clouds using convolutional neural networks', Frontiers in Physiology, **13***.*

Yamaguchi, T., Tsuchiya, T., Nakahara, S., Fukui, A., Nagamoto, Y., Murotani, K., Eshima, K., and Takahashi, N. (2016). 'Efficacy of left atrial voltage-based catheter ablation of

persistent atrial fibrillation', Journal of cardiovascular electrophysiology, **27***(9), pp. 1055–1063.*

Yang, B., Zhu, X., Liu, Y., and Liu, H. (2021a). 'A single-channel eeg based automatic sleep stage classification method leveraging deep one-dimensional convolutional neural network and hidden markov model', Biomedical Signal Processing and Control, **68***, 102581.*

Yang, K., Xi, X., Wang, T., Wang, J., Kong, W., Zhao, Y.-B., and Zhang, Q. (2021b). 'Effects of transcranial direct current stimulation on brain network connectivity and complexity in motor imagery', Neuroscience Letters, **757***, 135968.*

Yavin, H. D., Bubar, Z. P., Higuchi, K., Sroubek, J., Yarnitsky, J., and Anter, E. (2021). 'Propagation vectors facilitate differentiation between conduction block, slow conduction, and wavefront collision', Circulation: Arrhythmia and Electrophysiology, **14***(8), e010081.*

Yavin, H. D., Sroubek, J., Yarnitsky, J., Bubar, Z. P., Higuchi, K., Zilberman, I., Basu, S., and Anter, E. (2022). 'Direction-aware mapping algorithms have minimal impact on bipolar voltage maps created using high-resolution multielectrode catheters', Journal of cardiovascular electrophysiology, **33***(1), pp. 73–80.*

Yenduri, G., Ramalingam, M., Selvi, G. C., Supriya, Y., Srivastava, G., Maddikunta, P. K. R., Raj, G. D., Jhaveri, R. H., Prabadevi, B., Wang, W etxxxxx al.. (2024). 'Gpt (generative pre-trained transformer)–a comprehensive review on enabling technologies, potential applications, emerging challenges, and future directions', IEEE Access, .

Yeo, C., Tan, V. H., and Wang, Y. (2022). 'Omnipolar activation egm to identify the earliest breakout site of atrial tachycardia', Journal of Arrhythmia, **38***(5), pp. 801–804.*

Yin, K., Lim, E. Y., and Lee, S.-W. (2024). 'Gitgan: Generative inter-subject transfer for eeg motor imagery analysis', Pattern Recognition, **146***, 110015.*

Zaatari, G., Mitrani, R., Bohorquez, J., Ng, J., Ng, J., Rivner, H., Velasquez, A., Lambrakos, L., Arora, R., and Goldberger, J. J. (2023). 'Electrogram morphology recurrence for mapping persistent atrial fibrillation: Initial vs redo catheter ablation', JACC: Clinical Electrophysiology, .

Zander, T. O., Kothe, C., Welke, S., and Rötting, M. (2009). 'Utilizing secondary input from passive brain-computer interfaces for enhancing human-machine interaction', Foundations of Augmented Cognition. Neuroergonomics and Operational Neuroscience: 5th International Conference, FAC 2009 Held as Part of HCI International 2009 San Diego, CA, USA, July 19-24, 2009 Proceedings 5, Springer, pp. 759–771.

Zanini, P., Congedo, M., Jutten, C., Said, S., and Berthoumieu, Y. (2017). 'Transfer learning: A riemannian geometry framework with applications to brain–computer interfaces', IEEE Transactions on Biomedical Engineering, **65***(5), pp. 1107–1116.*

Zhang, L., Zhou, Y., Gong, P., and Zhang, D. (2024). 'Speech imagery decoding using eeg signals and deep learning: A survey', IEEE Transactions on Cognitive and Developmental Systems, .

Zhang, X., Yao, L., Wang, X., Monaghan, J., Mcalpine, D., and Zhang, Y. (2021). 'A survey on deep learning-based non-invasive brain signals: recent advances and new frontiers', Journal of neural engineering, **18***(3), 031002.*

Zhang, Y., Sun, L., Xuan, L., Pan, Z., Hu, X., Liu, H., Bai, Y., Jiao, L., Li, Z., Cui, L etxxxxx al.. (2018). 'Long non-coding rna ccrr controls cardiac conduction via regulating intercellular coupling', Nature communications, **9***(1), pp. 1–14.*

Zhou, Y., Song, H., and Ming, G.-l. (2024). 'Genetics of human brain development', Nature Reviews Genetics, **25***(1), pp. 26–45.*

Zhu, M., Biswas, S., Dinulescu, S. I., Kastor, N., Hawkes, E. W., and Visell, Y. (2022). 'Soft, wearable robotics and haptics: Technologies, trends, and emerging applications', Proceedings of the IEEE, **110***(2), pp. 246–272.*

Zich, C., Debener, S., Kranczioch, C., Bleichner, M. G., Gutberlet, I., and De Vos, M. (2015). 'Real-time eeg feedback during simultaneous eeg–fmri identifies the cortical signature of motor imagery', Neuroimage, **114***, pp. 438–447.*

Zubler, F., and Tzovara, A. (2023). 'Deep learning for eeg-based prognostication after cardiac arrest: from current research to future clinical applications', Frontiers in Neurology, **14***.*

Acronyms

1D-CNN	1−dimensional convolutional neural network
$1D$	1−dimensional
2D-CNN	2−dimensional convolutional neural network
$2D$	2−dimensional
3D	3−dimensional
ACS	atrial conduction system
AF	atrial fibrillation
AI	artificial intelligence
ARTs	assistive and rehabilitative technologies
AV	atrioventricular
BC	Bhattacharyya coefficient
BCI	brain-computer interface
CNN	convolutional neural network
CPC	cerebral performance category
CPSD	cross-power spectral density
CPU	central processing unit
CSP	common spatial pattern
CSS	covariate shift score
DSP	digital signal processing
ECG	electrocardiography
ECM	extracellular matrix
ECoG	electrocorticography
EEG	electroencephalogram
EGM	electrogram
FFT	Fast Fourier Transform
fMRI	Functional magnetic resonance imaging
fNIRS	functional near-infrared spectroscopy
FPR	false positive rate

GPU . . . . . graphics processing unit

ICF . . . . . International Classification of Functioning, Disability, and Health

ICU . . . . . intensive care unit

LDA . . . . . linear discriminant analysis

LSTM . . . . . long short-term memory

MEA . . . . . microelectrode array

MEG . . . . . magnetoencephalography

MI . . . . . motor imagery

PCA . . . . . principal component analysis

PSD . . . . . power spectral density

ReLU . . . . . rectified linear unit

RF . . . . . right foot

RH . . . . . right hand

SA . . . . . sinoatrial

SMR . . . . . sensorimotor

SR . . . . . sinus rhythm

TPR . . . . . true positive rate